UNDERSTANDING THE ROLE OF SULFUR IN CARTILAGE DEVELOPMENT:

HOW STRUCTURAL PROTEOGLYCANS ARE IMPLICATED IN CARTILAGE MATURATION

A Thesis Submitted to the College of
Graduate and Postdoctoral Studies
In Partial Fulfillment of the Requirements-
For the Degree of Master of Science
In the Department of Anatomy and Cell Biology
University of Saskatchewan
Saskatoon

By

DEVIN BROWN

Permission to Use

In presenting this thesis/dissertation in partial fulfillment of the requirements for a Postgraduate degree from the University of Saskatchewan, I agree that the Libraries of this University may make it freely available for inspection. I further agree that permission for copying of this thesis/dissertation in any manner, in whole or in part, for scholarly purposes may be granted by the professor or professors who supervised my thesis/dissertation work or, in their absence, by the Head of the Department or the Dean of the College in which my thesis work was done. It is understood that any copying or publication or use of this thesis/dissertation or parts thereof for financial gain shall not be allowed without my written permission. It is also understood that due recognition shall be given to me and to the University of Saskatchewan in any scholarly use which may be made of any material in my thesis/dissertation.

Disclaimer

References in this thesis/dissertation to any specific commercial products, process, or service by trade name, trademark, manufacturer, or otherwise, does not constitute or imply its endorsement, recommendation, or favoring by the University of Saskatchewan. The views and opinions of the author expressed herein do not state or reflect those of the University of Saskatchewan, and shall not be used for advertising or product endorsement purposes.

Requests for permission to copy or to make other uses of materials in this thesis/dissertation in whole or part should be addressed to:

Head of the department of Anatomy and Cell Biology

107 Wiggins Rd.

University of Saskatchewan

Saskatoon, Saskatchewan S7N 5E5

Canada

OR

Dean

College of Graduate and Postdoctoral Studies

University of Saskatchewan

105 Administration Place

Saskatoon, Saskatchewan S7N 5A2

Canada

Abstract

Cartilage is a vital tissue of the adult skeleton, which also serves as a transitional structure during early skeletal development. Sulfation of proteoglycans, especially chondroitin sulfate proteoglycans (CSPGs), lends unique mechanical properties to this tissue; but how CSPG sulfation relates to cartilage growth and development remains an open area of study. Though the basic biochemistry of addition and removal of sulfate groups from sulfated proteoglycans has been well studied, we reveal for the first time in the chicken the spatial distribution of sulfur throughout the cartilage template of a developing endochondral bone (the humerus) to show that changes in sulfation pattern are related to cartilage maturation. New techniques such as chemically specific X-ray fluorescence (XRF) imaging combined with immunohistochemistry allow the testing of the hypothesis that sulfate ester levels are correlated with the underlying cartilage maturation state. Our findings indicate that there is a significant decrease in sulfate ester levels in mature cartilage when compared with immature cartilage in the chicken. No significant decrease in PGs occurred at this time point in mature cartilage according to infrared imaging, suggesting an under-sulfated CSPG molecule in mature cartilage, and an unknown mechanism responsible for this shift in lowered sulfation levels. Decreasing sulfate esters in mature cartilage are now shown to be features of skeletal development for the chicken in addition to zebrafish.

Acknowledgements

I would like to first and foremost acknowledge and thank my supervisor, Dr. Brian Eames, for his mentorship and encouragement throughout my Master's project. I cannot thank him enough for pushing me in the right ways to get through significant struggles I faced pursuing my academic goals. Thank you very much to my committee members Dr. Ingrid Pickering and Dr. David Cooper for all of their input and help with overseeing my project from its very earliest inception. I would also like to acknowledge my fellow lab mates with special thanks to Mark Hackett, Julien Cotelesage, Patsy-Gómez-Picos and Rafaela Grecco for their help with this project.

A huge thank you to the sources of funding throughout my Master's project including the College of Medicine Departmental Scholarship, the Canadian Institutes of Health Research (CIHR) Training Grant in Health Research Using Synchrotron Techniques (CIHR-THRUST), and funding from Dr. Brian Eames obtained through CIHR.

Part of the research described in this thesis was performed at the Canadian Light Source, which is supported by the Canada Foundation for Innovation, NSERC, the University of Saskatchewan, the Government of Saskatchewan, Western Economic Diversification Canada, the National Research Council Canada, and the CIHR.

Lastly, I would like to mention that it was a great honor to be part of the CIHR-THRUST training program for new synchrotron researchers. The program presented many unique opportunities outside of funding, including a chance to present posters, give oral presentations, meeting and learning from other students and investigators using many different synchrotron techniques, attending of special seminars by field-leading experts, and it also provided a chance to be involved in a planning of our local, annual retreat. Thank you to the Canadian Light Source for granting beamtime to this project through four separate proposals at the VESPERS, Mid-IR and SXRMB beamlines and to all of the CLS staff for their help and moral support.

Dedication

I would like to dedicate this work to my late father, Darwin Brown, a man who walked tall and was a great friend to many, and my mother, Angela, who has always believed in me.

Table of Contents

List of Tables

List of Figures

List of Abbreviations

Bmp	bone morphogenetic protein
Chpf	chondroitin polymerizing factor
Chst	carbohydrate sulfotransferase
Chsy	chondroitin sulfate synthase
CS	chondroitin sulfate
Csgalnact	chondroitin sulfate N-acetylgalactosaminyltransferase
CSPG	chondroitin sulfate proteoglycan
CLS	Canadian Light Source synchrotron
DS	dermatan sulfate
ER	endoplasmic reticulum
Fgf	fibroblast growth factor
FTIR	Fourier-transform infrared
GAG	glycosaminoglycan
Gal	galactose
GalNAc	N-acetylgalactosamine
Galt	galactosyltransferase
Gat	glucuronyltransferase
GF	growth factor
GlcA	glucuronic acid
GlcNAc	N-acetylglucosamine
Hh	Hedgehog
HS	heparan sulfate
IR	infrared
KS	keratan sulfate
MIM	Mendelian Inheritance in Man
MPS	mucopolysaccharidosis
PG	proteoglycan
Ser	serine
SXRMB	Soft X-ray Characterization Beamline at the Canadian Light Source
UDP	uridine diphosphate
VESPERS	Very Sensitive Elemental and Structural Probe Employing Radiation from a Synchrotron beamline at Canadian Light Source
XRF	X-ray fluorescence
Xyl	xylose
Xylt	xylosyltransferase

CHAPTER 1

1.1 Introduction

This thesis is written in the form of manuscript-style chapters. The literature review and an introduction to the ideas explored further in the main study are presented in the second chapter, which have been published as a book chapter in the textbook Methods in Cell Biology:

Brown, DS, and Eames, BF (2016). Emerging tools to study proteoglycan function during skeletal development. Methods in Cell Biology 134: 485-530. PMID: 27312503

In this manuscript, the above-mentioned book chapter publication, I was granted first authorship and wrote it as a co-author with my supervisor Dr. Eames, whom was contacted by the publisher to contribute directly to a chapter. This manuscript has been altered from it's original published form. Several small changes to the wording and clarification of concepts in this manuscript have been made at the request of the thesis defense committee. The thrust of my contribution was that it should serve as a literature review for the role of matrix proteoglycans in development, their synthesis and degradation, and emerging techniques in the field to visualize proteoglycans *in-situ*. I authored the introduction, with input from Dr. Eames, along with the overview of proteoglycan synthesis and degradation, and the section on emerging new techniques to visualize proteoglycans focused on X-ray fluorescence imaging Fourier transform infrared imaging. I also co-authored the final discussion and conclusions as they went through several revisions. I was responsible for creating Figures 2.1 and 2.3 (as named within the manuscript). The figures included a schematic for proteoglycan synthesis and degradation pathways and locations within the cell for Figure 2.1 and Figure 2.3 included representative images I collected myself demonstrating different types of information captured by these various forms of imaging.

Writing a review paper served as a great background to my own research which is presented in Chapter 3. A working citation for the second, unpublished manuscript is:

Brown, DS., Grecco, R, Hackett, MJ, George, GN, Pickering, IJ, and Eames, BF., "Proteoglycan sulfation decreases in mature cartilage during endochondral ossification", in preparation

I am also the lead author on the second manuscript. The body of work pertains to experiments performed by myself throughout the course of my time in the lab of Dr. Eames. The rationale for this study was to determine whether sulfate ester levels decrease in mature cartilage in the chicken, as they were shown to in the zebrafish. After this was established, we wanted to try to understand if this sulfur loss can be attributed to loss of bulk PGs (through the lysosomal degradation pathway), or if sulfur may be decreasing in an independent fashion in the extracellular matrix (ECM). The latter would be a novel finding, pointing to an undiscovered mechanism regulating ECM sulfur levels. The main hypothesis of my thesis derives from previous experiments performed by Dr. Eames and Dr. Mark Hackett (then a post-doctoral fellow from the Department of Geological Sciences at the

University of Saskatchewan), which first identified the PG deficient *fam20b*$^{-/-}$ mutant zebrafish, and then proceeded to characterize it (Eames et al., 2011; Hackett et al., 2016). A trend was noticed in wild-type zebrafish sulfur levels spatially related to the different maturation states of cartilage (Hackett et al., 2016).

The hypothesis in the second manuscript, which is the same overriding hypothesis guiding my thesis, is sulfate ester levels of proteoglycans decrease in mature cartilage. This manuscript is furthering our understanding from these preliminary findings in two main ways. Firstly, the chicken as a well-accepted model organism for skeletal development may differ in significant ways from zebrafish: including the timing of overall maturation, the much greater amount of ECM in the chick relative to zebrafish, and the different environments of natural selection that each organism has experienced. Secondly, our methodology has some different technical elements to it compared to previous studies. Technical differences include the analysis of adjacent sections to look at the expression of the maturation marker protein COLX to more accurately draw our mature cartilage regions. We also had the chance to look at some newly validated proteoglycan markers in the infrared region to determine specifically whether it was bulk proteoglycans or sulfate esters specifically being lost from the mature region.

The plan for publishing the second manuscript is to include one more experimental result performed by another PhD student to add weight to our speculation on the cause for decreasing sulfur in mature cartilage. Based upon results of this thesis, we propose a mechanism behind what is driving these losses in sulfur in mature cartilage (i.e., a sulfatase, or combination of different sulfatases). With a mechanism finally proposed, this could directly lead to the possibility of creating an animal model which may lead to a significant breakthrough in understanding the role of sulfur in regulating developmental timing, as well as cartilage pathologies. The bulk of the work performed by myself during the course of my Master's work, essentially the second manuscript (Chapter 3), sets out to correlate sulfur levels and the maturation state of developing cartilage. I then tried to build a case for biological significance of these changes with respect to normal developmental regulation and also diseased states of cartilage.

An appendix was included at the end of the thesis. The rationale of this study was to look at sulfur speciation within normal and osteoarthritis (OA) affected cartilage, and to create maps showing the distribution of the different chemical forms of sulfur throughout both affected and unaffected tissue layers. This study employed the same chemically specific XRF imaging techniques used in Chapter 3 to look at sulfur in early development. High sulfation levels are an important factor in articular cartilage structural integrity. Sulfur exists in different chemical forms and this would be the first study looking at the spatial distribution of different chemical forms of sulfur in human OA tissue. This data may be put together later as a publication when coupled with more OA and non-OA, age-matched control samples imaged if more beamtime is granted for this purpose.

CHAPTER 2

2. Literature Review (published manuscript): Manuscript 1 – Emerging Tools to Study Proteoglycan Function during Skeletal Development (modified from the original version)

Brown, DS, and BF Eames (2016). Emerging tools to study proteoglycan function during skeletal development. Methods in Cell Biology 134: 485-530. PMID: 27312503

2.1 Introduction

2.1.1 Adding function to structure: Responsive architecture and PGs

The history of our understanding of proteoglycans PGs, which are special types of sugar-coated proteins, draws strong parallels to modern architectural trends. Responsive architecture is an evolving field that seeks to add functionality to structures, integrating technological components that allow buildings to interface with their environment (El-Khoury et al., 2012). For example, sensors in the walls determine if people are located in certain rooms at specific times of the day, and in response to these data, the performance of lighting and heating elements are optimized. So, in the history of architecture, walls in a building attained additional functions on top of their primary structural role. Just as responsive architecture adds function to structure, this review outlines similar progress in scientific understanding of the biological roles of PGs, interesting molecules that quite literally integrate the cell with the surrounding environment.

Biochemical studies of PGs began around the turn of the 20th century with crude preparations from biological tissues that were rich in extracellular matrix, including "chondromucoid" from cartilage and anticoagulant from liver (heparin) (reviewed in Esko *et al*., 2009). In the late 1970s, new chromatographic methods permitted purification and identification of different PGs (Yanagishita, 1993a), and in the 1980s through the 1990's, the PG synthesis pathway was dissected genetically (Banfield et al., 1995; Doege et al., 1994; Esko, 1992; Hardingham and Fosang, 1992; Li et al., 1993; Sarkar and Esko, 1995; Stirpe et al., 1987; Upholt et al., 1993; Valhmu et al., 1995; Watanabe et al., 1994; Wight et al., 1991). These and other advancements clarified greatly how this group of molecules are classified and synthesized.

PGs are a type of glycoprotein, comprised of a core protein onto which are attached one or many sidechains of repeating disaccharides, termed glycosaminoglycans (GAGs) (Hardingham and Fosang, 1992). Each specific class of PG is named based upon the exact sugars added in the GAG sidechain, including chondroitin sulfate (CS), heparan sulfate (HS), keratan sulfate (KS), and dermatan sulfate (DS) (Iozzo and Murdoch, 1996). CS differs from HS, for example, in that the repeating disaccharide of CS is made of glucuronic acid (GlcA) and N-acetylgalactosamine (GalNAc), whereas HS has GlcA and N-acetylglucosamine (GlcNAc) repeats (Bray et al., 1944). CS and HS are similar, however, because they both have the same four sugar (tetrasaccharide) linker region connecting the GAG sidechain to the core protein via a terminal hydroxyl-linked serine residue (Iozzo and Murdoch, 1996). Due to this linkage, CS and HS are termed O-linked glycans, whereas N-linked glycans, such as KS, are attached to asparagine residues (Vynios, 2014). Since most focus in the literature has been on biological roles of HSPG's (Bernfield et al., 1999; Esko and Lindahl, 2001; Lin, 2004; Tumova et al., 2000; Turnbull et al., 2001), this review emphasizes more recent advances on chondroitin sulfate proteoglycan (CSPG) functions (Cortes et al., 2009; Hintze et al., 2012; Khatri and Schipani, 2008; Lauing et al., 2014;

Mis et al., 2014; Mizumoto et al., 2009; Prydz, 2015; Salbach et al., 2012; Sato et al., 2011; Tompson et al., 2009; Watanabe et al., 2010).

Most tissues owe their structural features to the secretion of extracellular matrix by resident cells, a fact epitomized by skeletal cells, which secrete massive amounts of collagens and PGs to make cartilage and bone (Kearns et al., 1993; Sarmah et al., 2010). These secreted molecules and their extracellular interactions provide many of the mechanical properties of skeletal tissues. Collagen networks impart tensile strength, PG networks account for compressive resistant strength, and these networks also interact with each other directly (Aumailley and Gayraud, 1998; Merritt et al., 2007; Olsen, 1996). The most abundant cartilage PG is Aggrecan, a core protein decorated mostly with CS, but also with KS (Hardingham and Fosang, 1995; Kiani et al., 2002). In addition to collagen/PG interactions, cartilage structure also derives from interactions between Aggrecan core proteins and a secreted polysaccharide called hyaluronan via link proteins (Hardingham and Fosang, 1995; Iozzo and Murdoch, 1996; Kiani et al., 2002). In summary, initial characterization of CSPG's revealed these molecules to have mainly structural roles, but as in our analogy to responsive architecture above, subsequent studies added biological function to structure.

Responsive architecture relies on elements that can be altered to integrate responses to the environment, and the analogy in the world of PGs would be sulfation of sugars. In both responsive architecture and in PG synthesis and homeostasis, a structure can be manipulated in useful ways to create an additional level of functionality beyond the original scope of the basic unit of support. Sulfation of PGs, or addition of sulfate esters at specific sugars, fits these requirements, since a structural component is modified to give additional functionality (Gallagher, 1989; Hardingham and Fosang, 1992; Hintze et al., 2012; Salbach et al., 2012). Considering these glycosylation and sulfation events, PGs exemplify the importance of post-translational modifications. As we detail below, sulfation modifies both the structural and biological features of PGs. Incorporating this theme of adding function to structure, this review demonstrates the relevance of PGs to normal human biology; couples genetic and biochemical controls of sulfated PG synthesis with the cell secretory and degradation pathways; and highlights emerging genetic and imaging techniques to elucidate further the molecular mechanisms of cartilage PG functions.

2.1.2 Too much of a bad thing: PGs and disease

The importance of PGs to multicellular organisms is revealed by the variety of tissues that are affected in human diseases associated with PG defects: heart, cartilage, bone, liver, kidney, ear, brain, skin, and eye (Ashworth et al., 2006; Borlot et al., 2014; Braunlin et al., 2014; Lampe et al., 2013; Shapiro et al., 2015). Mutations underlying human disease can occur in core proteins or in the many classes of enzyme that regulate their post-translational modification. As outlined in this section, the fact that each class of enzyme in the PG synthesis pathway can be mutated and cause disease raises interesting questions about

genetic redundancy in this pathway and also whether mutant alleles are hypomorphic or null.

Perhaps due to the abundant secretion of PGs by resident cells, skeletal tissues commonly are affected when mutations occur in the PG synthesis pathway. In fact, studies on the molecular genetic bases for human skeletal disease have served as a tremendous resource for learning about the general PG synthesis pathway. Predominant defects in skeletal tissues (i.e., bone or cartilage) characterize mutations to five different PG core proteins (Table 2). Sometimes, mutations to one core protein can underlie many diseases. For example, the core protein Hspg2 (previously called Perlecan) is mutated in two human skeletal diseases: Silverman-Handmaker type dyssegmental dysplasia and type 1 Schwartz-Jampel syndrome (Iwata et al., 2015). As a side note about nomenclature, many of the proteins involved in PG synthesis were identified prior to the age of modern molecular genetics. Therefore, incredible degrees of discrepancy in terminology appear in the literature, when in many cases, authors refer to the same protein or gene. In order to help coordinate the field, terminology here follows accepted names according to the HUGO Gene Nomenclature Committee (genenames.org).

As detailed in the next section, derivatives of many types of sugar (e.g., glucose, xylose) are added to PG core proteins, typically by discrete classes of enzyme. Mutations to each class of these glycosyltransferases cause human skeletal disease (Table 2). Modifiers of these sugars cause skeletal diseases when mutated. For example, mutations to Fam20c, which phosphorylates xylose, cause Raine syndrome, an osteosclerotic (thick bone) disease (Faundes et al., 2014; Kinoshita et al., 2014). Also, enzymes that regulate the sulfation of GAGs cause phenotypes that are predominantly manifested in the skeleton when mutated, including those that add and remove sulfate groups (Khatri and Schipani, 2008). In total, at least twenty different PG core proteins and their post-translational modifiers, when mutated, are known to be associated with defects that are mainly confined to human skeletal tissues (bone or cartilage), and about ten more have skeletal defects that might be secondary to disruptions in craniofacial and digit patterning (Table 2). Furthermore, mutations to proteins that regulate metabolism and intracellular transport of PG precursors (like sugars and sulfur) result in a variety of human diseases typified by skeletal defects (Slc35d1, Mendelian Inheritance in Man (MIM) 610804; Slc26a2, MIM 606718; Papss2, MIM 603005; Cant1 MIM 613165; Impad1 MIM 614010). Therefore, many human PG diseases only affect skeletal tissues, and as a historical fact, much of the understanding of PG synthesis pathway derives from these genetic studies of skeletal diseases.

Table 2.1. Summary of human diseases associated with mutations to genes in the proteoglycan synthesis pathway.

protein	MIM	previous names	disease (MIM)	role in PG synthesis	major class of PG affected	organ(s)/tissue(s) affected
Aggrecan (Acan)	155760	Cspg1; Msk16; Sedk	aggrecan type spondyloepimetaphyseal dysplasia (612813); Kimberley type spondyloepiphyseal dysplasia (608361); osteochondritis dissecans, short stature, and early-onset osteoarthritis (165800)	core protein	CSPG	bone, cartilage
Heparan sulfate proteoglycan of basement membrane 2 (Hspg2)	142461	Perlecan (Plc); Sjs; Sja	Silverman-Handmaker type dyssegmental dysplasia (224410); type 1 Schwartz-Jampel syndrome	core protein	HSPG	bone, cartilage
Proteoglycan 4 (Prg4)	604283	Superficial zone protein (Szp); Lubricin; Megakaryocyte-stimulating factor (Msf); Hemangiopoietin (Hapo); Cacp; Jcap; Dol54	camptodactyly-arthropathy-coxa vara-pericarditis syndrome	core protein	CSPG	cartilage, synovium, heart
Structural maintenance of chromosomes 3 (Smc3)	606062	Chondroitin sulfate proteoglycan 6 (Cspg6); Bamacan (Bam); Human chromosome-associated polypeptide (Hcap); Cdls3; Mmip1	Cornelia de Lange syndrome 3	core protein (but has conserved function in DNA replication/mitosis)	CSPG	bone, cartilage, brain
Fras1-related extracellular matrix protein 1 (Frem1)	608944	Chromosome 9 open reading frame 154 (C9orf154); Bnar; Mota, Tilrr, Trigno2	bifid nose with or without anorectal and renal anomalies (608980); Manitoba oculotrichoanal syndrome (248450); trigonocephaly 2 (614485)	core protein	CSPG	craniofacial, kidney, anus/rectum, genital tract, eye
Fras1-related extracellular matrix protein 2 (Frem2)	608945		Fraser syndrome (219000)	core protein	CSPG	craniofacial, digits, kidney, lung, genital tract, brain
Glypican 3 (Gpc3)	300037	Oci5; Dgsx; Gtr2; Mxr7; Sdys; Sgb	type 1 Simpson-Golabi-Behmel syndrome (312870); Wilms tumor 1	core protein	HSPG	craniofacial, heart, eye, kidney, genital, brain
Glypican 6 (Gpc6)	604404	Omimd1	omodysplasia 1	core protein	HSPG	bone, cartilage, kidney, brain
Xylosyltransferase 1 (Xylt1)	608124	Xt1; UDP-D-xylose: proteoglycan core protein beta-D-xylosyltransferase 1; Dbqd2	Desbuquois dysplasia 2 (615777)	xylosyltransferase (1st sugar in tetrasaccharide linker region)	CSPG?	cartilage, bone, brain
Xylosyltransferase 2 (Xylt2)	608125	Xt2; UDP-D-xylose: proteoglycan core protein beta-D-xylosyltransferase 2; Sos	spondyloocular syndrome (605822)	xylosyltransferase (1st sugar in tetrasaccharide linker region)	CSPG?	bone, eye, brain, heart, craniofacial

Xylosylprotein beta 1,4-galactosyltransferase, polypeptide 7 (B4galt7)	604327	Xgpt1; Xgalt1; Edsp1; Galactosyltransferase 1; UDP-galactose: O-beta-D-xylosylprotein 4-beta-D-galactosyltransferase	progeroid type 1 Ehlers-Danlos syndrome (130070)	galactosyltransferase (2nd sugar in tetrasaccharide linker region)	DSPG?	bone, cartilage, muscle, skin, ectodermal appendages, brain
UDP-gal: beta-gal beta 1,3-galactosyltransferase, polypeptide 6 (B3galt6)	615291	Galactosyltransferase II (GaltII); Beta-1,3-galactosyltransferase 6; Beta-3-galt6; B3gnt1; Bgnt2; Edsp2; Semdjl1	progeroid type 2 Ehlers-Danlos syndrome (615349); type 1 spondyloepimetaphyseal dysplasia with joint laxity, with or without fractures (271640)	galactosyltransferase (3rd sugar in tetrasaccharide linker region)		bone, cartilage, muscle, skin, heart, ligament
Beta-1,3-glucuronyltransferase 3 (B3galt3)	606374	Glucuronylstranferase 1 (Glcat1); GlcUATI; Glct3; Glob; Galt3	multiple joint dislocations, short stature, craniofacial dysmorphism, and congenital heart defects (245600)	glucuronyltransferase (4th sugar in tetrasaccharide linker region)		bone, cartilage, heart, teeth, skin
Exostosin glycosyltransferase 1 (Ext1)	608177	Lgcr; Lgs; Trps2; Ttv; Dext1	chondrosarcoma (215300); type 1 multiple exostoses (133700)	glycosyltransferase (repeating HS disaccharide)	HSPG	cartilage, bone
Exostosin glycosyltransferase 2 (Ext2)	608210	Sotv	type 2 multiple exostoses (133701)	glycosyltransferase (repeating HS disaccharide)	HSPG	cartilage, bone
Exostosin glycosyltransferase 3 (Ext3)	600209	Ext2	type 3 multiple exostoses (600209?)	glycosyltransferase (repeating HS disaccharide)	HSPG	cartilage, bone
Chondroitin sulfate synthase 1 (Chsy1)	608183	Chondroitin synthase 1 (Css1); Carbohydrate synthase 1; KIAA0990; Tbps	Tentamy preaxial brachdactyly syndrome (605282)	galactosyltransferase (repeating CS disaccharide)	CSPG	craniofacial, digits, teeth, brain
Carbohydrate sulfotransferase 14 (Chst14)	608429	Dermatan-4-sulfotransferase 1 (D4st1); N-acetylgalactosamine 4-O sulfotransferase; Atcs; Edsmc1; Hnk1st	type 1 musculocontractural Ehlers-Danlos syndrome (601776)	sulfotransferase (4-O position of dermatan GalNAc)	DSPG	craniofacial, digits, joints, vertebrae, muscle, skin, brain
Carbohydrate sulfotransferase 3 (Chst3)	603799	Chondroitin 6-sulfotransferase (C6st); Hsd; Gst0	spondyloepiphyseal dysplasia with congenital joint dislocations (143095)	sulfotransferase (6-O position of chondroitin GalNAc)	CSPG	bone, joints, heart
Galactosamine-6-sulfate sulfatase (Galns)	612222	N-acetylgalactosamine-sulfate-sulfatase; Mps4a; Gas; Galnac6s; Galn6s	type IVa mucopolysaccharidosis (253000)	sulfatase (6-O position of GalNac)	CSPG	bone, teeth, eye
Arylsulfatase b (Arsb)	611542	G4s; Mps6; As1	type VI mucopolysaccharidosis (253200)	sulfatase (4-O position of GalNAc)	CSPG	bone, liver, spleen, joints, eye, heart, craniofacial
Arylsulfatase e (Arse)	300180	Cdpx	X-linked recessive chondrodysplasia punctata 1 (302950)	sulfatase		craniofacial, digits

Iduronate 2-sulfatase (Ids)	300823	Mps2; Sids	type II mucopolysaccharidosis (309900)	sulfatase		brain, nerves, craniofacial, heart
Beta-galactosamine 1 (Glb1)	611458	Elastin-binding protein (Ebp); S-Gal; Elastin receptor 1	type IVb mucopolysaccharidosis (253010); types I, II, and III GM1 gangliosidoses (230500, 230600, and 230650, respectively)	glycosidase	CSPG	nerves, liver, spleen, craniofacial, bone, eye
Beta-glucuronidase (Gusb)	611459		type VII mucopolysaccharidosis (253220)	glycosidase		brain, craniofacial, liver
Family with sequence similarity 20, member c (Fam20c)	611061	Dentin matrix protein 4 (Dmp4)	Raine syndrome (259775)	kinase		bone
Dermatan sulfate epimerase (Dse)	605942	Squamous cell carcinoma antigen recognized by T cells 2 (Sart2)	type 2 musculocontractural Ehlers-Danlos syndrome (615539)	sugar epimerase	DSPG	joints, skin, muscle, craniofacial

Other PG diseases in human specifically affect the eye and the brain, both of which are PG-rich (Ashworth et al., 2006; Avram et al., 2014; Shapiro et al., 2015). Mutations in the core proteins Versican, Decorin, Impg1, Impg2, Keratocan, and Nyctalopin (MIMs 118661, 125255, 602870, 607056, 603288, and 300278) respectively cause eye defects in Wagner vitreoretinopathy, congenital stromal corneal dystrophy, vitelliform macular dystrophy 4 and 5, retinitis pigmentosa 56, cornea plana 2, and type 1A congenital stationary night blindness. Eye defects in macular corneal dystrophy types 1 and 2 are associated with mutations in the PG posttranslational modifier Chst6 (MIM 605294). PG diseases that affect the brain include congenital myasthenic syndrome 8, autosomal recessive mental retardation 46, mucopolysaccharidosis (MPS) types IIId and IIIa, and multiple sulfatase deficiency; these diseases are associated with respective mutations in the PG pathway members Agrin, Ndst1, Gns, Sgsh, and Sumf1 (MIMs 103320, 600853, 607664, 605270, and 607939).

Since cartilage contains massive amounts of a class of PGs called chondroitin sulfate PGs (CSPGs), mutations to proteins involved in CSPG synthesis or modification often affect cartilage (and associated bone). The abundant cartilage core protein Aggrecan alone, for example, is mutated in three discrete cartilage diseases: Aggrecan-type spondyloepimetaphyseal dysplasia, Kimberley type spondyloepiphyseal dysplasia, and osteochondritis dissecans, short stature, and early-onset osteoarthritis (Lauing et al., 2014; Stattin et al., 2010). The CSPG posttranslational modifiers Galns, Glb1, and Arsb cause skeletal defects in MPS IVa, IVb, and VI when mutated (Table 2.1). The MPSs are a family of disorders that are linked to the breakdown of PGs, and they interfere with normal skeletal development (Lampe et al., 2013; Muenzer, 2011). For instance, MPS IV and VI are progressive diseases that cause major stunting of the skeleton and abnormal bone shape (Montano et al., 2007; Valayannopoulos et al., 2010). In addition to MPS IVb, mutations to Glb1 also cause types 1, 2, and 3 GM1 gangliosidoses, which are characterized by skeletal defects (Table 2.1).

Affecting about 50% of people over 60 years of age, osteoarthritis is a complex disease that is often characterized by loss of sulfated PGs in articular cartilage, leading some to suggest that mutations to PG-related genes might be causative. Indeed, *Chst11*, *Xylt1*, *Xylt2*, and *Aspn*, have been associated with osteoarthritis in genome-wide association and functional studies (arc et al., 2012; Schon et al., 2006; Valdes et al., 2007), but most of the statistical support for these and other genes is rather weak. The fact that osteoarthritis is a late-onset disease might be explained by two genetic hypotheses, which are not mutually exclusive. First, a large combination of genes might predispose to osteoarthritis, but the disease state only manifests after several decades of poor combined gene activity. Second, age-related epigenetic changes in chondrocytes might cause certain alleles to lose the ability to maintain articular cartilage homeostasis. Two recent large cohort studies, the Rotterdam study and stage 1 of the arcOGEN study did not find support for the polygenic hypothesis (reviewed in (Reynard and Loughlin, 2012). Therefore, future experiments are needed to test alternative hypotheses for the genetic causes of osteoarthritis.

Two final considerations of the genetic basis of PG diseases need mention: genetic redundancy and hypomorphic alleles. Most components of the PG synthesis pathway appear to demonstrate some degree of genetic redundancy, so it is interesting that mutations to only one gene can cause disease (Table 2.1). The fact that most PG diseases specifically affect tissues, such as cartilage, bone, eye, and brain, with abundant PGs suggests that the levels of PG synthesis in a given tissue dictate that tissue's susceptibility to disease when PG enzymes are mutated. From the other perspective, mutation to a single PG synthesis gene appears to be tolerated by many cells in the body. Another genetic issue related to levels of PG production is hypomorphism, which is to say that mutations associated with PG disease might not be null alleles, or complete losses of protein function. In fact, a few studies have shown residual enzyme activity in alleles of PG genes known to cause human disease (Baasanjav et al., 2011; Cortes et al., 2009; Dennis et al., 2009). The relatively minor decrease in overall levels of PG production observed in human disease likely reflects embryonic lethality in the case of complete loss of the PG synthetic pathway, but genetic experiments in animal models, such as zebrafish, could shed light on these open questions.

2.1.3 Pas de deux: Biochemistry and cell biology of PG synthesis

The array of enzymes that modify core proteins during PG synthesis is staggering, but this section highlights some interesting tricks that seem to have evolved to facilitate quality control. First, protein-protein interactions among enzymes are critical. For instance, the formation of multi-enzyme complexes is thought to allow the core protein to be modified sequentially, similar to an assembly line (Izumikawa et al., 2008; Mikami and Kitagawa, 2013). Also, later modifications appear to be coordinated through enzyme cooperativity (Izumikawa et al., 2007; Kitagawa et al., 2003; Kitagawa et al., 2001). Second, different stages of core protein post-translational modifications are confined to discrete cellular compartments. For example, the first sugars are added in the endoplasmic reticulum (ER) and cis Golgi, the next set of sugars are added in the trans Golgi, and sulfation of these sugars happens in the trans Golgi and perhaps even further in secretory vesicles (Fig. 2.1;

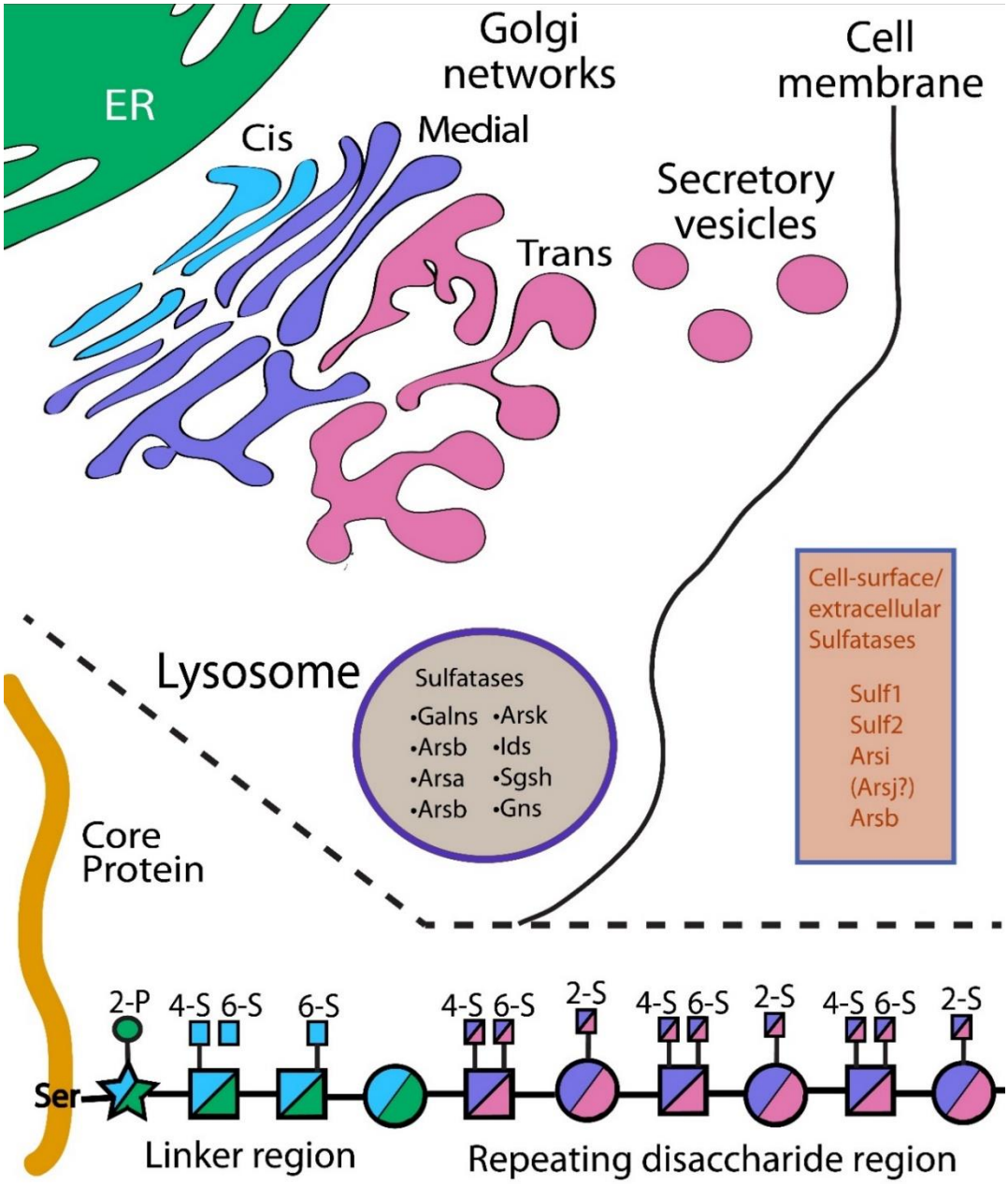

Figure 2.1 The cell biology of sulfated PG synthesis and degradation.

Below dashed line: schematized linker region of a CSPG showing specific sugars and post-translational modifications (while all possibilities of sulfation are shown, typically only certain sugars are sulfated at a given time). Above dashed line: CSPG components are color-coded with the schematic diagram to illustrate where each post-translational modification of the PG core protein occurs in the cell. In the linker region, most sugars and their modifications are added in the ER and cis Golgi. In the repeating disaccharide region, most sugars and their modifications are added in the medial and trans Golgi and secretory vesicles. Most sulfatases act on sulfated CSPGs in the lysosome during degradation, but some cell-surface/extracellular CSPG sulfatase activity may occur. Abbreviations: ER=endoplasmic reticulum; Gal=galactose; GalNAc=N- acetylgalactosamine; GlcA=glucuronic acid; Ser=serine residue on core protein; Xyl=xylose; 2-P=phosphorylation at 2-position of sugar ring; 2-S=sulfation at 2-position of sugar ring; 4-S=sulfation at 4-position of sugar ring; 6-S=sulfation at 6-position of sugar ring.

(Calabro and Hascall, 1994; Doms et al., 1989; Fransson et al., 1992; Klausner et al., 1992; Lippincott-Schwartz et al., 1989; Spiro et al., 1991; Sugumaran et al., 1992; Uhlin-Hansen and Yanagishita, 1993; Yanagishita, 1993b). These latter studies suggest the interesting hypothesis that the genetics of PG synthesis might be linked with cell secretion pathways. Skeletal cells are prime candidates for elucidating such a relationship, given the massive amounts of PG synthesis inherent in their differentiation. However, only a few reports have addressed the importance of components of the secretory pathway on skeletal tissue formation (Knapik et al., 2014; Lang et al., 2006; Melville et al., 2011; Sarmah et al., 2010; Unlu et al., 2014), so this is a critical area of future research. Finally, studies of human disease implicate PG sulfation with another cell biological process: lysosomal degradation (Diez-Roux and Ballabio, 2005; Khatri and Schipani, 2008). Therefore, PG synthesis may interact genetically with many basic cell biology pathways. To aid in these future studies, we correlate in this section the biochemistry of PG synthesis with cell biology, concluding with an explanation of why some PG defects have dramatic effects on cell biology.

2.1.4 Xylose: Where the "proteo-" meets the "-glycan"

PG synthesis occurs in many ordered steps, beginning with core protein translation and translocation via its signal sequence to the ER (Vertel et al., 1993). Once in this cellular compartment, core proteins becoming CSPGs or HSPGs have the first sugar, xylose (Xyl), added to a specific serine (Ser) residue within a core protein consensus sequence, although this can also occur in vesicles near the ER and in the early Golgi compartments (Fig. 2.1; (Kearns et al., 1993; Vertel et al., 1993). Then, the nascent PG is shuttled to the cis Golgi network, where three more sugars are added, initiating the GAG sidechain of CS or HS with a typical O-linked tetrasaccharide linker region (Kearns et al., 1991; Kearns et al., 1993; Vertel et al., 1993). Specifically, two galactose (Gal; not galactosamine) and one glucuronic acid (GlcA) residues are added to yield Ser-O-Xylβ1(1→4)Galβ(1→3)Galβ(1→3)GlcAβ, where 1→3 or 1→4 represents the carbon positions on the sugar involved in the glycosidic bond (Fig. 2.1). The addition of each monosaccharide is catalyzed by a particular glycosyltransferase, starting with the Xyl addition by a Xylosyltranferase (Xylt), followed by two Gal additions by a β1, 4-Galactosyltransferase I (B4galt) and a β1, 3-Galactosyltransferase II (B3galt), respectively, and finally GlcA addition by a β1,3-Glucuronyltransferase I (B3gat) (Mikami and Kitagawa, 2013). The efficiency of this process is thought to be increased by the formation of these linker region glycosyltransferases into a large, multi-enzyme complex, where each enzyme transfers its sugar, and then passes the substrate to an adjacent glycosyltransferase (Izumikawa et al., 2008; Mikami and Kitagawa, 2013). Even though CS and HS share the same tetrasaccharide linker region, they subsequently differ in the addition of a fifth residue: GalNAc or GlcNAc, respectively (Prydz, 2015; Sugumaran et al., 1992). In this way, the class of PG is determined before it moves beyond the cis-Golgi network.

The spatiotemporal sequence of events during PG linker region synthesis was visualized by electron microscopy and functionally confirmed using a compound called brefeldin A (BFA; reviewed in (Prydz and Dalen, 2000). For example, initial debate over whether PG xylosylation occurred in the rough ER or Golgi resulted from different interpretation of subcellular fractionation studies of cartilage cells (Geetha-Habib et al., 1984; Hoffmann et al., 1984). A well-designed experiment combining autoradiography, electron microscopy, subcellular fractionation, and immunohistochemical staining showed exactly where xylosylation was taking place (Kearns et al., 1993; Vertel et al., 1993). Typical of biology, the results supported a combination of the two initial hypotheses. Xylosylation occurred in the rough ER, but it also happened in transport vesicles near the nuclear membrane, as well as in early Golgi compartments. Functional confirmation of these results came from a technique involving BFA, which interferes with anterograde fusion of Golgi vesicles, causing accumulation of products from the cis and medial Golgi into the ER, whereas trans Golgi products remain separated (Doms et al., 1989; Klausner et al., 1992; Lippincott-Schwartz et al., 1989). BFA experiments confirmed that PG xylosylation did not happen in the trans Golgi (Calabro and Hascall, 1994; Doms et al., 1989; Fransson et al., 1992; Klausner et al., 1992; Lippincott-Schwartz et al., 1989; Spiro et al., 1991; Sugumaran et al., 1992; Uhlin-Hansen and Yanagishita, 1993). Similar experiments revealed the regulation of PG sugar addition in discrete compartments of the cell secretory pathway (Fig. 2.1; (Campbell and Schwartz, 1988; Geetha-Habib et al., 1984; Kimura and Ichihara, 1994; Lohmander et al., 1986; Ratcliffe et al., 1985; Sugumaran and Silbert, 1991; Vertel and Barkman, 1984; Vertel and Hitti, 1987).

The precursors utilized by PG glycosyltransferases are actually nucleotide (specifically uridine diphosphate, or UDP) sugars, all derived from UDP-glucose (Lennarz, 1980; Neufeld et al., 1958). For example, Ugdh converts UDP-glucose to UDP-glucuronic acid, which is converted to UDP-xylose by Uxs1 (Oka and Jigami, 2006). High levels of UDP-xylose can inhibit its own conversion, thus limiting itself in a negative feedback loop (Schwartz, 2000). Regulating the import of nucleotide sugars into Golgi vesicles is another control mechanism that links the rate of PG synthesis to resource availability. For instance, UDP-galactose is epimerized from UDP-glucose by Gale in the cytosol (Roper et al., 2005), and then specific UDP-galactose transport proteins regulate levels of UDP-galactose in the Golgi apparatus, thus limiting their availability for synthesis of the PG linker region (Toma et al., 1996). As might be expected, many components of this basic arm of the PG synthesis pathway are highly conserved from eukaryotes to prokaryotes (Eames et al., 2010).

In addition to limited UDP-sugar availability, linker tetrasaccharide synthesis is regulated by phosphorylation of serine-linked Xyl in the nascent GAG sidechain, which is carried out by the kinase Fam20b (Fig. 2.1; (Koike et al., 2009)). While this 2-*O*-phosphorylation is required for efficient addition of the next two linker sugars by B4galt7 and B3galnt6, respectively, rapid dephosphorylation of Xyl occurs after GlcA addition (Moses et al., 1997). Recently, the relevant phosphatase was identified (Koike et al., 2014). Untimely Xyl dephosphorylation can signal Extl2 to cap the linker region with an α-1, 4 GalNAc residue, which acts as a negative regulator since this capped pentasaccharide is no longer

able to serve as an acceptor for GAG biosynthesis (Mikami and Kitagawa, 2013). These data demonstrate that phosphorylation of Xyl is critical in ensuring an adequate number of tetrasaccharide primers are available during CS or HS synthesis, otherwise defective PG synthesis occurs (Eames et al., 2011; Wen et al., 2014).

Sulfation of linker sugars is the other important modification that regulates PG linker region synthesis. Sulfation of Gal residues in the linker region can actually determine whether the GAG sidechain is CS or HS. HS never has sulfur modifications of these linker sugars, while CS and DS are commonly sulfated at one or both Gal residues (Laremore et al., 2007). These observations are more than a coincidence, since sulfation at the 6 position of the first galactose (Gal1) greatly increases activity of enzymes that initiate the repeating GAG region, while 4,6-disulfation of Gal2 or 4-sulfation of Gal1 can completely inhibit this activity (Gulberti et al., 2005). However, a later study by the same group showed that sulfation in the linker region only had positive effects on the activity of subsequent glycosyltansferases (Gulberti et al., 2012). Therefore, the exact role of sulfation in the linker region is unclear, but the sulfation of Gal residues in the linker region can influence subsequent glycosyltransferase activity, even specifying the type of GAG chain produced.

2.1.5 Adding sugar like a kid after Halloween

After establishment of the tetrasaccharide linker region, the repeating disaccharides that are characteristic of the HS and CS GAG sidechains are added by specific glycosyltransferases in the cis, medial, and trans Golgi compartments, respectively (Fig. 2.1; (Dick et al., 2012). The repeating disaccharide of HS is added by Exostosins, mutations of which cause multiple hereditary exostoses (Kobayashi et al., 2000; Wuyts et al., 1998). Since their activities and regulation have been reviewed extensively (e.g., (Bernfield et al., 1999; Esko and Lindahl, 2001; Lin, 2004; Tumova et al., 2000; Turnbull et al., 2001), we focus on control of repeating disaccharide addition in CSPGs.

Six known glycosyltransferases catalyze synthesis of the repeating CS disaccharide (-GlcA-GalNAc-), the length of which is regulated by cooperativity among some of these enzymes. Initial characterizations of their *in vitro* activity designated these six as the Chondroitin sulfate synthases Chsy1 (formerly called Chsy, Css1, or Tpbs) and Chsy3 (formerly called Chsy2 or Css3); the Chondroitin polymerizing factors Chpf (formerly called Chsy2 or Css2) and Chpf2 (formerly called Csglcat or Chsy3); and the Chondroitin sulfate GalNAc transferases Csgalnact1 (formerly called Chgn or Beta4galnact) and Csgalnact2 (formerly called Chgn2 or Galnact2; (Mikami and Kitagawa, 2013). The first four of these enzymes can catalyze both glycosyltransferase activities needed to synthesize a growing CS GAG. The ability of each of these enzymes alone to add GalNAc to the repeating disaccharide is very limited, but it increases dramatically when any two of these enzymes are co-expressed (Izumikawa et al., 2008; Kitagawa et al., 2003; Yada et al., 2003). Therefore, cooperativity among these enzymes regulates CS chain elongation. Csgalnact1 and Csgalnact2, on the other hand, each can transfer GalNAc residues

efficiently to the linker and repeating disaccharide regions of the growing CS GAG when acting alone (Gotoh et al., 2002; Sato et al., 2003). Due to these independent activities, these enzymes are critical for initiating GAG sidechain growth, as well as determining the ultimate chain length (Mikami and Kitagawa, 2013; Uyama et al., 2002). In an experimental model of atherosclerosis, for example, CSPGs with unusually long chain length in the aorta were associated with increased Csgalnact2 expression (Anggraeni et al., 2011).

The number of CS GAGs attached to a core protein is another variable that seems to be regulated by glycosyltransferases. Loss of Csgalnact1 leads to a reduction in how many CS chains are produced (Ishimaru et al., 2014; Sato et al., 2011; Watanabe et al., 2010). Conversely, over-expression of Csgalnact1 in chondrosarcomas creates large CSPG aggregates with greater than the normal number of CS chains (Sakai et al., 2007). Thus, Csgalnact1 seems to control somehow the initiation of GAG synthesis based on the number of other CS chains attached to that particular core protein (Mikami and Kitagawa, 2013). The mechanism by which this occurs remains the subject of future research.

2.1.6 Don't be a quitter: Post-translational modifications of post-translational modifications

Similar to regulation of the linker region, sulfation of specific atoms on sugar residues is another major mechanism of control for GAG elongation efficiency, chain length, and chain number during PG synthesis. Addition of these sulfate groups occurs in the medial and trans Golgi (Fig. 2.1; (Sugumaran et al., 1992)). Three positions on the repeating disaccharide of CSPGs can be sulfated in various combinations: the 4 and 6 positions of GalNAc and the 2 position of GlcA (technically uronic acid). The repeating disaccharides of HSPGs also can be sulfated on the 2 position of GlcA, in addition to the 3 and 6 positions of GlcNAc (Bowman and Bertozzi, 1999; Mikami and Kitagawa, 2013). We focus our discussion on the 4 and 6 sulfation of GalNAc, since they are more CSPG-specific, and HSPG sulfation has received more attention in the literature (e.g., reviewed in (Bernfield et al., 1999; Esko and Lindahl, 2001; Lin, 2004; Tumova et al., 2000; Turnbull et al., 2001). Historically, classes of chondroitin sulfate that corresponded to these sulfation patterns were isolated using fractionation, and the naming convention has changed only slightly since (Levene and La Forge, 1913). Chondroitin sulfate A refers to chondroitin-4-sulfate; Chondroitin sulfate B is no longer used because it referred to dermatan sulfate; Chondroitin sulfate C refers to chondroitin-6-sulfate; Chondroitin sulfate D refers to chondroitin-2,6-sulfate; and Chondroitin sulfate E refers to chondroitin-4,6-sulfate.

Also similar to the linker region, enzyme cooperativity serves as an important regulatory control for the sulfation of CSPGs. Three different sulfotransferases catalyze sulfation of the 4 position of GalNAc in CSPG GAGs: Carbohydrate (chondroitin 4) sulfotransferases Chst11 (formerly called C4st1), Chst12 (formerly called C4st2 or C4s2), and Chst13

(formerly called C4st3; (Hiraoka et al., 2000; Kang et al., 2002; Yamauchi et al., 2000). Chst9 (formerly called Galnac4st2) also can perform this function (Kang et al., 2001), but it has not been studied extensively with respect to CSPG synthesis. Chst11 appears to be the major sulfotransferase involved in CSPG synthesis (Hiraoka et al., 2000; Kang et al., 2002; Mizumoto et al., 2009; Uyama et al., 2006; Yamauchi et al., 2000), because loss of Chst11 cannot be compensated for by over-expression of Chst12 or Chst13 (Hiraoka et al., 2000; Kang et al., 2002; Mizumoto et al., 2009; Uyama et al., 2006; Yamauchi et al., 2000). 4-sulfated GalNAc residues on the growing end of each CS chain are required for chain elongation, but these chains are only extended efficiently when catalyzed by Chst11, not Chst12 (Izumikawa et al., 2011). These and similar data suggested that a given sulfotransferase may have specific physical interactions with glycosyltransferases, an idea supported by many studies (Izumikawa et al., 2012; Schonherr et al., 1999). For example, Csgalnact2 over-expression increased the amount of CS produced in a manner that depended on Chst11, but not Chst12 (Izumikawa et al., 2011). Increased expression of both Chst11 and Csgalnact2 were observed in an experimental model of elevated CSPG production (Anggraeni et al., 2011). The fact that Csgalnact2 cannot catalyze GlcA addition in the repeating CS disaccharide indicates that the influence of Csgalnact2 and Chst11 on chain length determination must happen by enhancing chain elongation efficiency by other glycosyltransferases, such as Chsy1 or Chpf (Anggraeni et al., 2011). Techniques to visualize the organization of these enzymes *in vivo* would add tremendously to understanding how this complex process is spatially coordinated.

A proposed difference between CSPGs of humans and other vertebrates relates to the exact position of GalNAc where the majority of sulfation occurs: the 6 position in humans versus the 4 position in all other vertebrates (Vynios, 2014). At least two sulfotransferases (Chst3, Chst4) can catalyze addition of a sulfate group to the 6 position of GalNAc in CSPGs, but the most relevant appears to be Chst3 (formerly called C6st1; (Uchimura et al., 2002; Yamauchi et al., 2000). Differing levels of 6-sulfated GalNAc among vertebrates may explain differing phenotypes when Chst3 is mutated. Humans with loss-of-function mutations in *Chst3* can have severe chondrodysplasia (Table 2.1; (Thiele et al., 2004)) *Chst3* loss-of-function mice, however, show no overt phenotype, aside from lower levels of excreted 4-sulfated GalNAc (and lower levels of naïve T-lymphocytes; (Uchimura et al., 2002). This specific example may reflect broader evolutionary trends, where clade-specific GAG sulfation patterns can be selected, providing a robust set of molecules fine-tuned for different purposes (Sugiura et al., 2012).

The end of CSPG GAGs is marked by two characteristic sulfation events: 4,6-disulfated GalNAc and 2-sulfated uronic acid (GlcA) residues (Ohtake et al., 2005). Chst15 (previously called Brag or Galnac4s-6st) catalyzes 6-sulfation of a 4-sulfated GalNAc, and Ust (previously called 2ost) sulfates the 2-position of GlcA (Ohtake et al., 2001; Ohtake et al., 2005). These marks are not actually unique to the non-reducing end of the CS GAG, since they are also found in the internal disaccharides, but they seem to be enriched in the last disaccharide. Disulfated GalNAc residues are greater than 60 times more abundant at the non-reducing end of some (but not all) CS chains (Midura et al., 1995). 2-sulfation at the end of CS chains is found nested within the sequence GalNAc(4,6-S)-GlcA(2S)-

GalNAc(6S; (Kobayashi et al., 1999; Ohtake et al., 2005). Providing another example of the complex regulatory cascades governing PG synthesis, 2-sulfation greatly enhances the activity of Chst15, implying that 2-sulfation of uronic acid happens before the adjacent residue becomes di-sulfated (Ohtake et al., 2003).

2.1.7 Break it down for me, fellas

PG sulfation is an on-again, off-again affair, with sulfatases removing sulfate groups added by sulfotransferases. Based on sequence identity, there are at least seventeen human sulfatases, although two of these enzymes currently have undefined biochemical activities (i.e., Arsi, and Arsj) (Sardiello et al., 2005). Cellular localization of these sulfatases varies widely, which suggests differing substrates and functions. Many sulfatases are found predominantly in lysosomes and participate in the molecular degradation pathway (Arsa, Arsb, Arsg, Arsk, Ids, Sgsh, Gns, and Galns), while others are detected mainly in the Golgi (Arse), in the ER (Arsc, Arsd, Arsf, Arsi, and Arsj), or on the cell surface (Sulf1, Sulf2; (Diez-Roux and Ballabio, 2005; Wiegmann et al., 2013)). The two general classes, lysosomal and non-lysosomal, reflect the optimal activity of each enzyme at low or neutral pH, respectively (Diez-Roux and Ballabio, 2005). Each sulfatase demonstrates a surprising specificity for substrate recognition, and seven sulfatases are known to target sulfated GAGs (Ratzka et al., 2010). A given PG sulfatase is thought to remove sulfate groups from not only a specific sugar within a GAG chain, but a specific position on that sugar. For example, Gns is a sulfatase that removes sulfate from the 6 position of GlcNAc in HS (Rivera-Colon et al., 2012). The two known CS-specific sulfatases are Galns and Arsb, which remove sulfate groups from 4- and 6-sulfated GalNAc, respectively (Diez-Roux and Ballabio, 2005).

Due to the association of sulfatases and MPS diseases (Table 2.1), the major cell biological role for these enzymes thus far is PG degradation. The MPSs are a family of disorders that are all linked to the breakdown of the GAG chains of PGs. MPS types IV and VI are caused by mutations to the CS-specific sulfatases Galns and Arsb, respectively (Morrone et al., 2014; Tomatsu et al., 2005; Valayannopoulos et al., 2010). These diseases have major effects on cartilage-mediated skeletal growth, but they are characterized more generally as lysosomal storage diseases (Montano et al., 2007; Valayannopoulos et al., 2010). Sulfation of PGs may add a new layer of functionality, but it turns out that PG sulfation inhibits their degradation (Freeze, 2009). Careful study of sulfatase deficiencies, such as in MPS disorders, revealed that an inability to desulfate PGs leads to a block of autophagy and an inability to regulate PG levels (Opoka-Winiarska et al., 2013; Settembre et al., 2008).

Surely, the presence of Galns and Arsb in lysosomes suggests their role in CS catabolism, but surprisingly little is known about this process (Mikami and Kitagawa, 2013). Recycling of CSPG-rich matrix is thought to occur constantly in growth plate chondrocytes through the process of microautophagy (Settembre et al., 2008). In the current model, CS chains

are endocytosed in autophagosomes, which fuse with lysosomes, where at least three sets of enzymes break down the GAGs, releasing monosaccharides for recycling (Yamada, 2015). Endoglycosidases break down the repeating disaccharide chains into oligosaccharides of approximately 10 kDa, which are then cleaved into monosaccharides by exoglycosidases (Freeze, 2009; Prabhakar and Sasisekharan, 2006; Yamada, 2015). The sulfatases Arsb and Galns cooperate in this latter process, since exoglycosidases do not function well unless the terminal hydroxyl groups on oligosaccharides are unmodified by acetate, phosphate, or sulfate groups (Freeze, 2009). Interestingly, CS is passed in normal human urine largely intact, implying that a baseline level of excretion occurs that bypasses the energetically expensive breakdown of potentially recyclable chains (Lennarz, 1980).

While the specific lysosomal exoglycosidases responsible for CS metabolism in humans have been understood for some time, the corresponding endoglycosidases have only been identified recently. Along with β-glucuronidase, Hexosaminidase A and B (HexA and HexB) carry out exoglycosidase activity on CS chains (Yamada, 2015). More recently, a long-appreciated family of endoglyosidases have emerged as major CS degradation enzymes. Despite their name, Hyaluronidases, including Hyal1, Hyal4, and Spam1 (a testicular hyaluronidase), actually show a greater hydrolytic activity towards CS than to HA (Mikami and Kitagawa, 2013; Yamada, 2015).

Estimates of cartilage CSPG catabolism rates suggest the possibility of extracellular sulfatase activity, which is an interesting topic of future research. ^{35}S labelling indicated that the average CS turnover rate is approximately sixteen days in adult rat costal cartilage (Bostrom, 1952). Regarding the main cartilage CSPG core protein, Aggrecan in human articular cartilage was estimated from amino acid racemization rates to have a half-life of about three years, although smaller Aggrecan fragments may persist for about twenty years (Maroudas et al., 1998). If GAG sidechains are turned over much more quickly than the core protein for cartilage CSPGs, then are there extracellular CS sulfatase and glycosidase activities? A few studies suggest that this might be a fruitful avenue of cartilage research. Some cells in the liver express the “lysosomal” CS sulfatase Arsb on their cell surface (Mitsunaga-Nakatsubo et al., 2009). Also, lysosomal enzymes are secreted and circulate through the bloodstream and may participate in catabolism after being endocytosed (Elvevold et al., 2008; Natowicz et al., 1979). The notion of extracellular CS breakdown would be analogous to demonstrated roles of sulfatases and glycosidases that catabolize HS and HA (Esko and Selleck, 2002; Hacker et al., 2005; Harada et al., 2009).

Other key enzymes play a role in CS catabolism. An Aggrecan core protein with attached CS chains is too large to undergo endocytosis intact, so some degradation is thought to be required extracellularly (Vynios, 2014). Three classes of proteolytic enzymes in the extracellular matrix, including Matrix metalloproteinases (Mmp’s), A disintegrin and metalloproteinase with thrombospondin motifs (Adamts’s), and Calpains, can cleave Aggrecan, and thus are key regulators of CSPG turnover rates (Struglics and Hansson, 2010; Troeberg and Nagase, 2012). Of course, the complexity of CSPG catabolism is considerable, so these positive regulators of cartilage PG turnover are counteracted by negative regulators. For example, a family of proteins called Tissue inhibitors of

metalloproteinases (Timp's) can reduce both Mmp and Adamts activity in cartilage matrix (Vynios, 2014). The fragmented Aggrecan chains are internalized by the cell and directed to the lysosome for further proteolysis by Cathepsins, in addition to the degradation and recycling of GAG chains.

2.1.8 Adding function to structure by understanding PG-loss animal models

Our vertebrate cousin, the zebrafish, shares a remarkable conservation of gene function with humans. An example from skeletal studies is that mutations to the transcription factor Sox9 disrupt the ability to form cartilage in both zebrafish and human (Yan et al., 2002). As we discuss below, mutations to the PG synthesis enzyme Xylt1 were described first in zebrafish, and the exact same skeletal phenotype was published subsequently in the *Xylt1*$^{-}$ mouse (Eames et al., 2011; McCoy et al., 2012; Mis et al., 2014). In fact, innumerable studies over the past 20 years have supported zebrafish as a model for human development and disease (Ali et al., 2011; Zon, 1999), so here we discuss animal models of PG defects, focusing on the zebrafish. In particular, these studies illuminate an emerging hypothesis that, similar to HSPGs, CSPGs play a non-structural, biological role in growth factor (GF) signalling. This section highlights the powerful genetics and imaging capabilities of zebrafish in order to address the role of PGs in modulating GF signalling in developing skeletal tissues.

2.1.9 The old PG: Just another blockhead

PGs were characterized traditionally as passive, structural molecules, but work over the past 20 years has modified that notion tremendously. The structural role for PGs is exemplified best by the cartilage core protein, Aggrecan. Aggrecan self-assembles into large aggregate structures with the high-mass polysaccharide hyaluronic acid (aka hyaluronan) via link proteins (Hardingham and Fosang, 1995; Kiani et al., 2002). Hyaluronic acid, a repeating disaccharide of glucuronic acid and N-acetylglucosamine, is not a PG, since it has no core protein, making it unique amongst the secreted polysaccharides (Khatri and Schipani, 2008; Laurent and Fraser, 1992). Hyaluronic acid alone can have a mass as large as 20,000,000 Daltons, a sturdy substrate that can be bulked massively when linked with over one hundred Aggrecan molecules, each capable of being decorated with up to 100 CS and 60 KS chains (Kiani et al., 2002). This is where the "bottle-brush" metaphor for the structure of PGs comes from.

Sulfation of PG sugars leads to the structural function of PGs. The amount of PG sulfation is thought to be directly proportional to how much water it absorbs, which imparts cartilage matrix with its characteristic compressive-resistant strength (Chahine et al., 2005). In addition, hydration of Aggrecan aggregates creates the gel-like environment typical of

cartilage, an amazing evolutionary feat that currently cannot be mimicked by modern engineering, since it gives articular cartilage a lower coefficient of friction than Teflon (Gupta et al., 1985). Recent work indicates that PG sulfation also regulates a non-structural, biological role for PGs, but first we review a series of genetic studies leading to this concept.

2.1.10 PGs regulate the timing of skeletal development

A biological role for sulfated PGs in skeletal development was suggested by a few different animal models. For example, we isolated and analyzed zebrafish mutants that were defective in cartilage and bone development from an ENU mutagenesis screen (Eames et al., 2011; Miller et al., 2007). A class of mutants appeared to have decreased Alcian blue staining of PGs in their cartilage matrix, which consists predominantly of CSPGs (Eames et al., 2010). Using RAD-mapping, then meiotic mapping and sequencing, mutations were identified in two genes, *xylt1* and *fam20b* (Eames et al., 2011; Miller et al., 2007). Xylt1 had been known from biochemical studies of the 1970s to initiate GAG sidechain additions to PG core proteins (reviewed above; (Schwartz, 1977), but no vertebrate models of Xylt1 loss had been reported, so its *in vivo* role remained unproven.

The function of Fam20b was completely unknown, but a poster presentation of our genetic findings suggesting that Fam20b was involved in PG synthesis led to its biochemical characterization (Eames et al., 2008). The ortholog of Fam20b in the *Drosophila* fruit fly, Four-jointed, is a kinase that phosphorylates the cadherin domains of planar cell polarity proteins (Ishikawa et al., 2008; Matis and Axelrod, 2013). Pioneering work by the Kitagawa lab showed that Fam20b also functioned as a kinase, phosphorylating xylose in the nascent GAG sidechain (Koike et al., 2009). Although Fam20 members might phosphorylate the amino acids of proteins directly (Tagliabracci et al., 2014), the combination of these findings raises the question of whether Fam20 kinases only phosphorylate xylosylated proteins. Indeed, another major player in the planar cell polarity pathway, Notch, is known to be xylosylated (Bakker et al., 2009; Lee et al., 2013). Considering these cumulative data placing Xylt1 and Fam20b in the PG synthesis pathway, quantitative biochemical analyses of *xylt1* and *fam20b* mutant embryos confirmed that they had defects in PG synthesis (Eames et al., 2011).

Analyses of zebrafish *xylt1* and *fam20b* mutants revealed that PGs affect the timing of skeletal development. Specifically, cartilage PGs inhibit endochondral ossification, a process of bone formation involving a cartilage template that is subsequently replaced (Eames et al., 2003). A biological role for cartilage PGs was suggested by the fact that bone formation increased in the mutant perichondrium, the tissue layer surrounding the defective cartilage (Eames et al., 2011). The amount of perichondral bone observed in mutants appeared in the same location at later stages in wild types, prompting the idea that mutant bone formation was precocious. Leading to the hypothesis that PGs regulate the timing of endochondral ossification, mutants initiated perichondral bone and expressed molecular

markers of osteoblasts, or bone-forming cells, prior to wild-type siblings (Eames et al., 2011). An important question remained: How do cartilage PG defects cause early perichondral bone formation?

The key linking defects in cartilage PGs to adjacent bone formation is the known communication between chondrocytes and surrounding cells of the perichondrium during endochondral ossification. As wild-type chondrocytes undergo maturation, they signal to induce cells of the adjacent perichondrium to form bone (Eames et al., 2003; St-Jacques et al., 1999). Could decreased levels of cartilage PGs somehow cause early chondrocyte maturation and expression of perichondral bone-inducing genes? The transcription factors Sox9 and Runx2 are negative and positive regulators, respectively, of chondrocyte maturation (Eames et al., 2003; Eames et al., 2004). Indeed, expression of *sox9a* was decreased and *runx2* transcripts increased in *xylt1* and *fam20b* mutant chondrocytes (Eames et al., 2011). The inductive event for perichondral bone formation is mediated by Ihh, expressed in maturing chondrocytes and not in perichondrium (Long et al., 2004). Indeed, *ihh* transcripts were up-regulated early in *xylt1* and *fam20b* mutant chondrocytes, and genetic epistasis experiments showed that *ihha* function was necessary for the early bone of these PG mutants (Eames et al., 2011). In accordance with the primary defect being in cartilage, both *xylt1* and *fam20b* are expressed highly in chondrocytes, but at low or undetectable levels in perichondral osteoblasts (Eames et al., 2011). In total, these data argue strongly that decreased levels of cartilage PGs change chondrocyte gene expression, altering the timing of endochondral ossification.

As a brief aside, the specific findings of these mutant fish support an old hypothesis for the etiology of osteoarthritis. Osteoarthritis is a complex disease, associated with defects in articular cartilage and many other tissues, including subchondral bone and the surrounding synovial tissues and fluid (Felson et al., 2000). The etiology of osteoarthritis is unclear, but an old hypothesis is that breakdown of cartilage is the primary defect (Pitsillides and Beier, 2011). As summarized above, zebrafish models of PG loss not only support this hypothesis, but also add specific predictions. In *xylt1* and *fam20b* mutants, the primary defect is PG synthesis, and these fish produce less cartilage PGs; as a result of this primary defect, chondrocyte gene expression is mis-regulated, some of which induce extra bone in adjacent tissues (Eames et al., 2011). In osteoarthritis, common diagnostics are loss of sulfated PGs in articular cartilage, mis-expression of chondrocyte gene expression (specifically mis-expression of chondrocyte maturation genes in more superficial layers of articular cartilage), and extra bone (osteophytes) in adjacent tissues (Lindblad and Hedfors, 1987; Pullig et al., 2000). Therefore, the zebrafish studies predict that the primary defect in osteoarthritis is actually the loss of sulfated PGs, and these other diagnostic features are secondary consequences of PG loss. Careful sampling of early time points in experimental models of osteoarthritis could test this novel perspective on an old hypothesis.

Other PG mutant animal models support a role for PGs in the timing of skeletal development. Similar to *xylt1* and *fam20b* mutant zebrafish, both *Xylt1* mutant mice and Aggrecan-deficient (nanomelic) chicks displayed premature *Col10a1* expression and chondrocyte hypertrophy (Domowicz et al., 2009; Mis et al., 2014). All of these animal

models decreased levels of CSPGs, but did not abrogate their production. Equivalent phenotypes among these mutant zebrafish, chick, and mice confirm the evolutionary conservation of PG function during endochondral ossification, specifically supporting the idea that CSPGs normally delay endochondral ossification. Furthermore, these animals all showed dwarfism, suggesting that disruptions to the timing of endochondral ossification might cause dwarfism. Interestingly, many human PG diseases are characterized by dwarfism (Table 2.1), which might be attributed simply to defects in sufficient ECM secretion, but an alternative attractive hypothesis is that the timing of skeletal development is disrupted.

The timing of endochondral ossification is also disrupted in animal models that result in almost complete loss of sulfated PGs. For example, Uxs1 is required to make UDP-xylose, the substrate for Xylt1, and in *uxs1* null mutant zebrafish, *col10a1* expression and perichondral bone formation is delayed (Eames et al., 2010). Also, Papst1 generates sulfate precursors required for PG sulfation, and *papst1* mutant zebrafish show delayed or absent *col10a1* expression and perichondral bone formation (Clement et al., 2008). Defects in growth plate characteristics of other animal models of sulfated PG loss are consistent with disrupted developmental timing, although temporal analyses were not reported (Cortes et al., 2009; Kluppel et al., 2005). Interestingly, *ext2* mutant fish displayed delayed or absent *col10a1* expression and perichondral bone formation (Clement et al., 2008; Wiweger et al., 2014), suggesting that loss of cartilage HSPGs might have the opposite phenotype to loss of cartilage CSPGs. In general, these studies indicate that CSPG defects accelerate, whereas HSPG defects delay, endochondral ossification. By what molecular mechanism can cartilage PGs influence chondrocyte gene expression and developmental timing, and how might different classes of PGs elicit at times opposite effects?

2.1.11 The new PG: Regulator of growth factor signalling

Recently, non-structural roles for extracellular matrix molecules, such as PGs, have been elucidated (Fig. 2.2). As an example of how the surrounding extracellular matrix can impact gene expression in resident cells, PGs are known to modify growth factor (GF) signalling, which in turn regulates transcription (Kim et al., 2011; Schaefer and Schaefer, 2010). Revelatory work in *Drosophila* genetics almost 20 years ago showed that PGs regulate bone morphogenetic protein (Bmp) signalling *in vivo* (Jackson et al., 1997). Subsequent studies have shown that PGs affect a broad array of GF signalling pathways, including all the major developmental GF families (e.g., Bmp, Fgf, Hh, Wnt; (Bhattacharyya et al., 2015; Choocheep et al., 2010; Cortes et al., 2009; Han et al., 2005; Kluppel et al., 2005; Settembre et al., 2008). The mechanism through which PGs affect GF signalling is through direct binding (Bernfield et al., 1999; Harada et al., 2009; Hintze et al., 2012; Khan et al., 2011; Ni et al., 2014; Palma et al., 2011; Sardiello et al., 2005). Most of these studies focus on the role of HSPGs in GF signalling, perhaps because HSPGs are present in high numbers on cell membranes of most cell types (Hacker et al., 2005). For

example, the original

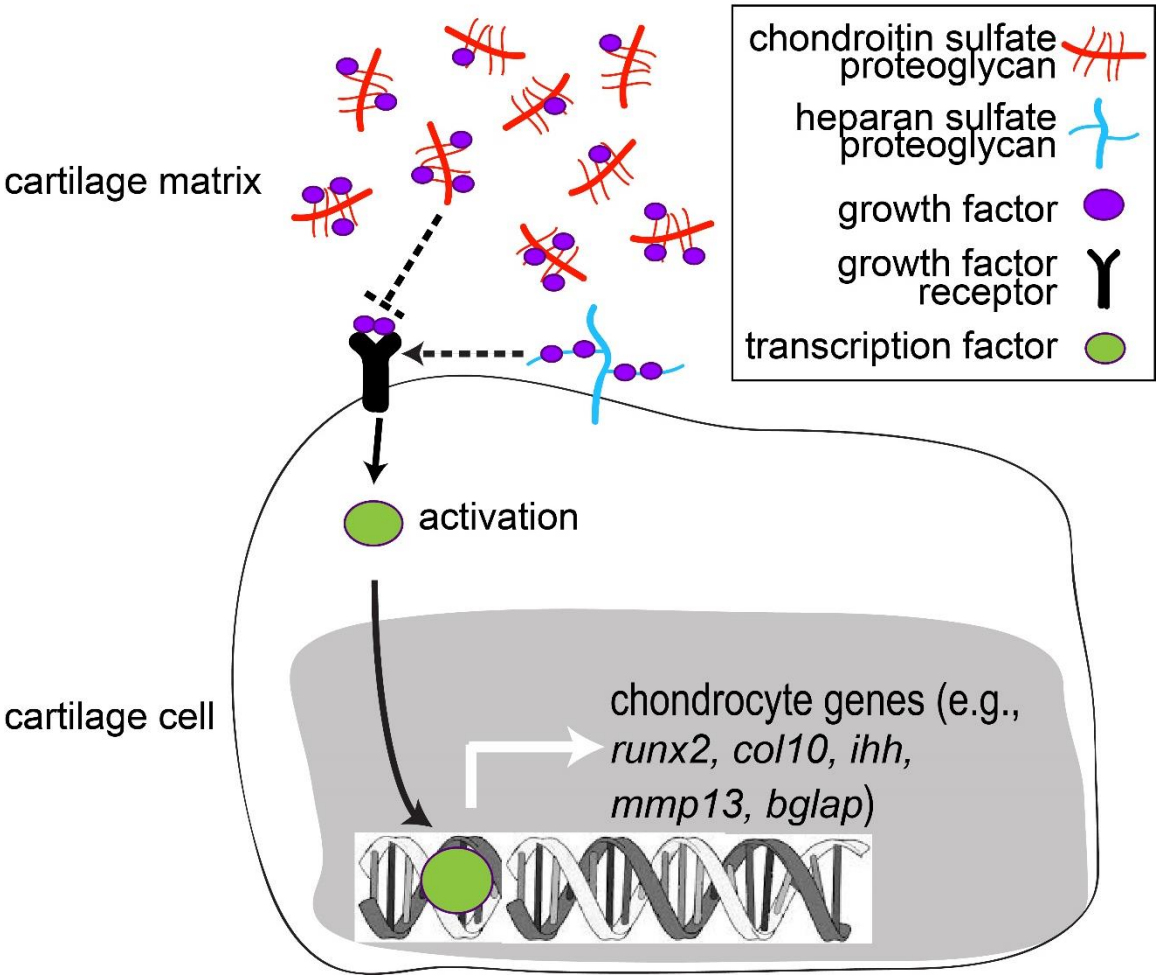

Figure 2.2 Schematic of the idea that cartilage PGs regulate GF signalling.

When bound to GFs, GF receptors modify transcription factors via a signal transduction cascade to regulate gene transcription. PGs surrounding developing chondrocytes can modulate GF signalling, and the specific effects may depend upon both the GF and the class of PGs involved. As depicted, CSPGs may inhibit binding between GF and receptor, acting as a sink; while HSPGs might facilitate binding of the same GF to its receptor.

Drosophila study showed that mutations to Dally, an HSPG core protein similar to Glypican, disrupted imaginal disc patterning (Han et al., 2005; Jackson et al., 1997).

The molecular mechanisms through which PGs regulate GF signalling include influences on GF-receptor binding and GF diffusion. In cultured primary mouse fibroblasts, Hh signalling is increased through direct binding of the ligand and the PG Hspg (previously known as Perlecan; (Palma et al., 2011). On the other hand, Vegf binding to its receptor is inhibited by the PG Decorin (Khan et al., 2011). Regarding GF diffusion, Wnt ligand distribution in the *Drosophila* imaginal disc is increased by the PG Dally (Han et al., 2005). Conversely, diffusion of an Fgf ligand is inhibited by binding to PGs (Harada et al., 2009).

As these studies illustrate, the overall effect of PGs on GF signalling can be positive or negative, depending on the specific GF, receptor, PG, and tissue under study. Regarding the influence of the class of PG on GF signalling, a signalling role for CSPGs has not been studied as extensively as HSPGs. However, CSPG-rich cartilage matrix provides a unique opportunity to evaluate *in vivo* interactions between CSPGs and GF signalling.

A few published studies demonstrate that CSPGs indeed regulate GF signalling in cartilage, but these reports suggest that molecular mechanisms of PG signalling might differ between CSPGs and HSPGs (Fig. 2.2). In 2005, a seminal study by Jeffrey Wrana and colleagues was among the first to analyze CSPG signalling *in vivo*, and they showed that CSPGs negatively regulated Bmp signalling (Kluppel et al., 2005). The notion derived from this finding was that cartilage CSPGs were a "sink", binding up GFs, perhaps acting as a GF reservoir. This negative role is opposite to the positive role for HSPGs in Bmp signalling that had been reported initially in *Drosophila* (Jackson et al., 1997), drawing attention to the potential divergence in signalling function between HSPGs and CSPGs. Similar to the different effects of HSPGs on signalling of different families of GFs, CSPG effects also vary. In cartilage, for example, CSPGs might promote Ihh signalling (Cortes et al., 2009; Domowicz et al., 2009; Gualeni et al., 2010; Mis et al., 2014; Sohaskey et al., 2008), but inhibit Bmp or Fgf signalling (Choocheep et al., 2010; Kluppel et al., 2005; Settembre et al., 2008).

Future studies assessing the role of PGs in GF signalling must be careful to evaluate the specificity of experimental perturbations employed. For example, do the approaches specifically affect HSPGs vs CSPGs, since they might have different functions? While many PG synthesis enzymes affect both HSPGs and CSPGs, other enzymes are dedicated to generating only one of those two classes of PG. For example, Ext2 and Chsy3 are exclusive to HSPG and CSPG synthesis, respectively (Holmborn et al., 2012; Kitagawa and Nadanaka, 2014). Also, enzymes that control PG sulfation, a post-translational modification that regulates PG function (Pitsillides and Beier, 2011; Valdes and Spector, 2010), are specific to a given class of PG, allowing another level of specificity when analyzing the effects of sulfated PGs on GF signalling. In addition, none of the above animal model studies used tissue-specific methods of gene alteration, so it is unclear whether the phenotypes attributed to cartilage CSPGs are actually due to defects in other tissues. To avoid this complication, Gateway and CRISPR technologies (Hwang et al., 2013; Kwan et al., 2007) can ensure tissue-specific genetic alterations. For example, many cartilage- and bone-specific drivers of gene expression have been identified in zebrafish (Dale and Topczewski, 2011; DeLaurier et al., 2010; Eames et al., 2013; Hammond and Moro, 2012).

On top of affecting the structural role of PGs, sulfation influences binding affinities (and thus signalling activity) of GFs and is actually required for normal GF signalling in cartilage matrix (Cortes et al., 2009; Otsuki et al., 2010; Rosen and Lemjabbar-Alaoui, 2010; Valdes and Spector, 2010). As reviewed above, PG sulfation is regulated genetically by an array of enzymes, including sulfotransferases and sulfatases, that add and remove, respectively, sulfate esters on specific sugar residues (Bandtlow and Zimmermann, 2000).

In fact, many of the studies on the signalling role of CSPGs originate from genetic perturbations to CSPG sulfation pathways (Bhattacharyya et al., 2015; Cortes et al., 2009; Gualeni et al., 2010; Kluppel et al., 2005; Melrose et al., 2012; Settembre et al., 2008; Sohaskey et al., 2008). Despite the importance of sulfation for PG function, our ability to visualize PG sulfation *in situ* is limited by detection methods that are either too indirect and non-specific (e.g., Alcian blue binding; (Clement et al., 2008)) or too specific (e.g., antibodies that recognize only certain chemical isoforms of sulfated PGs, such as anti-chondroitin sulfate-4S; (Cortes et al., 2009)). Novel synchrotron-based imaging modalities to visualize sulfur in cartilage matrix might address this limitation.

2.2 Here's looking at you, PG

2.2.1 XRF imaging

X-ray fluorescence (XRF) imaging starts with X-ray bombardment of a sample whereby a core shell electron is stripped and an electron from a higher energy orbital fills this gap, releasing a photon with an exact energy characteristic of that specific element (Fahrni, 2007). Synchrotron XRF imaging relies on very bright sources of X-rays provided by specialized synchrotron facilities, such as the Canadian Light Source (http://www.lightsource.ca/) or newly developed lab-based instruments. The advantages of synchrotron for XRF imaging are the small, very bright beam used, and the ability to detect low concentrations of elements, such are those typically present within biological samples. XRF originates when an X-ray beam hits a sample with sufficient energy to knock out a core electron from a given atom present in the beam path. The core ejected electron leaves a temporary low potential energy "hole", which is filled in by an electron from a higher potential energy shell, releasing a fluorescent photon with energy equivalent to the difference between the higher and lower potential energy shells (Paunesku et al., 2006; Pushie et al., 2014). Of course, many atoms have their electrons knocked out in the X-ray path, generating a complex spectrograph of emitted photons. Since each element has a specific higher to lower shell electron transition state (K-edge), however, the contribution of each element can be differentiated from other peaks through the choice of proper filters (thin metal sheets used for the purpose of attenuating beam intensity) and detectors. In the most common type of detector, a silicon drift detector, each incoming fluorescent photon hitting the detector plate creates an electron hole pair which "drifts" towards the anode on a silicon chip, allowing a measurement sensitive to incoming photon energy (Pushie et al., 2014). Measurement of fluorescent photons has a signal to noise advantage over other X-ray techniques based upon absorption and is ideally suited to hydrated biological specimens (Fahrni, 2007). The technique of K-edge subtraction (mapping at an energy above and below a K-edge jump to work out elemental distribution) is technically challenging since this technique relies on knowing the concentration of the element of interest beforehand. Critically, XRF can reflect the concentrations of elements, enabling quantitative analyses of XRF data (de Jonge and Vogt, 2010; Sole et al., 2007; Twining et al., 2003). X-ray

energies used to probe the fluorescence of atoms have the ability to image all of the elements in the periodic table down to about the mass of phosphorus, and absorbance techniques make it possible to evaluate the elements below this cutoff (Paunesku et al., 2006).

XRF has been utilized for a long time by various chemistry disciplines, but its recent adaptation as an imaging technique holds great promise for efforts to bridge biological and chemical realms. The main boost to imaging has come from the development of the silicon drift detector, which allows hundreds of thousands to millions of photon counts per second. With this technology, mapping can be performed on a single section in a reasonable amount of time at a high resolution (though still frequently requiring hours per scan). XRF imaging reveals spatially resolved patterns of elemental distribution by rastering a tissue section through the X-ray beam and registering the number of individual photons reaching the detector across all energies or "channels" at each raster position (Pushie et al., 2014). For example, perichondral bone in a tissue section can be highlighted using XRF imaging of a channel selected for Ca, due to high levels of hydroxyapatite in mineralized tissue (Fig. 2.3). In fact, as outlined above, data from each pixel includes information on the concentration of several elements simultaneously, which can be very useful. Since the advent of newer detector technology and wider adoption of these techniques by biologists, the number of publications retrieved from PubMed using the keywords 'X-ray fluorescence' and 'Biology' have grown dramatically (doubling between 2008 and 2014).

Newer XRF imaging techniques resulted from the desire to elucidate not only the chemical elements of the sample, but also the specific chemical species of those elements. For example, chemical states of a number of biologically important forms of sulfur, such as sulfate esters or disulfides, can be discriminated through chemically-specific XRF (Koudouna et al., 2014; Pickering et al., 2009). XRF data is generated only from the electrons of elements that can be excited at or below the energy of the incoming beam, and the exact chemical form of an element determines the characteristic energies at which its electrons will be excited (Pushie et al., 2014). Therefore, repeated scans of the same exact region of a tissue section taken using different incident energies can be used to work out the contribution of each specific chemical form of a given element (Pushie et al., 2014). Redox chemistry can also be deduced in this manner. For example, the ratio of oxidized to reduced glutathione can be used to reflect levels of oxidative stress (Hackett et al., 2012; Rompel et al., 1998). Each atomic element is present in the many types of molecule that comprise various tissues, but the chemical conformation of that element typically varies in a molecule-specific way. Taking advantage of this principle, chemically-specific XRF provides up to sub-micrometer resolution of molecular features of biological tissues without the need for special labelling. The practical size limit for imaging is strongly dependent upon the sample thickness, since self-absorption of sulfur K-edge fluorescent photons by the sample itself limits the detection by a small beam size where the number of photons is also restricted (even with a super-bright source such as a synchrotron).

As highlighted in this review, understanding of PG biology would benefit tremendously from XRF imaging. Importantly, the abundant secretion of extracellular matrix by skeletal

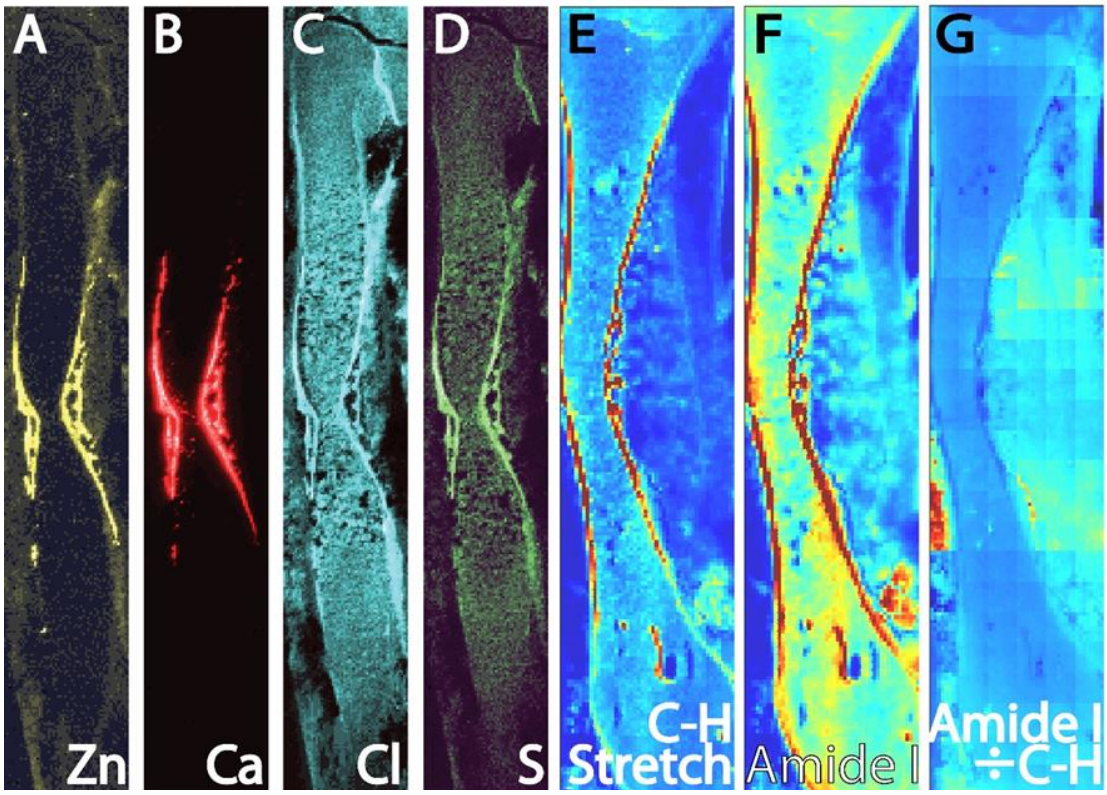

Figure 2.3 XRF and mid-IR maps can illustrate molecular features of developing cartilage.

All images are from 10 mm thick longitudinal sections of a flash-frozen, cryo-embedded HH36 chicken humerus. (A-D) XRF maps were gathered at the VESPERS beamline at the Canadian Light Source (CLS), using different channels during the same scan. Running peripherally along the middle of the element is newly forming perichondral bone, which shows up very strongly in the Zn and Ca channels. The higher levels of S reflect sulfated PGs in both cartilage and bone. (E-G) Infrared images were obtained at the Mid-IR beamline at CLS. Integrating the area under the band for the C-H stretching bond region (2800-3000 cm^{-1}) represents mainly carbohydrates (E), while the area under the total amide I band (1600-1700 cm^{-1}) represents total proteins (F). A second derivative map of the 1656 cm^{-1} protein band after normalization to total C-H stretching (G) demonstrates a low amount of protein in cartilage relative to the high amount of total C-H bonds contributed from carbohydrates. Abbreviations: C, carbon; Ca, calcium; Cl, chlorine; H, hydrogen; S, sulfur; Zn, zinc. (See color plate).

cells potentiates application of XRF to skeletal tissues. The concentration of sulfur present in cartilage PGs makes this tissue readily identifiable using XRF (Fig 2.3; (Althoff et al., 1982; Cichocki et al., 1989; Reinert et al., 2002; Reinert et al., 2001). Discrete sulfur forms are distinguishable by chemically-specific XRF, and the major form of sulfur in cartilage should be a sulfate ester, which is added to GAG sidechains by sulfotransferases (Mikami and Kitagawa, 2013). Indeed, the first demonstration was recently published of total sulfur and sulfate esters in normal and PG-defective zebrafish cartilage, opening up novel lines of research that seek to correlate directly PG function with PG-dependent biological process in cartilage (Hackett et al., 2016).

2.2.2 FTIR imaging

Fourier transform infrared (FTIR) imaging relies on the fact that most molecules absorb IR light, so complex absorption spectra can reveal information about the types of molecules in the probed sample (Baker et al., 2014). The common unit for specifying the energy probed in IR spectroscopy is wavenumber (cm^{-1}), which is basically the number of waves in a specified distance. Several interesting regions within the IR spectrum are used for analyzing biological tissues, but the most widely applied is mid-IR between ~3500 and 700 cm^{-1} (Movasaghi et al., 2008). Each molecule can absorb IR light in a number of different modes, including vibrational, rotational, and flexional, so complex spectra must be devolved using Fourier transform to reveal potential causative molecules (Baker et al., 2014). Non-linear molecules with N atoms have 3N-6 degrees of vibrational freedom (Stuart, 2004), so in a molecule of 10 atoms joined by 9 bonds, for example, there are 24 possible vibrational degrees of freedom, each absorbing a discrete amount of energy. Therefore, even relatively simple compounds, especially in the 1500-900 cm^{-1} (so-called "bio-fingerprint") region, exhibit complex, unique IR absorption plots (Baker et al., 2014). Using this complexity to its advantage, FTIR can positively identify organic substances and polymers, since the spectra acquired are so complex that only identical compounds will produce an identical absorption plot (Chen et al., 2013; Verhoef et al., 2005; Zimmermann et al., 2015).

FTIR imaging (also called "mapping") is carried out by shining a polychromatic IR beam (covering the entire IR region of interest, such as mid-IR or far-IR) either through or even reflected off the sample of interest onto a detector. Similar to XRF imaging, this process is repeated in a raster scan to produce an image of the tissue section. Each pixel in the "image" represents the average amplitude (intensity) of absorption of all the molecules at a given frequency, frequency range, or ratio of frequencies (Baker et al., 2014). From these data, IR biomarkers can be identified by selecting a pixel or group of pixels containing a particular biological feature of interest, and comparing the spectra from those pixels with those from other regions. In this manner, FTIR complements metabolomic studies in cancer biology to validate quickly and inexpensively tumorigenic phenotypes when a gold standard is lacking (Derenne et al., 2014; Noreen et al., 2012).

Of the wealth of FTIR data, only a few specific molecules can be associated with specific wavenumbers, but future work on this nascent application to biology may prove to be very productive. Experimentally, a molecule can be added or removed from a mixture, and multivariate analysis can be performed to identify diagnostic IR bands that covary with the presence or absence of that specific molecule (Chonanant et al., 2014; Kwon et al., 2014). In addition, proper normalization of data to account for local variations in sample thickness allows FTIR to be used as a quantitative tool (Petibois et al., 2008). As opposed to XRF imaging, however, FTIR is resolution-limited by the wavelength of light used, so resolution at the highest frequency used in Mid-IR runs into a limit at about 5 μm (Lasch and Naumann, 2006). Despite this limitation, distribution of PGs in cartilage matrix occurs on

a much larger scale, allowing their visualization and potential changes associated with pathological conditions, such as osteoarthritis (Fig. 2.3).

2.2.3 Visualizing sugars in vivo

The study of PG function *in vivo* took another leap forward with the advent of sugar visualization techniques. Using azide click chemistry, sugars incorporated into the GAG sidechains of PGs can be visualized in a dynamic fashion, not only revealing the location of specific PGs, but also showing the temporal turnover of GAGs in pulse-chase experiments (Flanagan-Steet and Steet, 2013; Laughlin et al., 2008). For example, HSPGs are labelled by injecting zebrafish embryos with Az-GlcNAc compounds, while CSPGs are labelled with Az-GalNac compounds. After the compounds are incorporated into developing tissues, they are converted to fluorophores *in vivo* by fluorescent click chemistry (Laughlin et al., 2008), and finally HSPGs and CSPGs are visualized by confocal imaging. More recently, modified sugars have been introduced similarly to block GAG synthesis, and to visualize mucin (O-linked) glycans (Beahm et al., 2014; Kramer et al., 2015). The fidelity and efficiency of these approaches to PG labelling are being optimized, but the technical imaging advances reviewed here and highlighted in zebrafish studies mean the future is bright for PG research.

2.3 Conclusion

PGs are recognized increasingly as critical structural and biological factors in many tissues, and we review here studies that revealed specific roles for PGs in cartilage matrix. When secreted abundantly in the extracellular matrix, PGs impart cartilage with mechanical properties, such as compressive resistance and low friction, both of which are required to facilitate movement at articulating surfaces of skeletal joints. Recent studies on biological roles for a specific class of PG, CSPGs, on growth factor (GF) signalling in cartilage have added complexity to our understanding of cartilage PGs. In fact, many diseases associated with defects in PG synthesis might reflect biological, as opposed to structural, functions of PGs.

Zebrafish is a unique experimental system to illuminate the role of cartilage PGs in GF signalling, due to the ease of combining in this model system novel imaging techniques with genetic techniques that can alter a specific class of PG in a specific tissue. Many of these techniques are innovative in the whole of biology, if not in their application to skeletal tissues. Using zebrafish to understand the genetic and molecular mechanisms by which PGs regulate GF signalling can impact and inform any therapeutic approach relying upon GF application. More generally, by identifying new functions of known PG synthesis genes, we might increase diagnostic and therapeutic targets for many diseases.

2.4 Acknowledgements

We wish to thank Mark Hackett for helping to generate and represent the synchrotron imaging data; Paul Koopman for his help relating PG functions to architectural practices; and the Canadian Light Source (supported by the Canada Foundation for Innovation, Natural Sciences and Engineering Research Council (NSERC), the University of Saskatchewan (UofS), the Government of Saskatchewan, Western Economic Diversification Canada, the National Research Council Canada, and the Canadian Institutes of Health Research (CIHR)) for the use of their facilities and the support from their great staff. This work was supported by UofS and CIHR-THRUST awards to DB; and Saskatchewan Health Research Foundation, NSERC, and CIHR grants to BFE.

CHAPTER 3

3. Proteoglycan Sulfation Decreases in Mature Cartilage During Endochondral Ossification

Brown, D. S., Hackett, M. J., Grecco, R., Picos-Gómez, P., George, G. N., Pickering, I. J., and Eames, B.F., "Proteoglycan sulfation decreases in mature cartilage during endochondral ossification", Cartilage, in preparation

3.1 Abstract

Cartilage plays an important biomechanical role within the skeleton in part due to the high degree of sulfated proteoglycans (PGs) present within the extracellular matrix (ECM). Exactly how PG sulfation levels are regulated, especially during cartilage development remains an open question. Changes to sulfur metabolism have been shown to alter normal skeletal development in the human mucopolysaccharidosis (MPS) disorders. Also, animal models containing under-sulfated PGs show stunted growth and early bone formation, suggesting that a correlation does exist between lowered levels of PGs in the ECM and in increased rate of cartilage maturation and early bone formation. New techniques, such as chemically specific X-ray fluorescence (XRF) imaging for sulfate esters, combined with Fourier transform infrared (FTIR) imaging to measure PG levels in the matrix can be used to discover if there is a connection between the distribution pattern of sulfur in the ECM and the maturation state of the underlying cartilage. Based on a trend noted in a previous XRF study in zebrafish, the hypothesis that we put forward is that sulfated PGs decrease in mature cartilage. From elemental and chemically specific XRF imaging, we showed that total sulfur, and specifically sulfate ester levels, decrease significantly in mature cartilage. An imaging strategy to measure PG levels directly with FTIR was carried out to determine if decreased sulfate esters were tied to PG losses, or if they were decreasing independently. The strategy used two marker bands at 985 – 1140 cm^{-1} and 1374 cm^{-1} (second derivative), which have been reported on previously. No significant change was observed for PG levels in mature cartilage according to this analysis for either band. We suggest that chondroitin sulfate (CS) PGs in mature cartilage are either losing sulfate esters directly from the ECM by an uncharacterized mechanism, or that they are differentially processed to contain less sulfur during turnover by pre-hypertrophic and hypertrophic chondrocytes. An understanding of how sulfur levels relate to differentiation states of chondrocytes could lead to new understandings for how sulfur may drive pathological states in cartilage.

3.2 Introduction

Chondroitin sulfate (CS) proteoglycans are the most abundant proteoglycan (PG) found in both developing and persistent cartilage, though their function in the development of the skeleton is still not well understood. The anionic properties of highly sulfated PGs in the extracellular matrix (ECM) heavily influence the mechanical properties of cartilage. While collagen proteins provide tensile strength and cohesion to the ECM, CS chains rich in sulfate esters grant cartilage its incredible resistance to compressive loads by increasing hydrostatic pressure (Aumailley and Gayraud, 1998; Chahine et al., 2005). Unlike heparin/heparan sulfate proteoglycans, which are known to be involved in the normal maturation of the chondrocytes endochondral bone formation (Bernfield et al., 1999; Hacker et al., 2005; Lin, 2004; Tumova et al., 2000; Turnbull et al., 2001), CS sulfate molecules have received very little attention until recently about these same roles attributed to heparin/heparan sulfate because their main function is to provide structural support to cartilage.

During endochondral ossification, cartilage acts as a biodegradable scaffold made up of chondrocytes at different stages of maturation, which are responsible for both the synthesis and degradation of the ECM. Immature chondrocytes appear after several longitudinal mitotic divisions of a proliferative chondrocyte which then begin to secrete large amounts of ECM composed of mainly Collagen type II (Col2) and Aggrecan. Aggrecan is the defining PG of cartilage and consists of its own core protein onto which is attached up to 100 CS chains and a smaller number of keratan sulfate (KS) chains (Roughley and Mort, 2014). As the cartilage element grows through appositional division and interstitial growth, pre-hypertrophic and hypertrophic chondrocytes (together termed mature chondrocytes) in the central region initiate matrix production focused on Collagen type 10 (Col10) (Vortkamp, 2000). The final stages of chondrocyte differentiation lead to the degradation of the ECM by matrix metalloproteinases, vascular invasion, and apoptosis of most mature chondrocytes – although direct transdifferentiation of chondrocytes to osteoblasts has been observed (Hinton et al., 2017; Karsenty and Wagner, 2002; Vu and Werb, 2000).

The synthesis of CS glycosaminoglycan (GAG) chains (which are composed of glucuronic acid (GlcA) and N-acetyl galactosamine (GalNAc) disaccharide repeats) occurs in the ER and early Golgi compartments, and sulfation of the newly synthesized chondroitin chain happens concomitantly with the action of sulfotransferases (Brown and Eames, 2016). CS synthesis is initiated in the ER through xylosylation of a serine residue on the core protein, and synthesis of a tetrasaccharide linker region (xylose -galactose –galactose -GlcA)(Schon et al., 2006). The determination of the GAG chain identity as either CS, keratan sulfate, or heparan/heparin sulfate is dependent on the initial sugar added to the tetrasaccharide linker. Polymerization of each GAG chain is carried out by the general CS polymerases GlcAT-II (GlcA transferase II) and GalNAcT-II (GalNAc transferase II) (Izumikawa et al., 2007; Kitagawa et al., 2003; Nadanaka and Kitagawa, 2008). Sulfate moieties are attached to growing CS chains in the form of O – linked sulfate esters. Sulfate

esters of CS can occupy the 4- and 6- carbons of the GalNAc sugar, or the 2-carbon of GlcA. CS GAGs are characterized starting out as an unsulfated O unit, and proceeding through either a 4-sulfation to yield an A unit, or initial 6-sulfation (C unit). CS A units commonly undergo additional 6-sulfation to yield a 4,6-sulfated disaccharide (E unit), and 6-sulfated C units can undergo 2-sulfation of GlcA, forming a 2,6-sulfated D unit (Brown and Eames, 2016; Kusche-Gullberg and Kjellen, 2003; Uyama et al., 2007). Postnatally, CS molecules have roughly equal proportions of 4- and 6- sulfated disaccharides; however, this ratio changes from approximately 50 % to 80 % 6-sulfation through the course of ageing from birth to 20 years of age (Bayliss et al., 1999). Along with shifts in the 4/6 -sulfated GAG ratio during development, changes in Aggrecan substituent chain lengths also occur as part of normal human development, with increasing chain lengths for KS and decreasing lengths seen for CS until the age of 20 (Brown et al., 1998; Plaas et al., 1997; Roughley, 1987; Roughley and White, 1980).

CS de-sulfation requires enzymes known as sulfatases which act on PGs during lysosomal degradation and which can affect growth plate dynamics. The family of known CS sulfatases includes three lysosomal enzymes, Arsb (EC 3.1.6.12; (Bhattacharyya et al., 2015)) and Galns (EC 3.1.6.4; (Tomatsu et al., 2005)) which act on GalNAc-4-S and GalNAc-6-S, respectively)] and the recently characterized sulfatase ARSK (EC:3.1.6.-), which acts on the GlcA-2-S D-unit of CS, (Dhamale et al., 2017; Wiegmann et al., 2013), and is also thought to act in the lysosome. There also exist several predicted sulfatases with unknown substrate-specificity and functions, which could very well act as CS sulfatases (Ratzka et al., 2010). In human skeletal development, sulfur PG misregulation in the form of mutations to either *ARSB* or *GALNS* are the cause for the mucopolysaccharidosis (MPS) disorders MPS IV and MPS VI, respectively (Muenzer, 2011). Both conditions cause a range of stunting during skeletal development depending on the severity of the mutation (Montano et al., 2007; Valayannopoulos et al., 2010). The severe effects that these sulfatase mutations have on skeletal development suggest that they might cause a problem with the cartilage maturation process during endochondral ossification.

Animal models of inherited diseases are invaluable tools in studying the specific genetic and biochemical etiology and prognosis of developmental disorders. Abnormal and stunted growth is characteristic of many animal PG mutant models, whether these mutations somehow affect PG synthesis, PG sulfation, or PG desulfation and degradation (Alliston, 2010; Cortes et al., 2009; Domowicz et al., 2009; Khatri and Schipani, 2008). The primary disruptive cellular process of the MPS-VI disorder in the feline model of the disorder is thought to arise due to the accumulation of DS GAGs in the lysosome leading to cell enlargement, dysfunction, and apoptosis (Simonaro et al., 2001; Valayannopoulos et al., 2010). Brd-U labelling has revealed that MPS cells divide up to 5 times faster than normal cells to offset high levels of apoptosis, such that the relative cell counts are the same in both cases (Simonaro et al., 2005). Despite similar cell counts in the growth plate, decreased bone growth in feline MPS-VI has been suggested to occur due to a slowed rate of hypertrophy (Nuttall et al., 1999). The absence of chick Aggrecan accelerates the process of cartilage maturation in the nanomelic long bone growth disorder (Domowicz et

al., 2009). Recent findings from zebrafish agree with conclusions from other studies on cartilage disorders in animal models, that the scarcity of the sulfated PG molecules within the ECM can have the opposite of delayed bone growth, that is, precocious bone development (Cortes et al., 2009; Domowicz et al., 2009; Eames et al., 2011; Hackett et al., 2016). The direct association between lowered PG levels and precocious bone formation is evidence that PG (and sulfation) levels are negatively related to the rate of cartilage maturation. The cartilage template relies on sulfated PGs to proceed through normal timing of growth and bone formation as evidenced by these mutant models. Evidence for the purposeful modulation of these levels by mature cartilage throughout development will come from studies of normal animal cartilage which will hopefully point to the exact mechanism or mechanisms responsible for these fine-tuned changes directing development.

Chemically-specific X-ray fluorescence (XRF) imaging has recently emerged as a tool which allows the visualization of tissue wide patterns of sulfation, data that is lacking from previous biochemical techniques focused on overall analysis of cartilage PGs. In zebrafish, chemically-specific XRF imaging was used to quantify sulfate ester levels, the main form of sulfur in cartilage, in the cartilage deficient *fam20b* mutant (Hackett et al., 2016). Analysis of sulfate ester levels in wild-type zebrafish cartilage revealed that there may be a correlation between cartilage maturation state and overall sulfated PG levels in the matrix. Losses of sulfate ester signal from *fam20b* mutant zebrafish also strongly argue that the sulfate esters in the matrix come directly from sulfated PGs. Previous bulk analysis of sulfur in developing chicken cartilage using electron probe also showed a significant decrease in the sulfur content of mature cartilage (Hargest et al., 1985), but this was based on bulk analysis of total sulfur and did not address whether sulfate esters from PGs were specifically decreasing, nor did it reveal the spatial nature of how sulfur was distributed.

Since the sulfate esters present in chicken are directly related to the sulfation of PG GAG chains, changes to the levels of sulfate esters within cartilage must reflect either a change in overall PG content, or a change in the sulfation level of the GAGs present. Changes to PG content in the ECM may reflect changes in individual PG chain lengths, or the total number of PG chains present. Fourier transform infrared (FTIR) imaging is another imaging based technique which has been used to quantitate overall PG levels in cartilage (Kim et al., 2005) and can be used to identify whether or not changes in PG levels are associated with changes in sulfate ester levels.

The human MPS-IV and MPS-VI growth disorders are caused by a decrease in the ability of lysosomes to efficiently degrade PGs due to a loss of function of sulfatase enzymes. Other animal models for mutations involving CSPG sulfation and synthesis are the cause of even more severe and even earlier onset changes which directly affect the maturation rate of chondrocytes and lead to early bone formation (Cortes et al., 2009; Domowicz et al., 2009; Eames et al., 2011). To try to better understand the link between tissue-wide sulfation patterns and the state of the underlying chondrocytes, the hypothesis set forth in this study is that PG sulfate ester levels decrease in mature cartilage during development. Directly related to the observations regarding sulfation levels and changes to the maturation

rate of cartilage, we demonstrated that sulfate ester levels in mature chicken cartilage decreased significantly when compared to immature cartilage, while proteoglycan levels in mature cartilage did not decrease significantly. These findings together indicate that mature PGs are under-sulfated with respect to immature PGs, and one possibility for this decrease in sulfation might be substrate level desulfation of CS occurring in the ECM.

3.3 Methods

3.3.1 Animal Model

White leghorn chicken eggs (N = 10) were incubated in a humidified, rocking incubator at 37 °C until they reached Hamburger-Hamilton stage 36 (~10.5 days of incubation) (Hamburger and Hamilton, 1951). This work was approved by the University of Saskatchewan's Animal Research Ethics Board, and adhered to the Canadian Council on Animal Care guidelines for humane animal use.

3.3.2 Sample preparation

Each embryo was killed by decapitation following its removal from the egg onto an empty glass receiving dish. Chick forelimbs were collected by dissection in phosphate buffered saline followed by embedding in OCT compound (Tissue Tek, Torrance, CA, USA) and immediately flash-frozen in liquid nitrogen-cooled isopentane. Chick forelimbs used for imaging were all from different individuals. 10 µm-thick sections of the humerus were cryo-sectioned and collected onto metal-free plastic coverslips (Thermanox, Mississauga, ON, Canada) for XRF imaging, and sections being prepared for Mid-IR analysis were collected onto an IR-grade CaF_2 window (Crystran, Dorset, UK). Eight to ten adjacent serial sections were collected onto Superfrost Plus™ glass slides (Fischer Scientific, Canada) for later immunohistochemistry (IHC) analyses or other potential applications, such as RNA *in-situ* hybridization analysis for looking at mRNA expression patterns. Sections imaged at the synchrotron were retained at -80 °C for later Safranin O staining.

3.3.3 Histology

For Safranin O tissue section staining, cryosectioned tissues were re-hydrated in water for 1 minute before staining. Sections were placed in Wiegert's hematoxylin for 5 minutes, rinsed in running tap water for 1 minute, and then counter-stained in fast green FCF (0.05 %) for 1 minutes. The tissues were then de-stained in 1 % acetic acid for 10 dips. Sections were then left in 0.1 % safranin O stain for 20 minutes and then dehydrated and mounted with a coverslip and Permount™ (Fisher Chemical, Mississauga, ON, Canada). Alizarin

red and Alcian blue whole mount staining on HH36 chick humeri was performed as previously described (Eames et al., 2011).

3.3.4 Pink-beam XRF at VESPERS

XRF imaging of total sulfur was performed at the Very Sensitive Elemental and Structural Probe Employing Radiation from a Synchrotron beamline at Canadian Light Source (VESPERS) beamline at the CLS. VESPERS is a bend magnet beamline which uses a Si (111) crystal monochromator pair and Kirkpatrick-Baez focusing mirrors (minimum 2 × 4 µm spot size) with several bandpass modes available. The detector used for fluorescence imaging was a Vortex®-ME4 4-element dispersive silicon drift detector (Hitachi, Troy, MI, USA). Each humerus sample on Thermanox™ was mounted vertically, inclined 45° relative to the incoming beam. Each humerus was raster-scanned with a 15 × 15 µm step size using 4 × 6 µm (horizontal × vertical) sized pink beam (15 keV excitation) with a 1 second dwell time for each pixel for the purpose of capturing data for multiple elements other than sulfur. Each humerus was approximately 3000 × 4000 µm in size resulting in approximate scan times of 7 hours. Upstream filters were used to cut down on incoming signal intensity reaching the detector to minimize dead-time effects. In total, 10 humerus samples were measured in this way at this beamline.

3.3.5 XANES data collection at the Canadian Light Source SXRMB beamline

X-ray absorption near-edge spectroscopy (XANES) spot scans were taken at SXRMB to determine all of the constitutive forms of sulfur present in mature and immature cartilage. X-ray absorption spectroscopy was carried out at the Soft X-ray Microcharacterization Beamline (SXRMB) at the CLS, where low energy X-rays are employed for observing the K-edges of lighter elements, particularly sulfur and phosphorus. Prior to the collection of spectra, the sample chamber was purged with He until the relative O_2 content within the chamber was <0.5%. XANES spectra were calibrated against the spectrum of an anhydrous $Na_2S_2O_3$ powder solid standard, with the lowest-energy peak thought to be 2469.2 eV, as described previously (Gnida et al., 2007; Pickering et al., 2001; Pickering et al., 1998; Pickering et al., 2009; Sekiyama et al., 1986). Spectra were collected across the energy range of 2450–2515 eV, with a total collection time of approximately 10 min, using the Acquaman software package (http://beamteam.usask.ca/mark/acquaman/index.html). Each spot scan measurement was taken as the averaged spectra of three replicate measurements at each spot. Spot scans were collected for at least 3 spots in the immature cartilage region and at least 3 spots in the mature region. The error for each measurement represents the standard error of the mean for each compound based on individual fittings. One sample out of four measured for XANES fitting in total was removed as an outlier because the sulfate ester and sulfonic acid percent fits were very different from the others. Spectra of calibration standards and model compounds were recorded at room temperature. Powdered solid standard

compounds used for fitting routines represented disulfides (oxidized glutathione), thiols (reduced glutathione), thio-ethers (methionine), sulfoxides (methionine sulfoxide), sulfinic acids (hypotaurine), sulfonic acids (taurine), O-linked sulfate esters (*N*-acetyl D-galactosamine 6-sulfate), N-linked sulfate esters (D-galactosamine 2-sulfate), and inorganic sulfates (Na_2SO_4). Spectra were collected from a total of four samples from different specimens. The number of spots used was not enough for a statistical comparison to be made between regions, since when directly comparing measurements, the individual measurement errors must be added together, resulting in error values which are bigger than the differences between regions for all of the forms of sulfur measured.

3.3.6 Chemically-specific XRF imaging at SXRMB

Chemically specific imaging of sulfate esters and sulfonic acids was performed at the SXRMB beamline at CLS. To create maps of sulfate esters and sulfonic acids, three XRF maps at different energies in the sulfur K-edge region and one map of total sulfur were created and processed as previously described (Hackett et al., 2016). The beamline relies on a bending magnet source, and operates in the 1-10 keV range with an energy resolution $\Delta E/E$ of 1.0×10^{-4}. Energy calibration was performed using a powder on tape standard composed of sodium thiosulfate placed in the ambient chamber in electron capture mode. Monochromator motors were calibrated at the start of each session. Humerus samples were mounted on an aluminum sample holder using carbon tape. Samples were mounted in a vacuum chamber with a 45° angle to the vertical plane relative to the incoming beam. The calibrated peak value of the secondary peak of sodium thiosulfate used at the SXRMB beamline is 2472.0, based on the value in the Handbook on Synchrotron Radiation published by the Lawrence Berkeley National Laboratory in 2011 (http://xdb.lbl.gov/). This calibration value is 2.8 eV higher than the energy used at SSRL, where the ideal peak fitting ratios were obtained solving for sulfonic acids and sulfate O – linked esters simultaneously. This may result in slightly off of white-line energies used for imaging, resulting in very slightly systematically shifted proportions of each of these two components from which the maps are derived. The four energies measured for chemically specific imaging at SXRMB were 2500.0 eV (for total sulfur) 2479.2 eV, 2477.6 eV and 2474.4 eV. In total, 6 humerus samples were measured in this way at this beamline, all of which were also imaged at the VESPERS beamline for total sulfur and included in the XRF quantitation.

3.3.7 Mid-Infrared (FTIR) Imaging

Fourier transform infrared (FTIR) imaging is being rapidly adopted as a research technique for the non-perturbative and label free analysis of biological tissues (Baker et al., 2014). It is a promising tool for looking at spatial changes to PG content by using wavenumber ranges correlated with cartilage matrix CSPGs (Saarakkala and Julkunen, 2010). FTIR imaging was performed at the mid-IR beamline at the CLS. FTIR imaging was performed

to assess if there was also a trend in overall PGs observed between regions that could account for decreasing sulfate esters from the ECM. Three different IR regions of interest were focused on to determine the relative abundance of total proteins and CS proteoglycans in mature versus immature cartilage. Normalization of spectra is important for infrared imaging because it accounts for confounding factors, such as thickness variations, and because otherwise differences in absorbance intensities will be highlighted, rather than biological differences (Baker et al., 2014). Total protein content is commonly used to normalize spectra to account for variations in thickness (Baker et al., 2014). Protein was estimated using the amide I band arising from C=O stretching of peptide bonds. Two IR regions, 985 – 1140 cm^{-1} and the 1374 cm^{-1} second derivative band, were chosen to give independent estimates of CS content based on previously validated studies (Boskey and Pleshko Camacho, 2007; Kim et al., 2005; Saarakkala et al., 2010).

All infrared data were collected with a Hyperion 3000 FTIR imaging system (Bruker Optics, Ettlingen, Germany) fitted with a mercury-cadmium-telluride (MCT) 64×64 focal plane array (FPA) detector with an upper objective of 15x magnification and a numerical aperture of 0.4, combined with a lower condenser of 15x magnification and 0.4 numerical aperture. This arrangement yielded a pixel size of 21.4 μm^2, using 8x8 binning. All scans were performed in transmission mode. Samples were mounted on IR-grade CaF_2 windows (Crystran Ltd.). A focal plane array detect was illuminated with a Globar source (aperture 3.5 mm, part of the Hyperion 3000 FTIR system used). FTIR-spectroscopic images were collected across the spectral region 3600 – 900 cm^{-1}, on a liquid nitrogen cooled focal plane array (FPA) detector with a spectral resolution of 4 cm^{-1} with the co-addition of 128 scans, with a background image similarly collected from blank substrate using 128 co-added scans. The background was collected immediately prior to each sample. In total, 8 humerus samples were measured in this way at this beamline.

3.3.8 Immunohistochemistry

COL10 IHC was performed on adjacent serial sections to those imaged at the CLS to visualize mature cartilage for drawing precise regions of interest used in subsequent quantitative analyses. Sections from storage at -80 °C were first adhered to glass slides by drying at 56 °C for 15 minutes. The sections were then post-fixed in 4 % PFA for 10 minutes at room temperature. Slides were then rinsed twice in PBS. Blocking was carried for 1 hour in blocking solution (10 % sheep serum in PBS). After blocking, 100 µL of 1:100 primary mouse α-COL10 antibody (X-AC9, Developmental Studies Hybridoma Bank (DSHB), Iowa City, IA) in dilution buffer (0.5 % sheep serum in PBS) was added and the slides were placed in an incubated chamber to rock at room temperature for 1 hour. The slides were then rinsed carefully in 2 changes of PBS for 5 minutes each. 100 µL of 1:2000 fluorescent rabbit α-mouse antibody (Chemicon, Temecula California) in dilution buffer were then added and left to rock in a humidified chamber in the dark at room temperature for an additional 30 minutes. Slides were rinsed twice in PBS as before and

nuclei were then stained with Hoechst stain for 10 minutes in the dark before applying cover slips.

3.3.9 Data processing and statistical analysis

All XRF maps collected at SXRMB and VESPERS were first opened in Sam's microprobe analysis toolkit (SMAK) version 1.40 (https://www.sams-xrays.com/smak) and normalized to the pre-sample ion chamber channel. To create chemically specific maps for sulfonic acids and sulfate esters, each map (e.g. 2500.0 eV, 2479.2 eV, 2477.6 eV and 2474.4 eV) was first normalized to the incoming beam current. Each map was then imported into a single file and the 2474.4 eV channel (background) was subtracted from the 2479.2 eV and 2477.6 eV maps. The "X-ray absorption near edge structure (XANES) fitting" sub-program was used to create the sulfate ester and sulfonic acids maps using the peak ratio parameters of 4.8:4.1 and 1.27:5.6 for 2477.6 eV and 2479.2 eV (both background subtracted as previously mentioned), respectively, as determined by determined by XANES measurements of pure standard compounds (Hackett et al., 2016). While referencing the optical microscope image of the same section in the XRF image, any small holes in the sample were removed by using a lower pixel intensity cut-off to get rid of false negative pixel intensity values. Sections with folds were avoided when choosing samples for synchrotron imaging.

All XRF files were then converted into a gray-scale text image using the program smak2txt created by Graham George (University of Saskatchewan), allowing them to be opened in ImageJ (https://imagej.nih.gov/ij/). Once open in ImageJ, the files were converted into a 16-bit grey value scale and then saved as a .tiff image to be opened in Adobe Photoshop CS6 (https://www.adobe.com/ca/). Adjacent sections were used to carry out immunohistochemistry protocols and imaged with a fluorescence microscope. In Adobe Photoshop, regions for analysis (mature versus immature cartilage) were selected based on the COL10 immunostaining pattern from an adjacent section (mature chondrocyte marker) by importing the IHC image as a new layer in the image and adjusting the layer transparency and contrast until the two outlines could be overlain to give the best possible fit. Sections which were too peripheral were either avoided all together or regions were drawn conservatively during analysis to avoid sulfur signal coming from the perichondrium.

Each region of interest for analysis was drawn using the polygon selection tool on the 16-bit greyscale sulfur map with the COL10 immunostain visible behind it (as a separate layer by reducing the sulfur layer opacity) visible, but with the sulfur map selected. The selected region was then copied into a new separate layer for analysis. Photoshop by default applies fuzziness to a clipped selection when copying it to a new layer or file to keep out of focus elements from appearing too crisp in a new layer for creating realistic images, but this default was overcome by setting the sharpness setting to 100 % immediately after copying to a new layer. The layers were transferred faithfully when using the 100 % sharpness setting, except for occasional clipped pixels along the outside edge which appeared very

dark and were excluded from the analysis. For each region, the filtered-out pixels (relating to tears) were hand selected and an inverse mask was applied, deselecting those pixels. This was necessary because Photoshop does not see null values generated by cut off value filters in other programs, but instead sees only grey values of 0, which affects the average of ROIs if they are included. Average pixel intensity, total pixel intensity, standard deviation, total pixels counted from the histogram toolbar were collected for statistical analysis.

XANES spectra (collected as above) were processed using the EXAFSPAK suite of programs (http://www-ssrl.slac.stanford.edu/exafspak.html). Using the DATFIT program, spectra from tissue sections were fitted with a linear combination of normalized reference spectra. Standards were excluded from the refinement algorithm if they contributed to <1 % of the total spectra.

Images of total protein distribution were calculated from the integrated area under the Amide I band (mainly C=O stretch) from 1590 – 1720 cm^{-1}. PG correlated bands 985 – 1140 cm^{-1} and the second derivative band at 1374 cm^{-1} were chosen based on biologically validated univariate models (Saarakkala et al., 2010). All data processing and image generation was performed using Cytospec software (Cytospec, Version 1.2.04) and Opus software (Version 6.5, Bruker, Ettlingen, Germany).

Statistics were carried out in SPSS version 23. Since only the relative difference in sulfur between regions was important for this study, the ratio between mature and immature mean sulfur values was used to normalize across different experimental runs, giving us an internally standardized look at increasing or decreasing relative sulfur levels. The One sample t-test was used to measure statistical significance between the mature region and the immature region mean intensity (defined as 1.0) with the deviation reported as ± the standard error of the mean. For cases where there were two immature regions present (corresponding to each end of the bone), the immature region was taken to be the calculated average of the two. The 95 % confidence interval with an associated p-value of < 0.05 was considered significant.

3.4 Results

3.4.1 XRF imaging at VESPERS shows a decrease in total sulfur in mature cartilage

To investigate a possible correlation between the maturation state of cartilage and sulfation levels, the ratio of total sulfur in mature cartilage versus immature cartilage was quantitated at the VESPERS beamline at the CLS. Whole-mount humeri and 10 µm-thick tissue sections were stained with Alcian blue stains and Safranin-O stains, respectively, which are both cationic dyes that bind to sulfated PGs and show a decrease in mature cartilage (Fig. 3.1 A-C)(Deutsch et al., 1995; Farquharson et al., 1994). Safranin-O tissue section

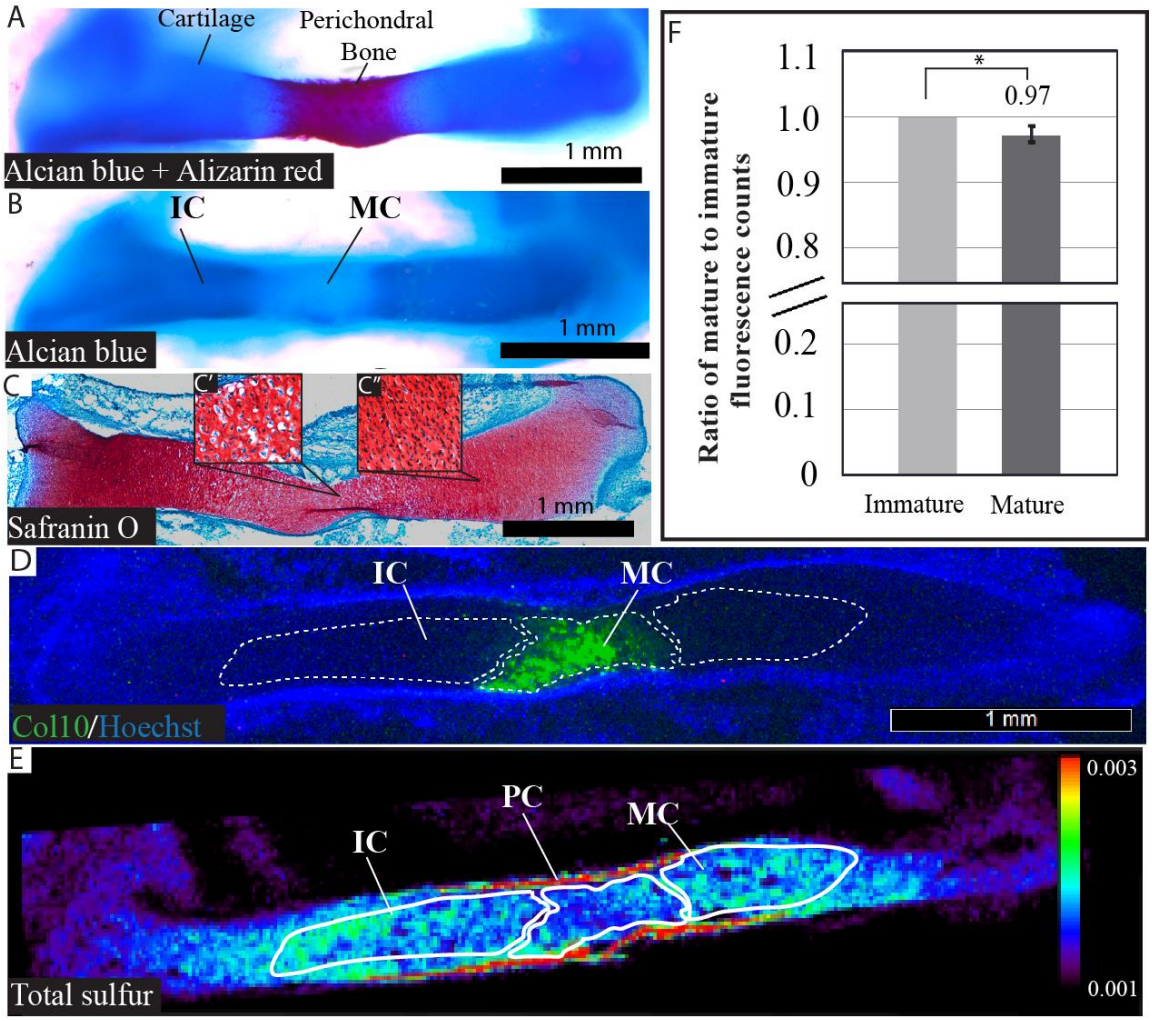

Figure 3.1 XRF imaging of total sulfur validates the loss of proteoglycan staining by Alcian blue/Safranin O in mature cartilage.

Mineralization of perichondral bone is depicted by Alizarin red staining (panel A) along with Alcian blue staining for sulfated proteoglycans. Alcian blue staining on its own (panel B) shows a decreased binding ability in the mature cartilage region. Safranin O staining of sulfated PGs depicts hypertrophy in mature cartilage (insert C') along with immature chondrocytes (C''). Immunohistochemistry images of COL10 (panel D) performed on adjacent sections were used to define the mature and immature regions for XRF image analysis (white dashed line). Total sulfur maps were collected at the VESPERS beamline at the Canadian Light Source (panel E). Quantitation of XRF images for total sulfur showed a decrease of 2.7 ± 1.1% in the average total sulfur content of mature cartilage relative to immature cartilage (panel F). N = 10. Error bars represent the standard error of the mean. P-values < 0.05 % were considered significant. Abbreviations: IC = immature cartilage; MC = mature cartilage; PC = perichondrium.

staining in the same region supports the case that decreased binding is due to lowered levels of sulfated GAGs in mature cartilage, and not a penetration issue as could occur with whole mounted humeri. COL10 immunostaining was used as an unbiased marker for identifying where to assign regions of interest for mature and immature cartilage (Fig. 3.1 D).

Sulfur was successfully imaged using XRF, with adjacent sections used for Col10 immunostaining for all 10 chicken humerus samples (Fig. 3.1 E). Qualitatively, a pattern

of decreasing sulfur in the central region was easily observed for most humerus samples scanned by sulfur XRF imaging. An additional seven 4 % PFA-fixed samples were also imaged in the same manner described in Section 3.3.4 VESPERS and the trend in decreasing cartilage was also observed (data not shown). A significant decrease ($p = 0.04$) in the average total sulfur content was shown to occur in mature cartilage compared to immature cartilage. This decrease in sulfur in mature cartilage was measured on the order of 3 ± 1 % (Fig. 3.1 F). This pattern was shown consistently for 9 of 10 samples imaged at the VESPERS beamline. Sections collected which exhibited narrowing in the mature region (more peripheral and closer to the perichondrium) showed a high sulfur content coming from the perichondrium itself (Fig. 3.1 E). Very strongly COL10 immunostained regions generally fit well within the low sulfur regions (Fig. 3.1 D-E). The question of the biological significance of this small detected decrease in mature cartilage may find an answer in knowing the exact chemical form of sulfur lost, whether sulfate esters or proteins, and how this loss relates to PG levels.

3.4.2 XANES analysis of sulfur K-edge achieves a good overall fit for cartilage using five standards

A total of 8 standard sulfur compounds (those shown in Fig. 3.2 A) were normalized to their respective edge-jump values and were tested in the fitting of combined mature and immature chicken cartilage XANES spot-scans. Inorganic (free) sulfate, N-linked sulfate esters, and sulfinic acids did not contribute >1 % to the total sulfur signal and were not included in the final fit. Five chemical forms of sulfur were determined to be present at > 1% abundance. The standard curve fitting using these 5 forms of sulfur gave an acceptable fit to averaged XANES spot scans from both mature and immature cartilage (Fig 3.2 B, C) (residual = 4.7×10^{-3}, 6.2×10^{-3}, respectively). As expected, most sulfur present in these spot scans was in the form of sulfate esters (77 ± 2 % for immature and 70 ± 11 % for mature). The secondary form of sulfur in mature and immature cartilage tissue was found to be sulfonic acids at 22 ± 11 % and 14 ± 2 %, respectively. Thioethers, sulfoxides and disulfides were measured to be 7± 1 %/6 ± 2 %, 1 ± 0.1 %/ 2 ± 1 %, and 0.9 ± 0.2%/ 1.0 ± 0.4 % for immature/mature cartilage, respectively.

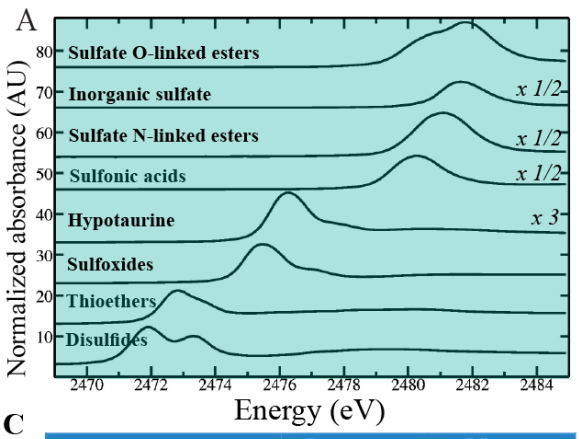

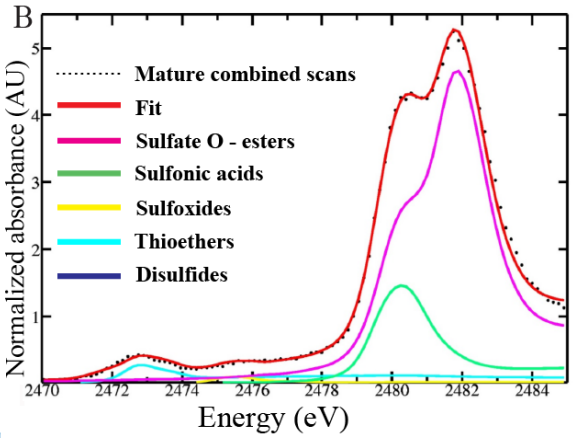

C

	Immature	Mature
Sulfate-O-esters	77 ± 2 %	70 ± 11 %
Sulfonic acids	14 ± 2 %	22 + 11 %
Thioethers	7 ± 1 %	6 ± 2 %
Disulfides	1 ± 0.1 %	2 ± 01 %
Sulfoxides	0.9 ± 0.2%	1 ± 0.4 %

Figure 3.2 Analysis of XANES spectra fittings with standard sulfur compounds has revealed the five major forms of sulfur present in chick cartilage.

The normalized standard absorption curves for a range of different forms of sulfur found in biology are shown in Panel A. The standard curve fittings for combined averaged XANES spot scans contributing >1 % abundance to mature cartilage are depicted in Panel B. The contributions of the five major forms of sulfur present in mature and immature cartilage are listed in the table in panel C. The relative abundances of the five forms of sulfur given in panel C are very similar between mature and immature cartilage. N = 4 using an averaged spectrum taken from 3-4 spots per region per sample. Error bars represent the standard error of the mean with respect to the variability of component composition between individual samples

3.4.3 Chemically specific XRF imaging reveals that PG sulfate esters decrease in mature cartilage

Chemically specific XRF maps of sulfonic acids and sulfate esters were generated for 6 humerus samples and indicated a significant decrease in sulfate ester levels in mature cartilage relative to immature cartilage. A map collected at 2474.4 eV composed of lower oxidation states of sulfur was subtracted from maps taken subsequently at 2477.6 and 2479.2 eV (Fig 3.3 A-D). A map of total sulfur taken at 2500 eV was also collected as a comparison between sulfate esters and total sulfur (Fig. 3.3 E). COL10 immunostaining on adjacent sections was used to determine the mature and immature cartilage regions as outlined by a white dotted line (Fig. 3.3 F). Sulfate esters maps were successfully generated, along with maps of sulfonic acids (Figs. 3.3 G, H). Quantitation of these images revealed that sulfate esters in mature cartilage were found to decrease significantly compared to immature cartilage, on the order of 14 ± 3% ($p = 0.008$), whereas total sulfur was found to decrease by 11 ± 4 %, though non-significantly ($p = 0.06$) (Fig. 3.3 I). Sulfonic acids, on the other hand, increased slightly (4 ± 3 %), but non-significantly ($p = 0.4$) in the mature cartilage region, and showing a large variation in patterns between samples. The much bigger difference between total sulfur and sulfate ester levels quantified at SXRMB might be partially explained by sulfonic acids increasing, whereas sulfate ester levels were found to decrease.

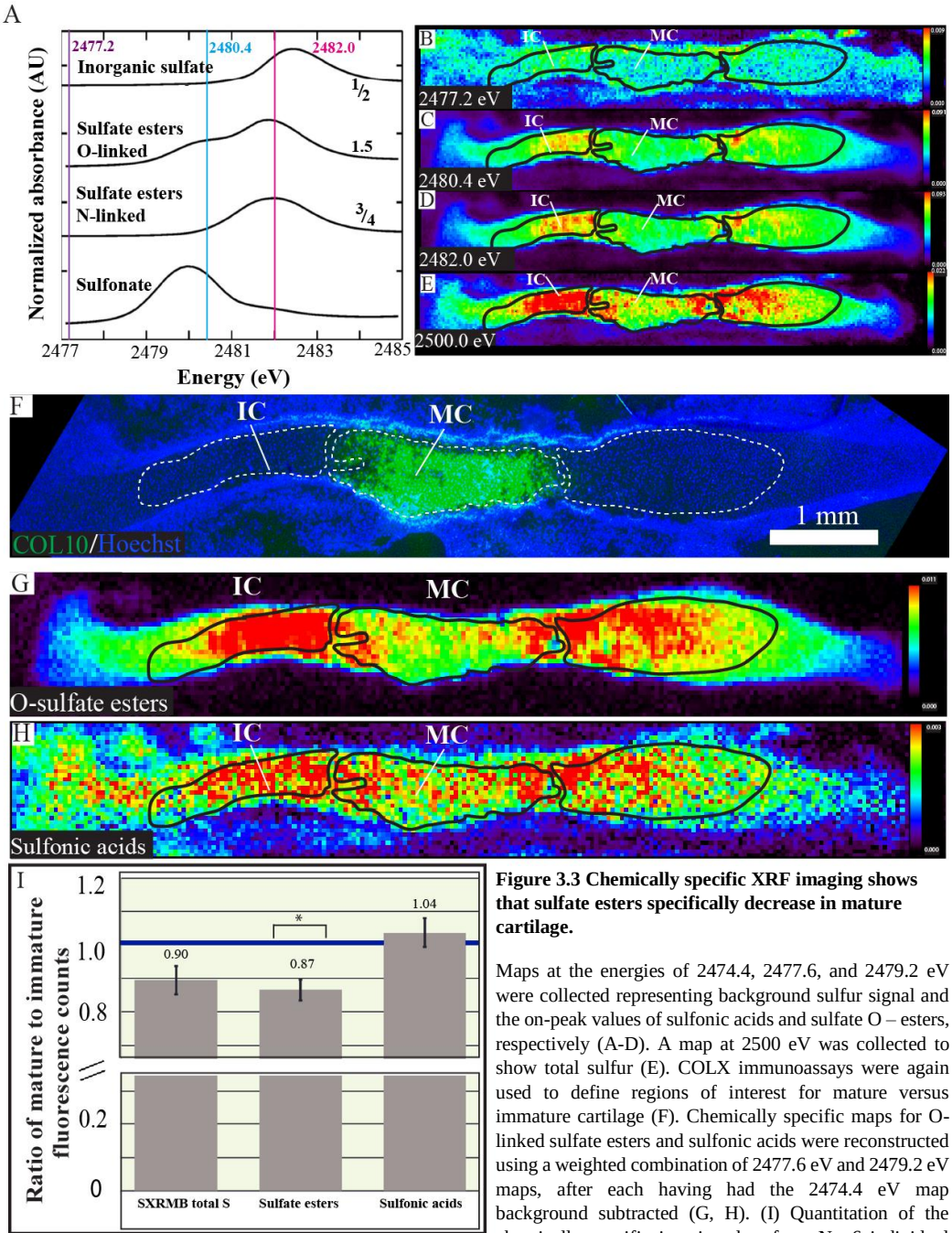

Figure 3.3 Chemically specific XRF imaging shows that sulfate esters specifically decrease in mature cartilage.

Maps at the energies of 2474.4, 2477.6, and 2479.2 eV were collected representing background sulfur signal and the on-peak values of sulfonic acids and sulfate O – esters, respectively (A-D). A map at 2500 eV was collected to show total sulfur (E). COLX immunoassays were again used to define regions of interest for mature versus immature cartilage (F). Chemically specific maps for O-linked sulfate esters and sulfonic acids were reconstructed using a weighted combination of 2477.6 eV and 2479.2 eV maps, after each having had the 2474.4 eV map background subtracted (G, H). (I) Quantitation of the chemically specific imaging data from N =6 individual chicken humeri shows that sulfate esters decreased 13 ± 3 % in mature cartilage compared to immature cartilage versus 11 ± 3 % for total sulfur. Quantitation of sulfonic acids revealed no significant difference between mature and immature cartilage. N = 6. All bars represent the mean ± standard error of the mean. Abbreviations: IC = immature cartilage; MC = mature cartilage.

3.4.4 FTIR imaging shows no significant decrease in proteins or PGs in mature cartilage

The integrated amide I peak (1590 – 1720 cm^{-1}) in the infrared spectrum map was used to depict total protein levels (3.4 A). The representative chondroitin sulfate (PG) bands 985 – 1140 cm^{-1}, and the second derivative peak at 1374 cm^{-1} are shown normalized to the amide I band to minimize tissue thickness differences (3.4 B and D). No significant differences were shown between mature and immature regions for proteins or either of the PG bands. To explore whether normalization by area scaling to the amide I band to control for thickness differences was masking differences between regions, the 985-1140 cm^{-1} integrated region was also measured without normalization to the amide I peak, and this analysis also showed no significant trend in mature PG content (Fig. 3.4 C). PGs measured with the 1374 cm^{-1} second derivative band were shown to decrease non-significantly. Regions of interest were assigned based on COL10 immunostaining of an adjacent section (Fig. 3.4 E). A side by side comparison showing the relative amounts of each of the 4 bands analyzed for mature versus immature cartilage is shown in Figure 3.4 F. FTIR image analysis reveals that in mature cartilage compared to immature cartilage, protein amide I content did not change significantly (decreasing 5 ± 3 % $p = 0.17$), while normalized PG content according to the bands 985 – 1140 cm^{-1} and 1374 cm^{-1} also did not decrease significantly (4 ± 4 %; $p = 0.25$ and 3 ± 3 %, $p = 0.33$), respectively. The non-normalized PG marker band of 985 – 1140 cm^{-1} also did not decrease significantly (7 ± 5 %; $p = 0.19$) in mature cartilage.

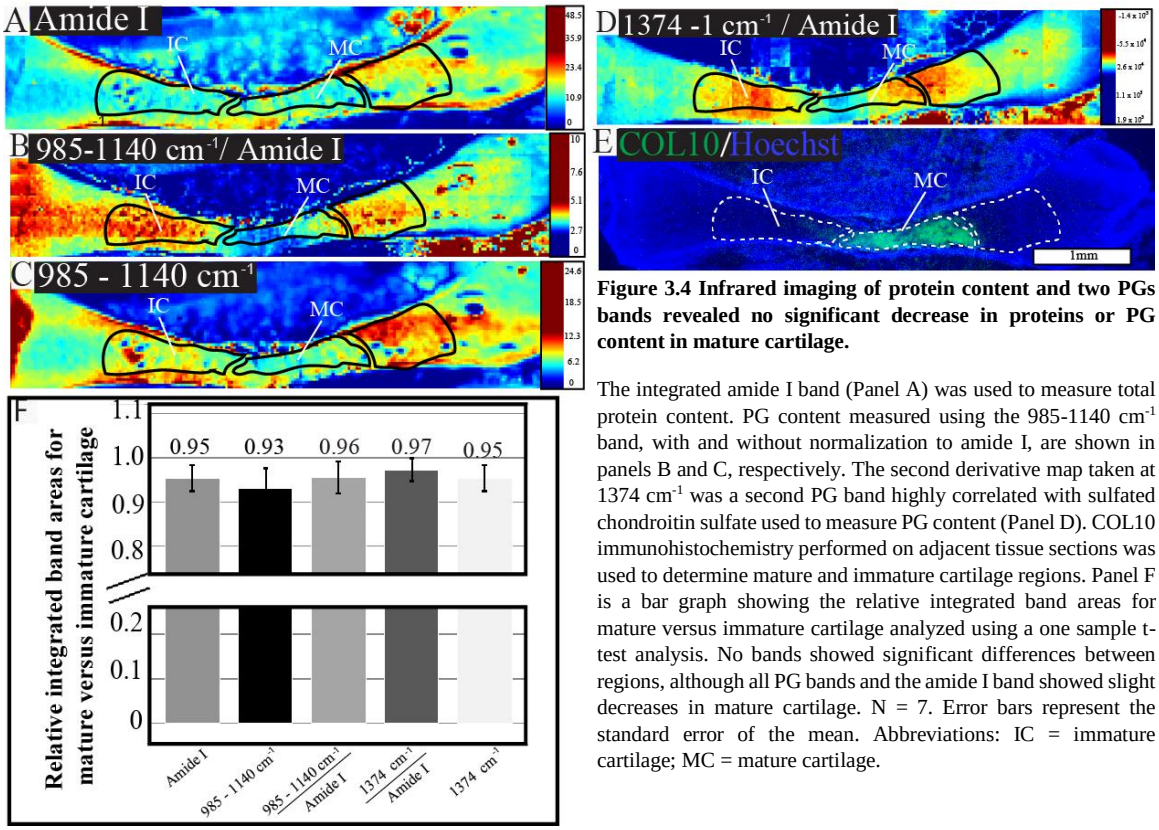

Figure 3.4 Infrared imaging of protein content and two PGs bands revealed no significant decrease in proteins or PG content in mature cartilage.

The integrated amide I band (Panel A) was used to measure total protein content. PG content measured using the 985-1140 cm^{-1} band, with and without normalization to amide I, are shown in panels B and C, respectively. The second derivative map taken at 1374 cm^{-1} was a second PG band highly correlated with sulfated chondroitin sulfate used to measure PG content (Panel D). COL10 immunohistochemistry performed on adjacent tissue sections was used to determine mature and immature cartilage regions. Panel F is a bar graph showing the relative integrated band areas for mature versus immature cartilage analyzed using a one sample t-test analysis. No bands showed significant differences between regions, although all PG bands and the amide I band showed slight decreases in mature cartilage. N = 7. Error bars represent the standard error of the mean. Abbreviations: IC = immature cartilage; MC = mature cartilage.

3.5 Discussion

The focus of this study was to present data exploring the relationship between the maturation state of cartilage and sulfate levels in the ECM and our findings did show a significant reduction in total sulfur (2.7 ± 1.1 %, p = 0.04) at the VESPERS beamline, and in sulfate esters (13 ± 3 %, p = 0.008) in mature cartilage relative to immature cartilage.

The decrease in total sulfur found (11 ± 4 % taken at SXRMB) is in agreement with a previous study using a different technique, electron probe, which showed an approximate 16 % decrease in (overall) sulfur content for spot scans in mature chick cartilage, (Hargest et al., 1985). This value could be somewhat biased compared to our data because of the much lower area examined by spot scan analysis compared to XRF image analysis. A decrease in bulk sulfur content between immature cartilage and fully mineralized cartilage was reported in pig, changing from 3.5 % to 0.2 % total dry weight (Althoff et al., 1982), although this is not a comparable decrease since we were not looking at late-stage fully mineralize cartilage. Compared to other imaging studies, our calculated value for the drop in total sulfur levels in mature cartilage is identical within the errors to the decrease in sulfur levels reported in zebrafish (11 ± 4 %, versus 11 ± 2 %), respectively (Hackett et al., 2016). Chemically specific XRF imaging based on regions given by COL10 expression have revealed a significant decrease of 13 ± 3 % in sulfate ester levels in mature cartilage.

Sulfate ester content in zebrafish was not reported so no comparison can be made (Hackett et al., 2016).

The methodology of using XRF imaging for spatially separating zones of maturation within a tissue is useful for tracking changes in the ECM occurring through process of hypertrophy, since mature chondrocytes arise adjacently from immature chondrocytes. The chemically specific imaging approach holds very important information about the matrix due to this spatial relationship between developing chondrocytes, and can even be used to zoom in at the level of the cell to see more local sulfur concentrations. There was a discrepancy in the total sulfur values for the six samples measured at both the VESPERS and SXRMB beamlines 4 ± 2 % versus 10 % ± 4 %, respectively. Due to the high energy pink beam X-rays used (15 keV), multiple elements are excited above the sulfur K-edge. Using a correlation plot to look at other elemental maps which may correlate with sulfur during total sulfur imaging at VESPERS, there seemed to be a linear trend between chlorine and sulfur levels. Chlorine is the main element of concern for overlap between K-edge peaks since chlorine is the Z+1 mass neighbour of sulfur. This is the most probable explanation of why the differences in total sulfur between immature and mature regions at VESPERS was much lower than the same measurement at SXRMB using a much lower excitation energy. The chlorine maps visually appeared to show a similar distribution to sulfur maps, but with more chlorine in the mature region than with the sulfur maps. This is a problem that does not occur at the SXRMB beamline, where monochromatic energies are used for each map.

Another expected source of error comes from the fact that the regions of interest were determined by the best fit of an adjacent section used for COL10 IHC, and that human judgement inevitably impacted to some extent where the boundaries of COL10 expression in regions were drawn. The fact that sections are adjacent to each other and not the same or identical makes it a source of error is introduced which can never be accounted for.

Sulfur XANES is a technique applicable to the determination of sulfur species contained in complex mixtures (Gambardella et al., 2015; George et al., 1991; Gnida et al., 2007; Greenfield et al., 2015; Hackett et al., 2012; Pickering et al., 1998). The same 5 sulfur species were present at greater or equal to 1 % abundance for both mature and immature cartilage. In decreasing order, these sulfoforms were: sulfate-O-esters, sulfonic acids, thioethers, disulfides, and sulfoxides. XANES spot scans estimated that 77 ± 2. % of sulfur for immature and 70 ± 11 % of sulfur for mature cartilage could be attributed to sulfate esters. Sulfate O-esters, sulfonic acids, and thioethers were all compounds identified in zebrafish cartilage by XANES measurements, though disulfides and sulfoxides were excluded from their final fit (Hackett et al., 2016). Sulfate ester degradation in the lysosome releases free sulfate as an end product of PG breakdown, and these free sulfate groups are generally not recycled back into PGs in tissue culture experiments (Harper et al., 1993; Rome and Hill, 1986). Including a free sulfate standard in our analysis, we found no free sulfate contributing to the overlapping peaks at 2478 eV. This is only to say that any sulfate esters lost in mature cartilage are not remaining as free sulfate for long in the ECM. The XANES data are based on spot sized data from individual samples, and since errors must

be added together when making a direct comparison, then statistical differences between regions for individual component comparisons (e.g. the sulfate ester difference measured by XANES spot scans for our data set would measure 8 ± 13%) could not be inferred accurately without using a larger number of spot scans.

The high levels of sulfonic acids (14 ± 2 % in immature, and 22 + 11 % in mature cartilage) are an interesting finding of this analysis, since the only other study using chemically specific XRF on developing cartilage noted negligible levels of sulfonic acids in zebrafish (Hackett et al., 2016). No significant relationship between sulfonic acid levels and maturation state was found for our samples. It is tempting to speculate that the identity of this sulfonic acid molecule could be the main sulfur donor to the sulfotransferase enzymes, phosphoadenosine phosphosulfate (PAPS)(Klaassen and Boles, 1997), especially because of the lack of a free sulfate detected by XANES fitting analysis.

FTIR analysis showed no significant changes to either PG band analyzed for mature cartilage versus immature cartilage, indicating that at least some of the sulfate esters in the mature matrix are disappearing independently of overall PG levels. The two spectral regions of 985-1140 cm^{-1} and 1374 cm^{-1} were used to represent overall PGs in the matrix (Boskey and Pleshko Camacho, 2007; Kim et al., 2005; Saarakkala et al., 2010). This method to measure CS proteoglycans is reliant on the strength of a univariate analysis which identified these two PG regions as the most significant changes seen varying with CS concentration. The 985-1140 cm^{-1} and 1374 cm^{-1} PG bands in their study were further assessed using varying amounts of Col2 and Aggrecan, by biochemical determination of GAG content based on estimates from this method, and they were also validated in articular cartilage - all of which add weight that most of the variance in these bands is due to CS, and not another component in cartilage (Boskey and Pleshko Camacho, 2007). If the PG content analysis is not faithfully estimating PG content and is overestimating losses observed in mature cartilage, then the same conclusions would be drawn from this study regardless; i.e. sulfate esters are decreasing despite no change to PG content between regions implying a loss of sulfate groups from PGs. If, however, FTIR analysis of PGs is significantly underestimating PG losses in mature cartilage, then it would weaken support for the notion that PG loss is the main reason for lowered sulfate esters in mature cartilage.

The loss of sulfate esters despite no significant loss of PGs in mature cartilage suggests two different but not exclusive possibilities as to how the sulfate levels might be changing. One possibility is that there is a less-sulfated CSPG product secreted in mature cartilage. Lowered levels of PG sulfation during mature cartilage PG synthesis compared to immature cartilage PG synthesis is not implausible - it is already known that *Carbohydrate sulfotransferase 11/Chondroitin-4-sulfotransferase-1 (CHST11/C4ST*-1)) gene expression ceases in mature cartilage, even though it is highly expressed in immature cartilage (Kluppel et al., 2002). A second possibility for disappearance of PG sulfur signals from mature cartilage is that sulfatases are acting in the ECM to release sulfate ester groups which are then removed or converted to another form of sulfur and removed through some clearance mechanism. The regulated removal of CS molecules *in-situ* in the ECM by sulfatases has not been reported in the literature; but in humans 15 sulfatases are known to

exist with 2 heparan sulfate specific sulfatases SULF1 and SULF2 acting exclusively in the ECM, and an additional 3 showing unknown substrate activity (Hanson et al., 2004).

Taken with the finding of significantly decreased sulfate esters in the matrix, and considering that no significant losses of PGs from the matrix were found, the obvious candidate for the cause of this loss of sulfate esters from that matrix is a sulfatase. Specifically, this sulfatase gene would be expected to be expressed highly in mature cartilage relative to immature cartilage, corresponding to the decrease seen for sulfate esters in mature chondrocytes. Our preliminary RNA *in-situ* hybridization analysis for *ARSB* and *GALNS* in chicken showed no substantial over-background signal (supplemental Fig. A1). Only three CS sulfatases are known, and both are found in lysosomes, although there is at least one published record of ARSB being found in the ECM in liver (Mitsunaga-Nakatsubo et al., 2009). There are other sulfatases, such as ARSJ, which have unknown substrate specificity and site of action and perhaps most interestingly, the sulfatase ARSI which has no clear substrate preference, has been shown to be secreted from human epithelial cells (Mikami and Kitagawa, 2013; Oshikawa et al., 2009). These may be good candidates for follow up studies to try to identify possible extracellular CS sulfatases.

Future studies will aim to address the exact mechanism responsible for sulfur loss in mature cartilage. It is important to keep in mind that cartilage is a mechanically responsive element, such that small local decreases in PGs can, in principle, have a large effect on mechanical forces and also growth factor distribution. Any direct evidence for the cause of differences in CS sulfation, which might lead cells towards certain developmental pathways could establish new avenues of treatment for cartilage diseases or better manipulation of artificial cartilage constructs (such as controlling range and/or the rate of growth factor diffusion). The loss of sulfated proteoglycans in mature cartilage is now shown to be a feature of endochondral bone formation that is shared for at least some bony fishes and avians, but data from more species are needed before making claims about conservation of this feature. Because of the sensitivity of XANES to sulfur neighboring groups, it would also be very interesting to see if it were possible to differentiate between and image different CS units directly, which differ only in their position(s) of sulfation.

3.6 Conclusions

Sulfate esters and PGs were visualized directly and quantitated to find out if the cartilage maturation state follows the same pattern as the sulfation status of PGs in the ECM. The hypothesis that we put forward was that sulfate esters levels decrease in mature cartilage. Indeed, sulfate ester levels were shown to decrease significantly by 13 ± 3 in mature cartilage. Sulfate ester level quantitation along with biochemical data gathered by FTIR indicates that sulfate ester levels in mature cartilage decrease, despite no significant decrease in PG levels. Two possibilities for these losses in sulfate esters include turnover of PGs with significantly less sulfation during replacement in MC, or that an uncharacterized enzyme or mechanism is removing sulfate esters from the ECM directly.

A clear connection has been demonstrated between sulfate esters levels and the maturation state of the underlying chondrocytes. This feature of endochondral bone development seems to have been passed down through vertebrates, appearing in at least both zebrafish and chicken. Sulfur is known to be critical to the function of PGs in the matrix, both biomechanically and related to the timing of development. A high amount of sulfation is required for PGs to function optimally within the skeleton. There may be a fine balance in cartilage between the high levels of sulfate esters required for optimal biomechanical functioning of PGs on one hand, and the lowering of sulfation levels to possibly sub-optimal levels at the correct time and by the correct amount to allow maturation to proceed on the other.

3.7 Supplemental

This supplemental is provided to include the results from the RNA *in-situ* hybridization experiments performed as part of my master's degree project. Gene expression data for *Galns* and *Arsb* have been published in the mouse (Ratzka et al., 2010), but not in the chicken, so the results obtained using a positive control along with data obtained from the mouse are the best indications of whether the probes and technique were successful, even if there was no strong expression shown for either probe in cartilage.

3.7.1 RNA in-situ hybridization results for GALNS and ARSB expression in stage HH36 cryo-sectioned chick humerus

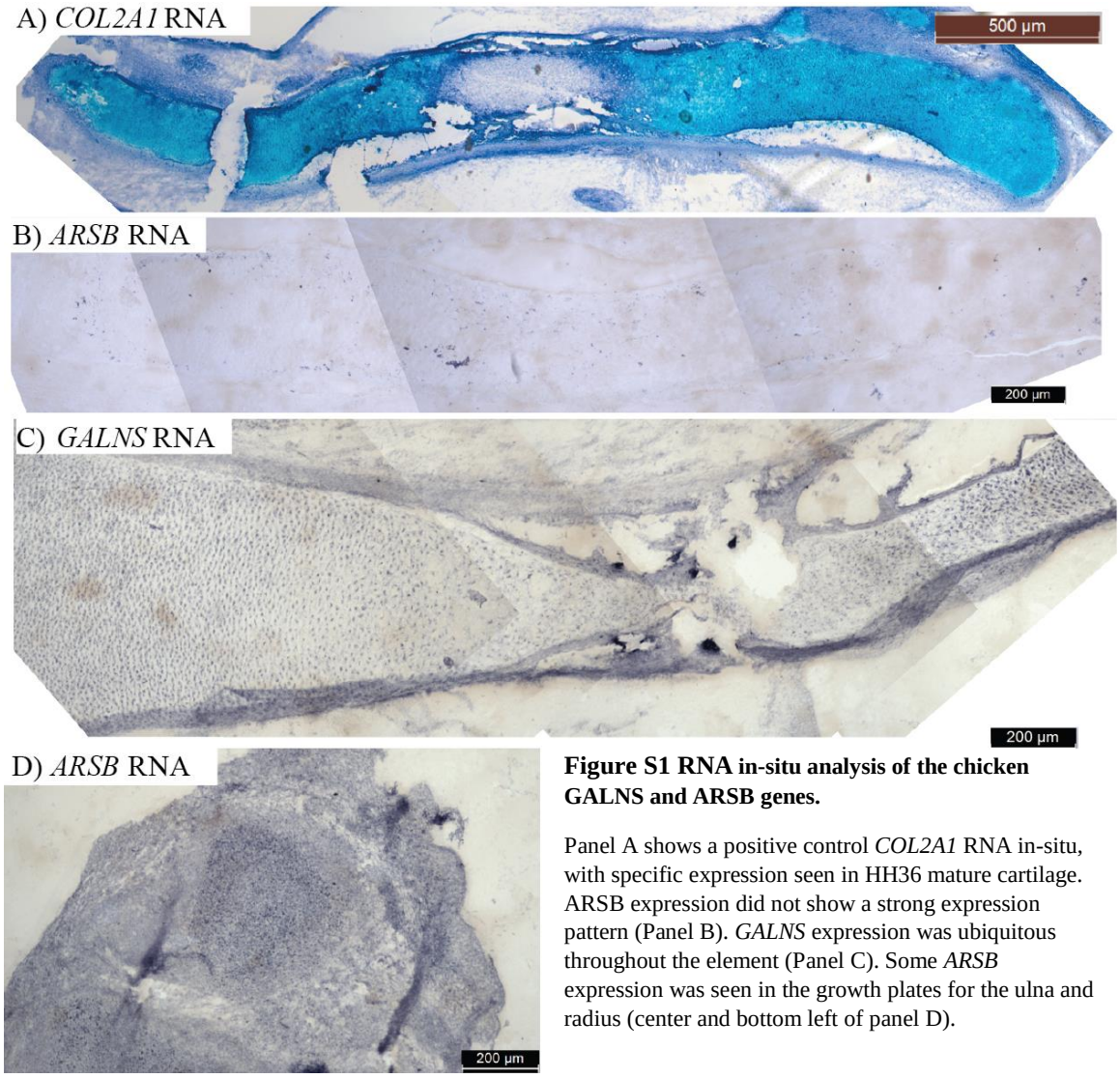

Figure S1 RNA in-situ analysis of the chicken GALNS and ARSB genes.

Panel A shows a positive control *COL2A1* RNA in-situ, with specific expression seen in HH36 mature cartilage. ARSB expression did not show a strong expression pattern (Panel B). *GALNS* expression was ubiquitous throughout the element (Panel C). Some *ARSB* expression was seen in the growth plates for the ulna and radius (center and bottom left of panel D).

3.8 Acknowledgements

We wish to thank Mark Hackett for helping to generate and represent the synchrotron imaging data, Patsy Gómes-Picos for her help with designing RNA *in-situ* hybridization probes. Research described in this paper was performed at the Canadian Light Source, which is supported by the Canada Foundation for Innovation, Natural Sciences and Engineering Research Council of Canada, the University of Saskatchewan, the Government of Saskatchewan, Western Economic Diversification Canada, the National Research Council Canada, and the Canadian Institutes of Health Research.

This work was supported by the UofS and CIHR-THRUST awards to DB; and Saskatchewan Health Research Foundation, NSERC, and CIHR grants to BFE.

CHAPTER 4

4.1 Discussion and Conclusions

Sulfated PGs in the cartilage ECM are necessary for normal biomechanical functioning of this tissue; but losses in PGs or sulfur regulating enzymes are known to cause severe growth defects related to altered maturation timing in chondrocytes. The hypothesis set out in Chapter 3 for the research based component of my thesis was that sulfate esters disappear from mature cartilage during endochondral bone development. The results of this research have provided valuable information regarding the spatial regulation of sulfur in development.

Total sulfur elemental mapping as well as chemically specific mapping was successfully carried out and differences were tested for statistical significance between mature and immature cartilage developmental regions. Previous findings have reported decreasing sulfur levels in mature cartilage based on a single chick electron probe study and one study in zebrafish. We reported a 10 ± 4 % decrease in total sulfur in mature cartilage in chicken at SXRMB. In zebrafish, XRF imaging analysis revealed a decrease of 11 ± 2 % (Hackett et al., 2016), which matches very closely with our data, even across species. A 16 % decrease was reported for sulfur levels in mature chicken cartilage measured by electron probe (spot scans), which is a slightly higher decrease than our estimate (Hargest et al., 1985). Our approach was technically limited because of the use of adjacent sections to define regions of interest, leading to a source of error in defining our mature and immature regions for analysis. In the future, sections used for synchrotron imaging would be best conserved and used for immunostaining to define regions more precisely. A similar limitation in drawing the regions by hand came from the human error associated with drawing regions, even though the approach was to base this drawing on marker protein expression. Even with the variability between immunostaining different tissues on different days, it would be good to run the analysis again with a computer assisted brightness cut-off value to see if very strong COL10 expression (capturing only morphologically mature chondrocytes) correlated any better with sulfur levels than we found in this study as we suspect it may.

FTIR imaging was used to get a measure of PG content differences between mature and immature cartilage regions in developing chick cartilage. The two bands used (985 – 1140 cm^{-1} and the 1374 cm^{-1} 2^{nd} derivative peak) were shown to be highly correlated with CS content in cartilage cell culture, articular cartilage sections, and in standard mixtures of PGs and collagen (Boskey and Pleshko Camacho, 2007; Kim et al., 2005; Saarakkala and Julkunen, 2010). Our analysis indicated that no significant decrease in PG content was occurring in mature cartilage compared to immature cartilage. These results suggest that the loss of sulfate esters in mature cartilage is not due to a loss in overall PGs from these regions. The two main possibilities that we suggest are that either sulfate esters are being

lost directly in the matrix due to the action of an unidentified sulfatase, or else that PGs are being recycled in this region with less sulfation upon their synthesis and re-secretion.

The many processes involved in PG synthesis and their turnover by the cell were outlined in Chapter 2. Human Aggrecan molecules in the growth plate have been estimated to have a three and a half year half-life, with smaller fragments estimated to persist for up to 20 years (Maroudas et al., 1998). At the same time, the pattern of sulfation happens throughout the lifetime of an individual, shifting towards more 6-O sulfation of GalNAc residues of CS. The sulfatase enzymes are required within cells to remove the sulfate groups for endoglycosidases in the lysosome to be able to degrade PGs into constituent monosaccharides (Diez-Roux and Ballabio, 2005; Hanson et al., 2004). Heparin/Heparan sulfate is known to interact with hormones and growth factors in the ECM, playing important roles in development, but this idea is not readily extended to the CS proteoglycans (Otsuki et al., 2010). The lysosomal CS sulfatase Arsb has been reported to be found pericellularly in mouse liver cells (Elvevold et al., 2008; Mitsunaga-Nakatsubo et al., 2009), and there remains a number of uncharacterized putative sulfatases which may be active in the ECM towards chondroitin sulfate (Ratzka et al., 2010).

The hypothesis put forth was ultimately supported based on quantitative sulfate ester XRF imaging analysis and FTIR imaging analysis for PG content in developing chick cartilage. Future studies should focus on identification of a sulfatase which could be acting to reduce sulfate esters in the ECM independently of PG degradation. This could be achieved with differential gene expression analysis to look for upregulated sulfatase genes found in mature cartilage compared to immature cartilage. Chemically specific XRF imaging is a powerful tool which can reveal much in the way of health-related information about a given sample. Osteoarthritis is one such example of a research field which could benefit from the use of chemically specific imaging to look at early signs of OA lesions. Critical losses of sulfate ester groups from the ECM in OA lesions, could be related to changes in the underlying state of chondrocytes in osteoarthritic tissue. It may be interesting to see what is happening to the sulfur pool in cartilage when sulfur is clearly not being replaced quickly enough to repair tissue – perhaps it is locked up in a different chemical state due to metabolic stresses places on this tissue, and perhaps this could lead to a shift in our understanding of how to re-energize the normal PG synthesis pathway.

APPENDIX

Appendix – OA Human Knee Imaging Study Overview

Introduction

Osteoarthritis is a not a degenerative disease of cartilage, but rather, it is a mechanical failure of function in areas of overloading causing irreplaceable damage to an articular cartilage surface which is actively trying to repair itself (Dieppe, 2011). The abnormalities in osteoarthritic cartilage which have been reported as pathologies, such as elevated cytokines, toxic radicals, and matrix degrading enzymes might be more accurately viewed as results of cartilage attempting to repair itself rather than a run-away process (Brandt et al., 2008, 2009). Articular chondrocytes implicated in the disease process exhibit many similarities to chondrocytes undergoing normal development which are closely related to the degradation of the extracellular matrix (ECM) and joint integrity (Pitsillides and Beier, 2011).

Sulfated proteoglycans (PGs) play a major role in resistance to compressive forces (Aumailley and Gayraud, 1998; Chahine et al., 2005), but as with losses of PG as seen in OA, there is a growing body of evidence that implicates developmental processes in the etiology of the disease (Pitsillides and Beier, 2011). In mutant animal models of cartilage diseases, lowered levels of PGs lead to stunting of bone growth, as well as precocious maturation of chondrocytes and early bone formation (Cortes et al., 2009; Domowicz et al., 2009; Eames et al., 2011; Hackett et al., 2016). Sulfate ester levels in normal zebrafish were shown to be correlated with the maturation state of the underlying cartilage (Hackett et al., 2016). The sulfation pattern of the most abundant cartilage PG, chondroitin sulfate (CS), refers to the ratio of 4-sulfated versus 6-sulfated CS disaccharides, and this has been shown to decreases through the normal course of ageing (even though healthy cartilage thickness does not change significantly with age)(Bayliss et al., 1999).

Chemically specific sulfur imaging is a valuable technique which can reveal the spatial distribution of both high and low oxidation state specific chemical forms of sulfur present in biological samples (Pickering et al., 1998; Pickering et al., 2009). Having previously characterized sulfate ester levels in chick cartilage during maturation (Chapter 3), we showed that decreases in sulfate ester levels were significantly correlated with cartilage maturation and also showed the differences in sulfur chemical speciation between regions by the use of X-ray absorption near edge structure (XANES) spectroscopy spot scan analysis. The hypothesis that we wanted to test with this OA human knee sample data set was that sulfate ester levels decrease first in the middle and deep zones (where most of the compressive strength is found) of damaged cartilage. This study would also be an exploration of the different chemical forms of sulfur present distributed in OA and non-OA tissue to look for key differences in how this sulfur is metabolised differently in the

two cases. The data set collected was a qualitative set of images from one OA knee sample imaged at both the VESPERS and SXRMB beamlines at the Canadian Light Source (CLS) to look for any observable trends (Fig. A1).

5.1.2 Results and Discussion

Qualitatively, chemically specific XRF imaging of sulfate esters shows major differences in sulfate ester, sulfonic acids, and phosphorus levels between OA lesion tissue and adjacent healthy cartilage, along with zone specific changes. Chemically specific XRF imaging was carried out at the SXRMB beamline at the CLS for one sample of OA tissue obtained from a knee replacement donor program. Four other samples comprising two OA samples obtained through the total knee replacement donor program, and two age-matched control samples obtained through the body bequeathal program were also imaged for total sulfur at the VESPERS beamline at the CLS (data not shown). Close-up images of the medial tibial plateau taken before cryosectioning (Fig. S1, panels A and B) shows a translucent appearance to cartilage and a milky white appearance (presumably the calcified layer of cartilage and underlying bone). The overall thickness of the normal appearing cartilage adjacent to the defect (panel C) is much greater than that within the defect (panel D). Chemically specific imaging was carried out at two locations, one at a normal adjacent cartilage site, and the other one at the defect (boxes, panel E). Chemical maps were processed for total sulfur, sulfate esters, sulfonic acids, and phosphorus in normal cartilage and the defect (Panel F). As can be seen in panel C, the presumptive cartilage region has higher levels of sulfur. Cell clusters in normal appearing cartilage are distributed evenly throughout the presumptive middle and deep zones. In the high resolution 4x4 images in panel C, the interterritorial cartilage, which is a region closely surrounding articular chondrocytes clusters, is seen as circles of very high sulfur content. It is thought that this territorial zone thickness is protectant of articular chondrocytes and contributes to their resilience (Muir, 1995). In comparison, OA regions 5 and 6 (panel D), which appear closest to the center of the defect, show very decreased levels of total sulfur. The highest levels of sulfur are in the presumptive underlying bone region, most obvious in zone 6 cartilage, where the remaining cartilage is the thinnest (panel D). Coincidentally, cells lose their even distribution pattern as well in zone 5 compared to zones 4 and 6. Territorial region as seen in the 4x4 images in panel D show no distinct demarcation of territorial bundles in zones 4 and 5; but interestingly, it shows up again in zone 6, which may be an indicator of regeneration. Chemically specific imaging of cartilage (panel F) reveals that total sulfur distribution shows differences with sulfate ester distribution in the cartilage of OA defect tissue, even though these two maps look very similar in normal thickness cartilage. Specifically, total sulfur levels dropped dramatically in the OA sample across all regions. Surprisingly, sulfate ester levels did not follow the same trend as total sulfur, and appeared to decrease most dramatically in lower regions, likely subchondral bone. Sulfonic acids may be one of the causes for this difference between sulfate esters and total sulfur, as they showed a major loss in superficial and deep regions. Phosphorus, which is associated with

matrix mineralization, was increased moderately in the superficial and deep regions. Interpreting whether this phosphorus change is real or artefactual is difficult because tissues were formalin fixed and demineralized, and phosphorus is a soluble ion.

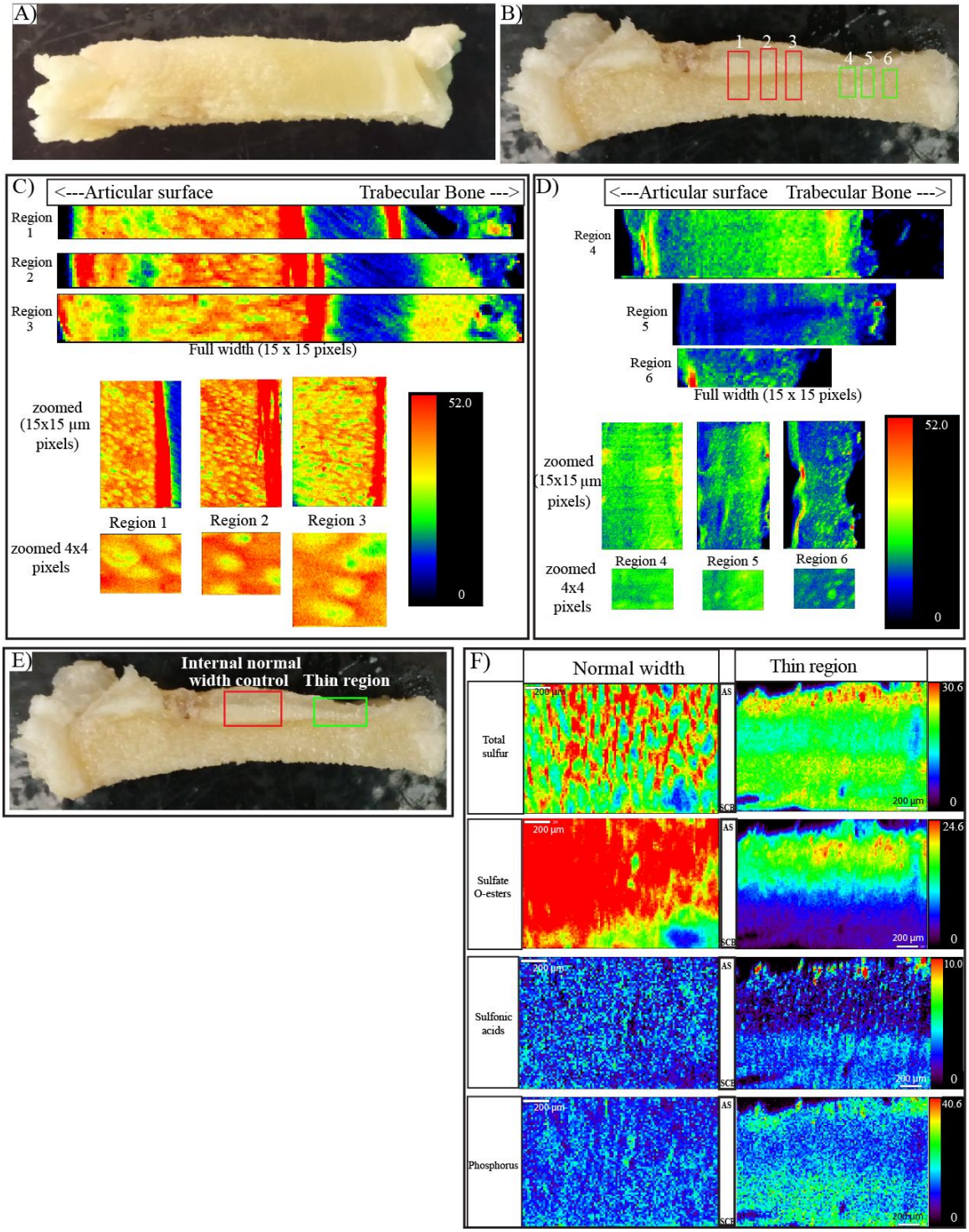
A)
B)
1 2 3
4 5 6
C)
<---Articular surface
Trabecular Bone --->
Region 1
Region 2
Region 3
Full width (15 x 15 pixels)
zoomed (15x15 µm pixels)
zoomed 4x4 pixels
Region 1
Region 2
Region 3
52.0
0
D)
<---Articular surface
Trabecular Bone --->
Region 4
Region 5
Region 6
Full width (15 x 15 pixels)
zoomed (15x15 µm pixels)
zoomed 4x4 pixels
Region 4
Region 5
Region 6
52.0
0
E)
Internal normal width control
Thin region
F)
Normal width
Thin region
Total sulfur
Sulfate O-esters
Sulfonic acids
Phosphorus
200 µm
AS
SCB
30.6
24.6
10.0
40.6
0

Figure A1 OA human knee imaging study overview.

Total sulfur and chemical specific XRF imaging analysis shows dramatic losses of total sulfur and sulfate O-esters in the OA defect, as well as differences in sulfonic acids and phosphorus distribution. The demineralized OA medial tibial plateau (A, B) was cut down in size and sectioned to 10 µm thickness for XRF imaging. Regions 1, 2, and 3 exhibited no evident wear and were relatively normal thickness for use as an internal normal control. Regions 4, 5, and 6 are directly from or adjacent to the defective area exhibiting very thin cartilage (B). Normal thickness cartilage was imaged at 15 × 15 µm and 4x4 pixel size to show sulfur distribution at different scales (C). Defective cartilage exhibited much less sulfur in across the thickness of the tissue (D). In region 6, closest to the defect, sulfur in the matrix was highly restricted to areas pericellular to chondrocyte clusters. Regions used for chemical specific imaging focused in below the articular cartilage to show a wider portion of the sample (E). Chemical specific imaging maps of total sulfur, sulfate O-esters, sulfonic acids, and phosphorus are shown for normal width and focal defect regions (F). Total sulfur decreased everywhere in the defective cartilage compared to normal control cartilage, but due to the disturbed zonal structure of the OA defect, conclusions on exact regional differences can not be drawn. Sulfate O-esters decreased throughout the chondral defect, but showed interesting differences from total sulfur; whereas phosphorus, a marker of calcification, increased in the cartilage defect. Abbreviations: AS = towards articular surface; OA = osteoarthritis; SCB = towards subchondral bone.

REFERENCES

Ali, S., Champagne, D.L., Spaink, H.P., Richardson, M.K., 2011. Zebrafish embryos and larvae: a new generation of disease models and drug screens. Birth Defects Res C Embryo Today 93, 115-133.

Alliston, T., 2010. Chondroitin sulfate and growth factor signalling in the skeleton: Possible links to MPS VI. J Pediatr Rehabil Med 3, 129-138.

Althoff, J., Quint, P., Krefting, E.R., Hohling, H.J., 1982. Morphological studies on the epiphyseal growth plate combined with biochemical and X-ray microprobe analyses. Histochemistry 74, 541-552.

Anggraeni, V.Y., Emoto, N., Yagi, K., Mayasari, D.S., Nakayama, K., Izumikawa, T., Kitagawa, H., Hirata, K., 2011. Correlation of C4ST-1 and ChGn-2 expression with chondroitin sulfate chain elongation in atherosclerosis. Biochem Biophys Res Commun 406, 36-41.

arc, O.C., arc, O.C., Zeggini, E., Panoutsopoulou, K., Southam, L., Rayner, N.W., Day-Williams, A.G., Lopes, M.C., Boraska, V., Esko, T., Evangelou, E., Hoffman, A., Houwing-Duistermaat, J.J., Ingvarsson, T., Jonsdottir, I., Jonnson, H., Kerkhof, H.J., Kloppenburg, M., Bos, S.D., Mangino, M., Metrustry, S., Slagboom, P.E., Thorleifsson, G., Raine, E.V., Ratnayake, M., Ricketts, M., Beazley, C., Blackburn, H., Bumpstead, S., Elliott, K.S., Hunt, S.E., Potter, S.C., Shin, S.Y., Yadav, V.K., Zhai, G., Sherburn, K., Dixon, K., Arden, E., Aslam, N., Battley, P.K., Carluke, I., Doherty, S., Gordon, A., Joseph, J., Keen, R., Koller, N.C., Mitchell, S., O'Neill, F., Paling, E., Reed, M.R., Rivadeneira, F., Swift, D., Walker, K., Watkins, B., Wheeler, M., Birrell, F., Ioannidis, J.P., Meulenbelt, I., Metspalu, A., Rai, A., Salter, D., Stefansson, K., Stykarsdottir, U., Uitterlinden, A.G., van Meurs, J.B., Chapman, K., Deloukas, P., Ollier, W.E., Wallis, G.A., Arden, N., Carr, A., Doherty, M., McCaskie, A., Willkinson, J.M., Ralston, S.H., Valdes, A.M., Spector, T.D., Loughlin, J., 2012. Identification of new susceptibility loci for osteoarthritis (arcOGEN): a genome-wide association study. Lancet 380, 815-823.

Ashworth, J.L., Biswas, S., Wraith, E., Lloyd, I.C., 2006. The ocular features of the mucopolysaccharidoses. Eye (Lond) 20, 553-563.

Aumailley, M., Gayraud, B., 1998. Structure and biological activity of the extracellular matrix. J Mol Med (Berl) 76, 253-265.

Avram, S., Shaposhnikov, S., Buiu, C., Mernea, M., 2014. Chondroitin sulfate proteoglycans: structure-function relationship with implication in neural development and brain disorders. Biomed Res Int 2014, 642798.

Baasanjav, S., Al-Gazali, L., Hashiguchi, T., Mizumoto, S., Fischer, B., Horn, D., Seelow, D., Ali, B.R., Aziz, S.A., Langer, R., Saleh, A.A., Becker, C., Nurnberg, G., Cantagrel, V., Gleeson, J.G., Gomez, D., Michel, J.B., Stricker, S., Lindner, T.H., Nurnberg, P., Sugahara, K., Mundlos, S., Hoffmann, K., 2011. Faulty initiation of proteoglycan synthesis causes cardiac and joint defects. Am J Hum Genet 89, 15-27.

Baker, M.J., Trevisan, J., Bassan, P., Bhargava, R., Butler, H.J., Dorling, K.M., Fielden, P.R., Fogarty, S.W., Fullwood, N.J., Heys, K.A., Hughes, C., Lasch, P., Martin-Hirsch, P.L., Obinaju, B., Sockalingum, G.D., Sule-Suso, J., Strong, R.J., Walsh, M.J., Wood, B.R., Gardner, P., Martin, F.L., 2014. Using Fourier transform IR spectroscopy to analyze biological materials. Nat Protoc 9, 1771-1791.

Bakker, H., Oka, T., Ashikov, A., Yadav, A., Berger, M., Rana, N.A., Bai, X., Jigami, Y., Haltiwanger, R.S., Esko, J.D., Gerardy-Schahn, R., 2009. Functional UDP-xylose transport across the endoplasmic reticulum/Golgi membrane in a Chinese hamster ovary cell mutant defective in UDP-xylose Synthase. J Biol Chem 284, 2576-2583.

Bandtlow, C.E., Zimmermann, D.R., 2000. Proteoglycans in the developing brain: new conceptual insights for old proteins. Physiol Rev 80, 1267-1290.
Banfield, B.W., Leduc, Y., Esford, L., Schubert, K., Tufaro, F., 1995. Sequential isolation of proteoglycan synthesis mutants by using herpes simplex virus as a selective agent: evidence for a proteoglycan-independent virus entry pathway. J Virol 69, 3290-3298.
Bayliss, M.T., Osborne, D., Woodhouse, S., Davidson, C., 1999. Sulfation of chondroitin sulfate in human articular cartilage. The effect of age, topographical position, and zone of cartilage on tissue composition. J Biol Chem 274, 15892-15900.
Beahm, B.J., Dehnert, K.W., Derr, N.L., Kuhn, J., Eberhart, J.K., Spillmann, D., Amacher, S.L., Bertozzi, C.R., 2014. A visualizable chain-terminating inhibitor of glycosaminoglycan biosynthesis in developing zebrafish. Angew Chem Int Ed Engl 53, 3347-3352.
Bernfield, M., Gotte, M., Park, P.W., Reizes, O., Fitzgerald, M.L., Lincecum, J., Zako, M., 1999. Functions of cell surface heparan sulfate proteoglycans. Annu Rev Biochem 68, 729-777.
Bhattacharyya, S., Feferman, L., Tobacman, J.K., 2015. Regulation of chondroitin-4-sulfotransferase (CHST11) expression by opposing effects of arylsulfatase B on BMP4 and Wnt9A. Biochim Biophys Acta 1849, 342-352.
Borlot, F., Arantes, P.R., Quaio, C.R., Franco, J.F., Lourenco, C.M., Bertola, D.R., Kim, C.A., 2014. New insights in mucopolysaccharidosis type VI: neurological perspective. Brain Dev 36, 585-592.
Boskey, A., Pleshko Camacho, N., 2007. FT-IR imaging of native and tissue-engineered bone and cartilage. Biomaterials 28, 2465-2478.
Bostrom, H., 1952. On the metabolism of the sulfate group of chondroitinsulfuric acid. J Biol Chem 196, 477-481.
Bowman, K.G., Bertozzi, C.R., 1999. Carbohydrate sulfotransferases: mediators of extracellular communication. Chem Biol 6, R9-R22.
Brandt, K.D., Dieppe, P., Radin, E.L., 2008. Etiopathogenesis of osteoarthritis. Rheum Dis Clin North Am 34, 531-559.
Brandt, K.D., Dieppe, P., Radin, E.L., 2009. Commentary: is it useful to subset "primary" osteoarthritis? A critique based on evidence regarding the etiopathogenesis of osteoarthritis. Semin Arthritis Rheum 39, 81-95.
Braunlin, E., Orchard, P.J., Whitley, C.B., Schroeder, L., Reed, R.C., Manivel, J.C., 2014. Unexpected coronary artery findings in mucopolysaccharidosis. Report of four cases and literature review. Cardiovasc Pathol 23, 145-151.
Bray, H.G., Gregory, J.E., Stacey, M., 1944. Chemistry of tissues: I. Chondroitin from cartilage. Biochem J 38, 142-146.
Brown, D.S., Eames, B.F., 2016. Emerging tools to study proteoglycan function during skeletal development. Methods Cell Biol 134, 485-530.
Brown, G.M., Huckerby, T.N., Bayliss, M.T., Nieduszynski, I.A., 1998. Human aggrecan keratan sulfate undergoes structural changes during adolescent development. J Biol Chem 273, 26408-26414.
Calabro, A., Hascall, V.C., 1994. Differential effects of brefeldin A on chondroitin sulfate and hyaluronan synthesis in rat chondrosarcoma cells. J Biol Chem 269, 22764-22770.
Campbell, S.C., Schwartz, N.B., 1988. Kinetics of intracellular processing of chondroitin sulfate proteoglycan core protein and other matrix components. J Cell Biol 106, 2191-2202.
Chahine, N.O., Chen, F.H., Hung, C.T., Ateshian, G.A., 2005. Direct measurement of osmotic pressure of glycosaminoglycan solutions by membrane osmometry at room temperature. Biophys J 89, 1543-1550.

Chen, J., Sun, S., Zhou, Q., 2013. Direct observation of bulk and surface chemical morphologies of Ginkgo biloba leaves by Fourier transform mid- and near-infrared microspectroscopic imaging. Anal Bioanal Chem 405, 9385-9400.
Chonanant, C., Bambery, K.R., Jearanaikoon, N., Chio-Srichan, S., Limpaiboon, T., Tobin, M.J., Heraud, P., Jearanaikoon, P., 2014. Discrimination of micromass-induced chondrocytes from human mesenchymal stem cells by focal plane array-Fourier transform infrared microspectroscopy. Talanta 130, 39-48.
Choocheep, K., Hatano, S., Takagi, H., Watanabe, H., Kimata, K., Kongtawelert, P., Watanabe, H., 2010. Versican facilitates chondrocyte differentiation and regulates joint morphogenesis. J Biol Chem 285, 21114-21125.
Cichocki, T., Gonsior, B., Hofert, M., Jarczyk, L., Raith, B., Rokita, E., Strzalkowski, A., Sych, M., 1989. The analysis of mineral deposits and proteoglycans content in the cartilage of mouse trachea using PIXE in combination with proton microprobe. Acta histochemica 85, 39-45.
Clement, A., Wiweger, M., von der Hardt, S., Rusch, M.A., Selleck, S.B., Chien, C.B., Roehl, H.H., 2008. Regulation of zebrafish skeletogenesis by ext2/dackel and papst1/pinscher. PLoS Genet 4, e1000136.
Cortes, M., Baria, A.T., Schwartz, N.B., 2009. Sulfation of chondroitin sulfate proteoglycans is necessary for proper Indian hedgehog signalling in the developing growth plate. Development 136, 1697-1706.
Dale, R.M., Topczewski, J., 2011. Identification of an evolutionarily conserved regulatory element of the zebrafish col2a1a gene. Dev Biol 357, 518-531.
de Jonge, M.D., Vogt, S., 2010. Hard X-ray fluorescence tomography--an emerging tool for structural visualization. Curr Opin Struct Biol 20, 606-614.
DeLaurier, A., Eames, B.F., Blanco-Sanchez, B., Peng, G., He, X., Swartz, M.E., Ullmann, B., Westerfield, M., Kimmel, C.B., 2010. Zebrafish sp7:EGFP: a transgenic for studying otic vesicle formation, skeletogenesis, and bone regeneration. Genesis 48, 505-511.
Dennis, J.W., Nabi, I.R., Demetriou, M., 2009. Metabolism, cell surface organization, and disease. Cell 139, 1229-1241.
Derenne, A., Vandersleyen, O., Goormaghtigh, E., 2014. Lipid quantification method using FTIR spectroscopy applied on cancer cell extracts. Biochim Biophys Acta 1841, 1200-1209.
Deutsch, A.J., Midura, R.J., Plaas, A.H., 1995. Structure of chondroitin sulfate on aggrecan isolated from bovine tibial and costochondral growth plates. J Orthop Res 13, 230-239.
Dhamale, O.P., Lawrence, R., Wiegmann, E.M., Shah, B.A., Al-Mafraji, K., Lamanna, W.C., Lubke, T., Dierks, T., Boons, G.J., Esko, J.D., 2017. Arylsulfatase K is the Lysosomal 2-Sulfoglucuronate Sulfatase. ACS Chem Biol 12, 367-373.
Dick, G., Akslen-Hoel, L.K., Grondahl, F., Kjos, I., Prydz, K., 2012. Proteoglycan synthesis and Golgi organization in polarized epithelial cells. J Histochem Cytochem 60, 926-935.
Dieppe, P., 2011. Developments in osteoarthritis. Rheumatology (Oxford) 50, 245-247.
Diez-Roux, G., Ballabio, A., 2005. Sulfatases and human disease. Annu Rev Genomics Hum Genet 6, 355-379.
Doege, K.J., Garrison, K., Coulter, S.N., Yamada, Y., 1994. The structure of the rat aggrecan gene and preliminary characterization of its promoter. J Biol Chem 269, 29232-29240.
Domowicz, M.S., Cortes, M., Henry, J.G., Schwartz, N.B., 2009. Aggrecan modulation of growth plate morphogenesis. Dev Biol 329, 242-257.
Doms, R.W., Russ, G., Yewdell, J.W., 1989. Brefeldin A redistributes resident and itinerant Golgi proteins to the endoplasmic reticulum. J Cell Biol 109, 61-72.
Eames, B.F., de la Fuente, L., Helms, J.A., 2003. Molecular ontogeny of the skeleton. Birth Defects Res C Embryo Today 69, 93-101.

Eames, B.F., DeLaurier, A., Ullmann, B., Huycke, T.R., Nichols, J.T., Dowd, J., McFadden, M., Sasaki, M.M., Kimmel, C.B., 2013. FishFace: interactive atlas of zebrafish craniofacial development at cellular resolution. BMC Dev Biol 13, 23.
Eames, B.F., Sharpe, P.T., Helms, J.A., 2004. Hierarchy revealed in the specification of three skeletal fates by Sox9 and Runx2. Dev Biol 274, 188-200.
Eames, B.F., Singer, A., Smith, G.A., Wood, Z.A., Yan, Y.L., He, X., Polizzi, S.J., Catchen, J.M., Rodriguez-Mari, A., Linbo, T., Raible, D.W., Postlethwait, J.H., 2010. UDP xylose synthase 1 is required for morphogenesis and histogenesis of the craniofacial skeleton. Dev Biol 341, 400-415.
Eames, B.F., Swartz, M.E., Kimmel, C.B., 2008. Fam20b and Xylosyltransferase1 (Xylt1) drive cartilage matrix production and inhibit perichondral bone during endochondral ossification. Dev Biol 319, 480.
Eames, B.F., Yan, Y.L., Swartz, M.E., Levic, D.S., Knapik, E.W., Postlethwait, J.H., Kimmel, C.B., 2011. Mutations in fam20b and xylt1 reveal that cartilage matrix controls timing of endochondral ossification by inhibiting chondrocyte maturation. PLoS Genet 7, e1002246.
El-Khoury, R., Marcopoulos, C.M., Marcopoulos, C., Moukheiber, C., University of Toronto. Faculty of Architecture, L., Design, 2012. Make Alive: Prototypes for Responsive Architectures. Oscar Riera Ojeda Publishers Limited.
Elvevold, K., Simon-Santamaria, J., Hasvold, H., McCourt, P., Smedsrod, B., Sorensen, K.K., 2008. Liver sinusoidal endothelial cells depend on mannose receptor-mediated recruitment of lysosomal enzymes for normal degradation capacity. Hepatology 48, 2007-2015.
Esko, J.D., 1992. Animal cell mutants defective in heparan sulfate polymerization. Adv Exp Med Biol 313, 97-106.
Esko, J.D., Lindahl, U., 2001. Molecular diversity of heparan sulfate. J Clin Invest 108, 169-173.
Esko, J.D., Selleck, S.B., 2002. Order out of chaos: assembly of ligand binding sites in heparan sulfate. Annu Rev Biochem 71, 435-471.
Fahrni, C.J., 2007. Biological applications of X-ray fluorescence microscopy: exploring the subcellular topography and speciation of transition metals. Curr Opin Chem Biol 11, 121-127.
Farquharson, C., Whitehead, C.C., Loveridge, N., 1994. Alterations in glycosaminoglycan concentration and sulfation during chondrocyte maturation. Calcif Tissue Int 54, 296-303.
Faundes, V., Castillo-Taucher, S., Gonzalez-Hormazabal, P., Chandler, K., Crosby, A., Chioza, B., 2014. Raine syndrome: an overview. Eur J Med Genet 57, 536-542.
Felson, D.T., Lawrence, R.C., Dieppe, P.A., Hirsch, R., Helmick, C.G., Jordan, J.M., Kington, R.S., Lane, N.E., Nevitt, M.C., Zhang, Y., Sowers, M., McAlindon, T., Spector, T.D., Poole, A.R., Yanovski, S.Z., Ateshian, G., Sharma, L., Buckwalter, J.A., Brandt, K.D., Fries, J.F., 2000. Osteoarthritis: new insights. Part 1: the disease and its risk factors. Ann Intern Med 133, 635-646.
Flanagan-Steet, H.R., Steet, R., 2013. "Casting" light on the role of glycosylation during embryonic development: insights from zebrafish. Glycoconj J 30, 33-40.
Fransson, L.A., Karlsson, P., Schmidtchen, A., 1992. Effects of cycloheximide, brefeldin A, suramin, heparin and primaquine on proteoglycan and glycosaminoglycan biosynthesis in human embryonic skin fibroblasts. Biochim Biophys Acta 1137, 287-297.
Freeze, H.H., 2009. Genetic Disorders of Glycan Degradation, in: Varki, A., Cummings, R.D., Esko, J.D., Freeze, H.H., Stanley, P., Bertozzi, C.R., Hart, G.W., Etzler, M.E. (Eds.), Essentials of Glycobiology, 2nd ed, Cold Spring Harbor (NY).
Gallagher, J.T., 1989. The extended family of proteoglycans: social residents of the pericellular zone. Curr Opin Cell Biol 1, 1201-1218.
Gambardella, A.A., Schmidt Patterson, C.M., Webb, S.M., Walton, M.S., 2015. Sulfur K-edge XANES of Lazurite: Toward Determining

the Provenance of Lapis Lazuli. Microchem. J. 125, 299-307.
Geetha-Habib, M., Campbell, S.C., Schwartz, N.B., 1984. Subcellular localization of the synthesis and glycosylation of chondroitin sulfate proteoglycan core protein. J Biol Chem 259, 7300-7310.
George, G.N., Gorbaty, M.L., Kelemen, S.R., Sansone, M., 1991. Direct Determination and Quantification of Sulfur Forms in Coals

from the Argonne Premium Sample Program. Energy Fuels 5, 93-97.
Gnida, M., Sneeden, E.Y., Whitin, J.C., Prince, R.C., Pickering, I.J., Korbas, M., George, G.N., 2007. Sulfur X-ray absorption spectroscopy of living mammalian cells: an enabling tool for sulfur metabolomics. In situ observation of uptake of taurine into MDCK cells. Biochemistry 46, 14735-14741.
Gotoh, M., Sato, T., Akashima, T., Iwasaki, H., Kameyama, A., Mochizuki, H., Yada, T., Inaba, N., Zhang, Y., Kikuchi, N., Kwon, Y.D., Togayachi, A., Kudo, T., Nishihara, S., Watanabe, H., Kimata, K., Narimatsu, H., 2002. Enzymatic synthesis of chondroitin with a novel chondroitin sulfate N-acetylgalactosaminyltransferase that transfers N-acetylgalactosamine to glucuronic acid in initiation and elongation of chondroitin sulfate synthesis. J Biol Chem 277, 38189-38196.
Greenfield, M.L., Byrne, M., Mitra-Kirtley, S., Kercher, E.M., Bolin, T.B., Wu, T., Craddock, P.R., Bake, K.D., Pomerantz, A.E., 2015. XANES Measurements of Sulfur Chemistry during Asphalt Oxidation. Fuel 162, 179-185.
Gualeni, B., Facchini, M., De Leonardis, F., Tenni, R., Cetta, G., Viola, M., Passi, A., Superti-Furga, A., Forlino, A., Rossi, A., 2010. Defective proteoglycan sulfation of the growth plate zones causes reduced chondrocyte proliferation via an altered Indian hedgehog signalling. Matrix Biol 29, 453-460.
Gulberti, S., Jacquinet, J.C., Chabel, M., Ramalanjaona, N., Magdalou, J., Netter, P., Coughtrie, M.W., Ouzzine, M., Fournel-Gigleux, S., 2012. Chondroitin sulfate N-acetylgalactosaminyltransferase-1 (CSGalNAcT-1) involved in chondroitin sulfate initiation: Impact of sulfation on activity and specificity. Glycobiology 22, 561-571.
Gulberti, S., Lattard, V., Fondeur, M., Jacquinet, J.C., Mulliert, G., Netter, P., Magdalou, J., Ouzzine, M., Fournel-Gigleux, S., 2005. Phosphorylation and sulfation of oligosaccharide substrates critically influence the activity of human beta1,4-galactosyltransferase 7 (GalT-I) and beta1,3-glucuronosyltransferase I (GlcAT-I) involved in the biosynthesis of the glycosaminoglycan-protein linkage region of proteoglycans. J Biol Chem 280, 1417-1425.
Gupta, B.S., Wolf, K.W., Postlethwait, R.W., 1985. Effect of suture material and construction on frictional properties of sutures. Surg Gynecol Obstet 161, 12-16.
Hacker, U., Nybakken, K., Perrimon, N., 2005. Heparan sulphate proteoglycans: the sweet side of development. Nat Rev Mol Cell Biol 6, 530-541.
Hackett, M.J., George, G.N., Pickering, I.J., Eames, B.F., 2016. Chemical Biology in the Embryo: In Situ Imaging of Sulfur Biochemistry in Normal and Proteoglycan-Deficient Cartilage Matrix. Biochemistry 55, 2441-2451.
Hackett, M.J., Smith, S.E., Paterson, P.G., Nichol, H., Pickering, I.J., George, G.N., 2012. X-ray absorption spectroscopy at the sulfur K-edge: a new tool to investigate the biochemical mechanisms of neurodegeneration. ACS Chem Neurosci 3, 178-185.
Hamburger, V., Hamilton, H.L., 1951. A series of normal stages in the development of the chick embryo. Developmental Dynamics 195, 231-272.
Hammond, C.L., Moro, E., 2012. Using transgenic reporters to visualize bone and cartilage signalling during development in vivo. Front Endocrinol (Lausanne) 3, 91.

Han, C., Yan, D., Belenkaya, T.Y., Lin, X., 2005. Drosophila glypicans Dally and Dally-like shape the extracellular Wingless morphogen gradient in the wing disc. Development 132, 667-679.
Hanson, S.R., Best, M.D., Wong, C.H., 2004. Sulfatases: structure, mechanism, biological activity, inhibition, and synthetic utility. Angew Chem Int Ed Engl 43, 5736-5763.
Harada, M., Murakami, H., Okawa, A., Okimoto, N., Hiraoka, S., Nakahara, T., Akasaka, R., Shiraishi, Y., Futatsugi, N., Mizutani-Koseki, Y., Kuroiwa, A., Shirouzu, M., Yokoyama, S., Taiji, M., Iseki, S., Ornitz, D.M., Koseki, H., 2009. FGF9 monomer-dimer equilibrium regulates extracellular matrix affinity and tissue diffusion. Nat Genet 41, 289-298.
Hardingham, T.E., Fosang, A.J., 1992. Proteoglycans: many forms and many functions. FASEB J 6, 861-870.
Hardingham, T.E., Fosang, A.J., 1995. The structure of aggrecan and its turnover in cartilage. J Rheumatol Suppl 43, 86-90.
Hargest, T.E., Gay, C.V., Schraer, H., Wasserman, A.J., 1985. Vertical distribution of elements in cells and matrix of epiphyseal growth plate cartilage determined by quantitative electron probe analysis. J Histochem Cytochem 33, 275-286.
Harper, G.S., Rozaklis, T., Bielicki, J., Hopwood, J.J., 1993. Lysosomal sulfate efflux following glycosaminoglycan degradation: measurements in enzyme-supplemented Maroteaux-Lamy syndrome fibroblasts and isolated lysosomes. Glycoconj J 10, 407-415.
Hinton, R.J., Jing, Y., Jing, J., Feng, J.Q., 2017. Roles of Chondrocytes in Endochondral Bone Formation and Fracture Repair. J Dent Res 96, 23-30.
Hintze, V., Miron, A., Moeller, S., Schnabelrauch, M., Wiesmann, H.P., Worch, H., Scharnweber, D., 2012. Sulfated hyaluronan and chondroitin sulfate derivatives interact differently with human transforming growth factor-beta1 (TGF-beta1). Acta Biomater 8, 2144-2152.
Hiraoka, N., Nakagawa, H., Ong, E., Akama, T.O., Fukuda, M.N., Fukuda, M., 2000. Molecular cloning and expression of two distinct human chondroitin 4-O-sulfotransferases that belong to the HNK-1 sulfotransferase gene family. J Biol Chem 275, 20188-20196.
Hoffmann, H.P., Schwartz, N.B., Roden, L., Prockop, D.J., 1984. Location of xylosyltransferase in the cisternae of the rough endoplasmic reticulum of embryonic cartilage cells. Connect Tissue Res 12, 151-163.
Holmborn, K., Habicher, J., Kasza, Z., Eriksson, A.S., Filipek-Gorniok, B., Gopal, S., Couchman, J.R., Ahlberg, P.E., Wiweger, M., Spillmann, D., Kreuger, J., Ledin, J., 2012. On the roles and regulation of chondroitin sulfate and heparan sulfate in zebrafish pharyngeal cartilage morphogenesis. J Biol Chem 287, 33905-33916.
Hwang, W.Y., Fu, Y., Reyon, D., Maeder, M.L., Tsai, S.Q., Sander, J.D., Peterson, R.T., Yeh, J.R., Joung, J.K., 2013. Efficient genome editing in zebrafish using a CRISPR-Cas system. Nat Biotechnol 31, 227-229.
Iozzo, R.V., Murdoch, A.D., 1996. Proteoglycans of the extracellular environment: clues from the gene and protein side offer novel perspectives in molecular diversity and function. FASEB J 10, 598-614.
Ishikawa, H.O., Takeuchi, H., Haltiwanger, R.S., Irvine, K.D., 2008. Four-jointed is a Golgi kinase that phosphorylates a subset of cadherin domains. Science 321, 401-404.
Ishimaru, D., Sugiura, N., Akiyama, H., Watanabe, H., Matsumoto, K., 2014. Alterations in the chondroitin sulfate chain in human osteoarthritic cartilage of the knee. Osteoarthritis Cartilage 22, 250-258.
Iwata, S., Ito, M., Nakata, T., Noguchi, Y., Okuno, T., Ohkawara, B., Masuda, A., Goto, T., Adachi, M., Osaka, H., Nonaka, R., Arikawa-Hirasawa, E., Ohno, K., 2015. A missense mutation

in domain III in HSPG2 in Schwartz-Jampel syndrome compromises secretion of perlecan into the extracellular space. Neuromuscul Disord 25, 667-671.
Izumikawa, T., Koike, T., Kitagawa, H., 2012. Chondroitin 4-O-sulfotransferase-2 regulates the number of chondroitin sulfate chains initiated by chondroitin N-acetylgalactosaminyltransferase-1. Biochem J 441, 697-705.
Izumikawa, T., Koike, T., Shiozawa, S., Sugahara, K., Tamura, J.I., Kitagawa, H., 2008. Identification of chondroitin sulfate glucuronyltransferase as chondroitin synthase-3 involved in chondroitin polymerization - Chondroitin polymerization is achieved by multiple enzyme complexes consisting of chondroitin synthase family members. Journal of Biological Chemistry 283, 11396-11406.
Izumikawa, T., Okuura, Y., Koike, T., Sakoda, N., Kitagawa, H., 2011. Chondroitin 4-O-sulfotransferase-1 regulates the chain length of chondroitin sulfate in co-operation with chondroitin N-acetylgalactosaminyltransferase-2. Biochem J 434, 321-331.
Izumikawa, T., Uyama, T., Okuura, Y., Sugahara, K., Kitagawa, H., 2007. Involvement of chondroitin sulfate synthase-3 (chondroitin synthase-2) in chondroitin polymerization through its interaction with chondroitin synthase-1 or chondroitin-polymerizing factor. Biochem J 403, 545-552.
Jackson, S.M., Nakato, H., Sugiura, M., Jannuzi, A., Oakes, R., Kaluza, V., Golden, C., Selleck, S.B., 1997. dally, a Drosophila glypican, controls cellular responses to the TGF-beta-related morphogen, Dpp. Development 124, 4113-4120.
Kang, H.G., Evers, M.R., Xia, G., Baenziger, J.U., Schachner, M., 2002. Molecular cloning and characterization of chondroitin-4-O-sulfotransferase-3. A novel member of the HNK-1 family of sulfotransferases. J Biol Chem 277, 34766-34772.
Karsenty, G., Wagner, E.F., 2002. Reaching a genetic and molecular understanding of skeletal development. Dev Cell 2, 389-406.
Kearns, A.E., Campbell, S.C., Westley, J., Schwartz, N.B., 1991. Initiation of chondroitin sulfate biosynthesis: a kinetic analysis of UDP-D-xylose: core protein beta-D-xylosyltransferase. Biochemistry 30, 7477-7483.
Kearns, A.E., Vertel, B.M., Schwartz, N.B., 1993. Topography of glycosylation and UDP-xylose production. J Biol Chem 268, 11097-11104.
Khan, G.A., Girish, G.V., Lala, N., Di Guglielmo, G.M., Lala, P.K., 2011. Decorin is a novel VEGFR-2-binding antagonist for the human extravillous trophoblast. Mol Endocrinol 25, 1431-1443.
Khatri, R., Schipani, E., 2008. About the importance of being desulfated. Genes Dev 22, 2750-2754.
Kiani, C., Chen, L., Wu, Y.J., Yee, A.J., Yang, B.B., 2002. Structure and function of aggrecan. Cell Res 12, 19-32.
Kim, M., Bi, X., Horton, W.E., Spencer, R.G., Camacho, N.P., 2005. Fourier transform infrared imaging spectroscopic analysis of tissue engineered cartilage: histologic and biochemical correlations. J Biomed Opt 10, 031105.
Kim, S.H., Turnbull, J., Guimond, S., 2011. Extracellular matrix and cell signalling: the dynamic cooperation of integrin, proteoglycan and growth factor receptor. J Endocrinol 209, 139-151.
Kimura, M., Ichihara, I., 1994. The Golgi apparatus and acid phosphatase-negative cisternal portions of the trans-Golgi network: ultrastructural and cytochemical studies of secretory epithelial cells in the rat lateral prostate. Okajimas Folia Anat Jpn 71, 297-310.
Kinoshita, Y., Hori, M., Taguchi, M., Fukumoto, S., 2014. Functional analysis of mutant FAM20C in Raine syndrome with FGF23-related hypophosphatemia. Bone 67, 145-151.

Kitagawa, H., Izumikawa, T., Uyama, T., Sugahara, K., 2003. Molecular cloning of a chondroitin polymerizing factor that cooperates with chondroitin synthase for chondroitin polymerization. J Biol Chem 278, 23666-23671.
Kitagawa, H., Nadanaka, S., 2014. Chondroitin Polymerizing Factor, Chondroitin Polymerizing Factor 2, Chondroitin Sulfate Synthase 1,3 (CHPF, CHPF2, CHSY1, CHSY3), in: Taniguchi, N., Honke, K., Fukuda, M., Narimatsu, H., Yamaguchi, Y., Angata, T. (Eds.), Handbook of Glycosyltransferases and Related Genes. Springer Japan, pp. 947-963.
Kitagawa, H., Uyama, T., Sugahara, K., 2001. Molecular cloning and expression of a human chondroitin synthase. J Biol Chem 276, 38721-38726.
Klaassen, C.D., Boles, J.W., 1997. Sulfation and sulfotransferases 5: the importance of 3'-phosphoadenosine 5'-phosphosulfate (PAPS) in the regulation of sulfation. FASEB J 11, 404-418.
Klausner, R.D., Donaldson, J.G., Lippincott-Schwartz, J., 1992. Brefeldin A: insights into the control of membrane traffic and organelle structure. J Cell Biol 116, 1071-1080.
Kluppel, M., Vallis, K.A., Wrana, J.L., 2002. A high-throughput induction gene trap approach defines C4ST as a target of BMP signalling. Mech Dev 118, 77-89.
Kluppel, M., Wight, T.N., Chan, C., Hinek, A., Wrana, J.L., 2005. Maintenance of chondroitin sulfation balance by chondroitin-4-sulfotransferase 1 is required for chondrocyte development and growth factor signalling during cartilage morphogenesis. Development 132, 3989-4003.
Knapik, D.M., Perera, P., Nam, J., Blazek, A.D., Rath, B., Leblebicioglu, B., Das, H., Wu, L.C., Hewett, T.E., Agarwal, S.K., Jr., Robling, A.G., Flanigan, D.C., Lee, B.S., Agarwal, S., 2014. Mechanosignalling in bone health, trauma and inflammation. Antioxid Redox Signal 20, 970-985.
Kobayashi, M., Sugumaran, G., Liu, J., Shworak, N.W., Silbert, J.E., Rosenberg, R.D., 1999. Molecular cloning and characterization of a human uronyl 2-sulfotransferase that sulfates iduronyl and glucuronyl residues in dermatan/chondroitin sulfate. J Biol Chem 274, 10474-10480.
Kobayashi, S., Morimoto, K., Shimizu, T., Takahashi, M., Kurosawa, H., Shirasawa, T., 2000. Association of EXT1 and EXT2, hereditary multiple exostoses gene products, in Golgi apparatus. Biochem Biophys Res Commun 268, 860-867.
Koike, T., Izumikawa, T., Sato, B., Kitagawa, H., 2014. Identification of phosphatase that dephosphorylates xylose in the glycosaminoglycan-protein linkage region of proteoglycans. J Biol Chem 289, 6695-6708.
Koike, T., Izumikawa, T., Tamura, J., Kitagawa, H., 2009. FAM20B is a kinase that phosphorylates xylose in the glycosaminoglycan-protein linkage region. Biochem J 421, 157-162.
Koudouna, E., Young, R.D., Ueno, M., Kinoshita, S., Quantock, A.J., Knupp, C., 2014. Three-dimensional architecture of collagen type VI in the human trabecular meshwork. Mol Vis 20, 638-648.
Kramer, J.R., Onoa, B., Bustamante, C., Bertozzi, C.R., 2015. Chemically tunable mucin chimeras assembled on living cells. Proc Natl Acad Sci U S A 112, 12574-12579.
Kusche-Gullberg, M., Kjellen, L., 2003. Sulfotransferases in glycosaminoglycan biosynthesis. Curr Opin Struct Biol 13, 605-611.
Kwan, K.M., Fujimoto, E., Grabher, C., Mangum, B.D., Hardy, M.E., Campbell, D.S., Parant, J.M., Yost, H.J., Kanki, J.P., Chien, C.B., 2007. The Tol2kit: a multisite gateway-based construction kit for Tol2 transposon transgenesis constructs. Dev Dyn 236, 3088-3099.
Kwon, Y.K., Ahn, M.S., Park, J.S., Liu, J.R., In, D.S., Min, B.W., Kim, S.W., 2014. Discrimination of cultivation ages and cultivars of ginseng leaves using Fourier transform infrared spectroscopy combined with multivariate analysis. J Ginseng Res 38, 52-58.
Lampe, C., Bellettato, C.M., Karabul, N., Scarpa, M., 2013. Mucopolysaccharidoses and other lysosomal storage diseases. Rheum Dis Clin North Am 39, 431-455.

Lang, M.R., Lapierre, L.A., Frotscher, M., Goldenring, J.R., Knapik, E.W., 2006. Secretory COPII coat component Sec23a is essential for craniofacial chondrocyte maturation. Nat Genet 38, 1198-1203.
Laremore, T.N., Zhang, F., Linhardt, R.J., 2007. Ionic liquid matrix for direct UV-MALDI-TOF-MS analysis of dermatan sulfate and chondroitin sulfate oligosaccharides. Anal Chem 79, 1604-1610.
Lasch, P., Naumann, D., 2006. Spatial resolution in infrared microspectroscopic imaging of tissues. Biochim Biophys Acta 1758, 814-829.
Laughlin, S.T., Baskin, J.M., Amacher, S.L., Bertozzi, C.R., 2008. In vivo imaging of membrane-associated glycans in developing zebrafish. Science 320, 664-667.
Lauing, K.L., Cortes, M., Domowicz, M.S., Henry, J.G., Baria, A.T., Schwartz, N.B., 2014. Aggrecan is required for growth plate cytoarchitecture and differentiation. Dev Biol 396, 224-236.
Laurent, T.C., Fraser, J.R., 1992. Hyaluronan. FASEB J 6, 2397-2404.
Lee, T.V., Sethi, M.K., Leonardi, J., Rana, N.A., Buettner, F.F., Haltiwanger, R.S., Bakker, H., Jafar-Nejad, H., 2013. Negative regulation of notch signalling by xylose. PLoS Genet 9, e1003547.
Lennarz, W.J., 1980. The Biochemistry of Glycoproteins and Proteoglycans, 1 ed. Plenum Press, New York.
Levene, P.A., La Forge, F.B., 1913. On Chondroitin Sulphuric Acid. J. Biol. Chem. 15, 69-79.
Li, H., Schwartz, N.B., Vertel, B.M., 1993. cDNA cloning of chick cartilage chondroitin sulfate (aggrecan) core protein and identification of a stop codon in the aggrecan gene associated with the chondrodystrophy, nanomelia. J Biol Chem 268, 23504-23511.
Lin, X., 2004. Functions of heparan sulfate proteoglycans in cell signalling during development. Development 131, 6009-6021.
Lindblad, S., Hedfors, E., 1987. Arthroscopic and immunohistologic characterization of knee joint synovitis in osteoarthritis. Arthritis & Rheumatism 30, 1081-1088.
Lippincott-Schwartz, J., Yuan, L.C., Bonifacino, J.S., Klausner, R.D., 1989. Rapid redistribution of Golgi proteins into the ER in cells treated with brefeldin A: evidence for membrane cycling from Golgi to ER. Cell 56, 801-813.
Lohmander, L.S., Hascall, V.C., Yanagishita, M., Kuettner, K.E., Kimura, J.H., 1986. Post-translational events in proteoglycan synthesis: kinetics of synthesis of chondroitin sulfate and oligosaccharides on the core protein. Arch Biochem Biophys 250, 211-227.
Long, F., Chung, U.I., Ohba, S., McMahon, J., Kronenberg, H.M., McMahon, A.P., 2004. Ihh signalling is directly required for the osteoblast lineage in the endochondral skeleton. Development 131, 1309-1318.
Maroudas, A., Bayliss, M.T., Uchitel-Kaushansky, N., Schneiderman, R., Gilav, E., 1998. Aggrecan turnover in human articular cartilage: use of aspartic acid racemization as a marker of molecular age. Arch Biochem Biophys 350, 61-71.
Matis, M., Axelrod, J.D., 2013. Regulation of PCP by the Fat signalling pathway. Genes Dev 27, 2207-2220.
McCoy, S.Y., Falgowski, K.A., Srinivasan, P.P., Thompson, W.R., Selva, E.M., Kirn-Safran, C.B., 2012. Serum xylosyltransferase 1 level increases during early posttraumatic osteoarthritis in mice with high bone forming potential. Bone 51, 224-231.
Melrose, J., Isaacs, M.D., Smith, S.M., Hughes, C.E., Little, C.B., Caterson, B., Hayes, A.J., 2012. Chondroitin sulphate and heparan sulphate sulphation motifs and their proteoglycans are involved in articular cartilage formation during human foetal knee joint development. Histochem Cell Biol 138, 461-475.

Melville, D.B., Montero-Balaguer, M., Levic, D.S., Bradley, K., Smith, J.R., Hatzopoulos, A.K., Knapik, E.W., 2011. The feelgood mutation in zebrafish dysregulates COPII-dependent secretion of select extracellular matrix proteins in skeletal morphogenesis. Dis Model Mech 4, 763-776.
Merritt, T.M., Bick, R., Poindexter, B.J., Alcorn, J.L., Hecht, J.T., 2007. Unique matrix structure in the rough endoplasmic reticulum cisternae of pseudoachondroplasia chondrocytes. Am J Pathol 170, 293-300.
Midura, R.J., Calabro, A., Yanagishita, M., Hascall, V.C., 1995. Nonreducing end structures of chondroitin sulfate chains on aggrecan isolated from Swarm rat chondrosarcoma cultures. J Biol Chem 270, 8009-8015.
Mikami, T., Kitagawa, H., 2013. Biosynthesis and function of chondroitin sulfate. Biochim Biophys Acta 1830, 4719-4733.
Miller, M.R., Atwood, T.S., Eames, B.F., Eberhart, J.K., Yan, Y.L., Postlethwait, J.H., Johnson, E.A., 2007. RAD marker microarrays enable rapid mapping of zebrafish mutations. Genome Biol 8, R105.
Mis, E.K., Liem, K.F., Jr., Kong, Y., Schwartz, N.B., Domowicz, M., Weatherbee, S.D., 2014. Forward genetics defines Xylt1 as a key, conserved regulator of early chondrocyte maturation and skeletal length. Dev Biol 385, 67-82.
Mitsunaga-Nakatsubo, K., Kusunoki, S., Kawakami, H., Akasaka, K., Akimoto, Y., 2009. Cell-surface arylsulfatase A and B on sinusoidal endothelial cells, hepatocytes, and Kupffer cells in mammalian livers. Med Mol Morphol 42, 63-69.
Mizumoto, S., Mikami, T., Yasunaga, D., Kobayashi, N., Yamauchi, H., Miyake, A., Itoh, N., Kitagawa, H., Sugahara, K., 2009. Chondroitin 4-O-sulfotransferase-1 is required for somitic muscle development and motor axon guidance in zebrafish. Biochem J 419, 387-399.
Montano, A.M., Tomatsu, S., Gottesman, G.S., Smith, M., Orii, T., 2007. International Morquio A Registry: clinical manifestation and natural course of Morquio A disease. J Inherit Metab Dis 30, 165-174.
Morrone, A., Caciotti, A., Atwood, R., Davidson, K., Du, C., Francis-Lyon, P., Harmatz, P., Mealiffe, M., Mooney, S., Oron, T.R., Ryles, A., Zawadzki, K.A., Miller, N., 2014. Morquio A syndrome-associated mutations: a review of alterations in the GALNS gene and a new locus-specific database. Hum Mutat 35, 1271-1279.
Moses, J., Oldberg, A., Cheng, F., Fransson, L.A., 1997. Biosynthesis of the proteoglycan decorin--transient 2-phosphorylation of xylose during formation of the trisaccharide linkage region. Eur J Biochem 248, 521-526.
Movasaghi, Z., Rehman, S., Rehman, I., 2008. Fourier Transform Infrared (FTIR) Spectrocopy of Biological Tissues. Applied Spectroscopy Reviews 43, 134-179.
Muenzer, J., 2011. Overview of the mucopolysaccharidoses. Rheumatology (Oxford) 50 Suppl 5, v4-12.
Nadanaka, S., Kitagawa, H., 2008. Heparan sulphate biosynthesis and disease. J Biochem 144, 7-14.
Natowicz, M.R., Chi, M.M., Lowry, O.H., Sly, W.S., 1979. Enzymatic identification of mannose 6-phosphate on the recognition marker for receptor-mediated pinocytosis of beta-glucuronidase by human fibroblasts. Proc Natl Acad Sci U S A 76, 4322-4326.
Neufeld, E.F., Feingold, D.S., Hassid, W.Z., 1958. Enzymatic Conversion of Uridine Diphosphate D-Glucuronic Acid to Uridine Diphosphate Galacturonic Acid, Uridine Diphosphate Xylose, and Uridine Diphosphate Arabinose. J Am Chem Soc 80, 4430-4431.
Ni, G.X., Li, Z., Zhou, Y.Z., 2014. The role of small leucine-rich proteoglycans in osteoarthritis pathogenesis. Osteoarthritis Cartilage 22, 896-903.

Noreen, R., Moenner, M., Hwu, Y., Petibois, C., 2012. FTIR spectro-imaging of collagens for characterization and grading of gliomas. Biotechnol Adv 30, 1432-1446.
Nuttall, J.D., Brumfield, L.K., Fazzalari, N.L., Hopwood, J.J., Byers, S., 1999. Histomorphometric analysis of the tibial growth plate in a feline model of mucopolysaccharidosis type VI. Calcif Tissue Int 65, 47-52.
Ohtake, S., Ito, Y., Fukuta, M., Habuchi, O., 2001. Human N-acetylgalactosamine 4-sulfate 6-O-sulfotransferase cDNA is related to human B cell recombination activating gene-associated gene. J Biol Chem 276, 43894-43900.
Ohtake, S., Kimata, K., Habuchi, O., 2003. A unique nonreducing terminal modification of chondroitin sulfate by N-acetylgalactosamine 4-sulfate 6-o-sulfotransferase. J Biol Chem 278, 38443-38452.
Ohtake, S., Kimata, K., Habuchi, O., 2005. Recognition of sulfation pattern of chondroitin sulfate by uronosyl 2-O-sulfotransferase. J Biol Chem 280, 39115-39123.
Oka, T., Jigami, Y., 2006. Reconstruction of de novo pathway for synthesis of UDP-glucuronic acid and UDP-xylose from intrinsic UDP-glucose in Saccharomyces cerevisiae. FEBS J 273, 2645-2657.
Olsen, B.R., 1996. Role of cartilage collagens in formation of the skeleton. Ann N Y Acad Sci 785, 124-130.
Opoka-Winiarska, V., Jurecka, A., Emeryk, A., Tylki-Szymanska, A., 2013. Osteoimmunology in mucopolysaccharidoses type I, II, VI and VII. Immunological regulation of the osteoarticular system in the course of metabolic inflammation. Osteoarthritis Cartilage 21, 1813-1823.
Oshikawa, M., Usami, R., Kato, S., 2009. Characterization of the arylsulfatase I (ARSI) gene preferentially expressed in the human retinal pigment epithelium cell line ARPE-19. Mol Vis 15, 482-494.
Otsuki, S., Hanson, S.R., Miyaki, S., Grogan, S.P., Kinoshita, M., Asahara, H., Wong, C.H., Lotz, M.K., 2010. Extracellular sulfatases support cartilage homeostasis by regulating BMP and FGF signalling pathways. Proc Natl Acad Sci U S A 107, 10202-10207.
Palma, V., Carrasco, H., Reinchisi, G., Olivares, G., Faunes, F., Larrain, J., 2011. SHh activity and localization is regulated by perlecan. Biol Res 44, 63-67.
Paunesku, T., Vogt, S., Maser, J., Lai, B., Woloschak, G., 2006. X-ray fluorescence microprobe imaging in biology and medicine. J Cell Biochem 99, 1489-1502.
Petibois, C., Wehbe, K., Belbachir, R., Noreen, R., Deleris, G., 2008. Current Trends in the Development of FTIR Imaging for the Quantitative Analysis of Biological Samples. Acta Physica Polonica A 115, 507-512.
Pickering, I.J., George, G.N., Yu, E.Y., Brune, D.C., Tuschak, C., Overmann, J., Beatty, J.T., Prince, R.C., 2001. Analysis of sulfur biochemistry of sulfur bacteria using X-ray absorption spectroscopy. Biochemistry 40, 8138-8145.
Pickering, I.J., Prince, R.C., Divers, T., George, G.N., 1998. Sulfur K-edge X-ray absorption spectroscopy for determining the chemical speciation of sulfur in biological systems. FEBS Lett 441, 11-14.
Pickering, I.J., Sneeden, E.Y., Prince, R.C., Block, E., Harris, H.H., Hirsch, G., George, G.N., 2009. Localizing the chemical forms of sulfur in vivo using X-ray fluorescence spectroscopic imaging: application to onion (Allium cepa) tissues. Biochemistry 48, 6846-6853.
Pitsillides, A.A., Beier, F., 2011. Cartilage biology in osteoarthritis--lessons from developmental biology. Nat Rev Rheumatol 7, 654-663.
Plaas, A.H., Wong-Palms, S., Roughley, P.J., Midura, R.J., Hascall, V.C., 1997. Chemical and immunological assay of the nonreducing terminal residues of chondroitin sulfate from human aggrecan. J Biol Chem 272, 20603-20610.

Prabhakar, V., Sasisekharan, R., 2006. The biosynthesis and catabolism of galactosaminoglycans. Adv Pharmacol 53, 69-115.
Prydz, K., 2015. Determinants of Glycosaminoglycan (GAG) Structure. Biomolecules 5, 2003-2022.
Prydz, K., Dalen, K.T., 2000. Synthesis and sorting of proteoglycans. J Cell Sci 113 Pt 2, 193-205.
Pullig, O., Weseloh, G., Ronneberger, D., Kakonen, S., Swoboda, B., 2000. Chondrocyte differentiation in human osteoarthritis: expression of osteocalcin in normal and osteoarthritic cartilage and bone. Calcif Tissue Int 67, 230-240.
Pushie, M.J., Pickering, I.J., Korbas, M., Hackett, M.J., George, G.N., 2014. Elemental and chemically specific X-ray fluorescence imaging of biological systems. Chem Rev 114, 8499-8541.
Ratcliffe, A., Fryer, P.R., Hardingham, T.E., 1985. Proteoglycan biosynthesis in chondrocytes: protein A-gold localization of proteoglycan protein core and chondroitin sulfate within Golgi subcompartments. J Cell Biol 101, 2355-2365.
Ratzka, A., Mundlos, S., Vortkamp, A., 2010. Expression patterns of sulfatase genes in the developing mouse embryo. Dev Dyn 239, 1779-1788.
Reinert, T., Reibetanz, U., Schwertner, M., Vogt, J., Butz, T., Sakellariou, A., 2002. The architecture of cartilage: Elemental maps and scanning transmission ion microscopy/tomography. Nuclear Instruments and Methods in Physics Research Section B: Beam Interactions with Materials and Atoms 188, 1-8.
Reinert, T., Reibetanz, U., Vogt, J., Butz, T., Werner, A., Gründer, W., 2001. Spatially resolved elemental distributions in articular cartilage. Nuclear Instruments and Methods in Physics Research Section B: Beam Interactions with Materials and Atoms 181, 516-521.
Reynard, L.N., Loughlin, J., 2012. Genetics and epigenetics of osteoarthritis. Maturitas 71, 200-204.
Rivera-Colon, Y., Schutsky, E.K., Kita, A.Z., Garman, S.C., 2012. The structure of human GALNS reveals the molecular basis for mucopolysaccharidosis IV A. J Mol Biol 423, 736-751.
Rome, L.H., Hill, D.F., 1986. Lysosomal degradation of glycoproteins and glycosaminoglycans. Efflux and recycling of sulphate and N-acetylhexosamines. Biochem J 235, 707-713.
Rompel, A., Cinco, R.M., Latimer, M.J., McDermott, A.E., Guiles, R.D., Quintanilha, A., Krauss, R.M., Sauer, K., Yachandra, V.K., Klein, M.P., 1998. Sulfur K-edge x-ray absorption spectroscopy: a spectroscopic tool to examine the redox state of S-containing metabolites in vivo. Proc Natl Acad Sci U S A 95, 6122-6127.
Roper, J.R., Guther, M.L., Macrae, J.I., Prescott, A.R., Hallyburton, I., Acosta-Serrano, A., Ferguson, M.A., 2005. The suppression of galactose metabolism in procylic form Trypanosoma brucei causes cessation of cell growth and alters procyclin glycoprotein structure and copy number. J Biol Chem 280, 19728-19736.
Rosen, S.D., Lemjabbar-Alaoui, H., 2010. Sulf-2: an extracellular modulator of cell signalling and a cancer target candidate. Expert Opin Ther Targets 14, 935-949.
Roughley, P.J., 1987. Structural changes in the proteoglycans of human articular cartilage during aging. J Rheumatol 14 Spec No, 14-15.
Roughley, P.J., Mort, J.S., 2014. The role of aggrecan in normal and osteoarthritic cartilage. J Exp Orthop 1, 8.
Roughley, P.J., White, R.J., 1980. Age-related changes in the structure of the proteoglycan subunits from human articular cartilage. J Biol Chem 255, 217-224.

Saarakkala, S., Julkunen, P., 2010. Specificity of Fourier Transform Infrared (FTIR) Microspectroscopy to Estimate Depth-Wise Proteoglycan Content in Normal and Osteoarthritic Human Articular Cartilage. Cartilage 1, 262-269.
Saarakkala, S., Rieppo, L., Rieppo, J., Jurvelin, J.S., 2010. Fourier Transform Infrared (FTIR) Microspectroscopy of Immature, Mature and Degenerated Articular Cartilage. Microscopy: Science, Technology, Applications and Education, 403-414.
Sakai, K., Kimata, K., Sato, T., Gotoh, M., Narimatsu, H., Shinomiya, K., Watanabe, H., 2007. Chondroitin sulfate N-acetylgalactosaminyltransferase-1 plays a critical role in chondroitin sulfate synthesis in cartilage. J Biol Chem 282, 4152-4161.
Salbach, J., Kliemt, S., Rauner, M., Rachner, T.D., Goettsch, C., Kalkhof, S., von Bergen, M., Moller, S., Schnabelrauch, M., Hintze, V., Scharnweber, D., Hofbauer, L.C., 2012. The effect of the degree of sulfation of glycosaminoglycans on osteoclast function and signalling pathways. Biomaterials 33, 8418-8429.
Sardiello, M., Annunziata, I., Roma, G., Ballabio, A., 2005. Sulfatases and sulfatase modifying factors: an exclusive and promiscuous relationship. Hum Mol Genet 14, 3203-3217.
Sarkar, A.K., Esko, J.D., 1995. Synthesis and glycosaminoglycan priming activity of three disaccharides related to the linkage region tetrasaccharide of proteoglycans. Carbohydr Res 279, 161-171.
Sarmah, S., Barrallo-Gimeno, A., Melville, D.B., Topczewski, J., Solnica-Krezel, L., Knapik, E.W., 2010. Sec24D-dependent transport of extracellular matrix proteins is required for zebrafish skeletal morphogenesis. PLoS One 5, e10367.
Sato, T., Gotoh, M., Kiyohara, K., Akashima, T., Iwasaki, H., Kameyama, A., Mochizuki, H., Yada, T., Inaba, N., Togayachi, A., Kudo, T., Asada, M., Watanabe, H., Imamura, T., Kimata, K., Narimatsu, H., 2003. Differential roles of two N-acetylgalactosaminyltransferases, CSGalNAcT-1, and a novel enzyme, CSGalNAcT-2. Initiation and elongation in synthesis of chondroitin sulfate. J Biol Chem 278, 3063-3071.
Sato, T., Kudo, T., Ikehara, Y., Ogawa, H., Hirano, T., Kiyohara, K., Hagiwara, K., Togayachi, A., Ema, M., Takahashi, S., Kimata, K., Watanabe, H., Narimatsu, H., 2011. Chondroitin sulfate N-acetylgalactosaminyltransferase 1 is necessary for normal endochondral ossification and aggrecan metabolism. J Biol Chem 286, 5803-5812.
Schaefer, L., Schaefer, R.M., 2010. Proteoglycans: from structural compounds to signalling molecules. Cell Tissue Res 339, 237-246.
Schon, S., Huep, G., Prante, C., Muller, S., Christ, R., Hagena, F.W., Kuhn, J., Kleesiek, K., Gotting, C., 2006. Mutational and functional analyses of xylosyltransferases and their implication in osteoarthritis. Osteoarthritis Cartilage 14, 442-448.
Schonherr, E., O'Connell, B.C., Schittny, J., Robenek, H., Fastermann, D., Fisher, L.W., Plenz, G., Vischer, P., Young, M.F., Kresse, H., 1999. Paracrine or virus-mediated induction of decorin expression by endothelial cells contributes to tube formation and prevention of apoptosis in collagen lattices. Eur J Cell Biol 78, 44-55.
Schwartz, N., 2000. Biosynthesis and regulation of expression of proteoglycans. Front Biosci 5, D649-655.
Schwartz, N.B., 1977. Regulation of chondroitin sulfate synthesis. Effect of beta-xylosides on synthesis of chondroitin sulfate proteoglycan, chondroitin sulfate chains, and core protein. J Biol Chem 252, 6316-6321.
Sekiyama, H., Kosugi, N., Kuroda, H., Ohta, T., 1986. Sulfur K-edge absorption spectra of Na2SO4, Na2SO3, Na2S2O3, and

Na2S2Ox (x = 5−8). Bull. Chem. Soc. Jpn. 59, 575-579.

Settembre, C., Arteaga-Solis, E., McKee, M.D., de Pablo, R., Al Awqati, Q., Ballabio, A., Karsenty, G., 2008. Proteoglycan desulfation determines the efficiency of chondrocyte autophagy and the extent of FGF signalling during endochondral ossification. Genes Dev 22, 2645-2650.
Shapiro, E.G., Nestrasil, I., Rudser, K., Delaney, K., Kovac, V., Ahmed, A., Yund, B., Orchard, P.J., Eisengart, J., Niklason, G.R., Raiman, J., Mamak, E., Cowan, M.J., Bailey-Olson, M., Harmatz, P., Shankar, S.P., Cagle, S., Ali, N., Steiner, R.D., Wozniak, J., Lim, K.O., Whitley, C.B., 2015. Neurocognition across the spectrum of mucopolysaccharidosis type I: Age, severity, and treatment. Mol Genet Metab 116, 61-68.
Simonaro, C.M., D'Angelo, M., Haskins, M.E., Schuchman, E.H., 2005. Joint and bone disease in mucopolysaccharidoses VI and VII: identification of new therapeutic targets and biomarkers using animal models. Pediatr Res 57, 701-707.
Simonaro, C.M., Haskins, M.E., Schuchman, E.H., 2001. Articular chondrocytes from animals with a dermatan sulfate storage disease undergo a high rate of apoptosis and release nitric oxide and inflammatory cytokines: a possible mechanism underlying degenerative joint disease in the mucopolysaccharidoses. Lab Invest 81, 1319-1328.
Sohaskey, M.L., Yu, J., Diaz, M.A., Plaas, A.H., Harland, R.M., 2008. JAWS coordinates chondrogenesis and synovial joint positioning. Development 135, 2215-2220.
Sole, V.A., Papillon, E., Cotte, M., Walter, P., Susini, J., 2007. Spectrochimica Acta Part B: Atomic Spectroscopy. Spectrochimica Acta 62, 63-68.
Spiro, R.C., Freeze, H.H., Sampath, D., Garcia, J.A., 1991. Uncoupling of chondroitin sulfate glycosaminoglycan synthesis by brefeldin A. J Cell Biol 115, 1463-1473.
St-Jacques, B., Hammerschmidt, M., McMahon, A.P., 1999. Indian hedgehog signalling regulates proliferation and differentiation of chondrocytes and is essential for bone formation. Genes Dev 13, 2072-2086.
Stattin, E.L., Wiklund, F., Lindblom, K., Onnerfjord, P., Jonsson, B.A., Tegner, Y., Sasaki, T., Struglics, A., Lohmander, S., Dahl, N., Heinegard, D., Aspberg, A., 2010. A missense mutation in the aggrecan C-type lectin domain disrupts extracellular matrix interactions and causes dominant familial osteochondritis dissecans. Am J Hum Genet 86, 126-137.
Stirpe, N.S., Argraves, W.S., Goetinck, P.F., 1987. Chondrocytes from the cartilage proteoglycan-deficient mutant, nanomelia, synthesize greatly reduced levels of the proteoglycan core protein transcript. Dev Biol 124, 77-81.
Struglics, A., Hansson, M., 2010. Calpain is involved in C-terminal truncation of human aggrecan. Biochem J 430, 531-538.
Stuart, B., 2004. INFRARED SPECTROSCOPY: FUNDAMENTALS AND APPLICATIONS. John Wiley and Sons Ltd.
Sugiura, N., Shioiri, T., Chiba, M., Sato, T., Narimatsu, H., Kimata, K., Watanabe, H., 2012. Construction of a chondroitin sulfate library with defined structures and analysis of molecular interactions. J Biol Chem 287, 43390-43400.
Sugumaran, G., Katsman, M., Silbert, J.E., 1992. Effects of brefeldin A on the localization of chondroitin sulfate-synthesizing enzymes. Activities in subfractions of the Golgi from chick embryo epiphyseal cartilage. J Biol Chem 267, 8802-8806.
Sugumaran, G., Silbert, J.E., 1991. Subfractionation of chick embryo epiphyseal cartilage Golgi. Localization of enzymes involved in the synthesis of the polysaccharide portion of proteochondroitin sulfate. J Biol Chem 266, 9565-9569.
Tagliabracci, V.S., Engel, J.L., Wiley, S.E., Xiao, J., Gonzalez, D.J., Nidumanda Appaiah, H., Koller, A., Nizet, V., White, K.E., Dixon, J.E., 2014. Dynamic regulation of FGF23 by Fam20C phosphorylation, GalNAc-T3 glycosylation, and furin proteolysis. Proc Natl Acad Sci U S A 111, 5520-5525.

Thiele, H., Sakano, M., Kitagawa, H., Sugahara, K., Rajab, A., Hohne, W., Ritter, H., Leschik, G., Nurnberg, P., Mundlos, S., 2004. Loss of chondroitin 6-O-sulfotransferase-1 function results in severe human chondrodysplasia with progressive spinal involvement. Proc Natl Acad Sci U S A 101, 10155-10160.
Toma, L., Pinhal, M.A., Dietrich, C.P., Nader, H.B., Hirschberg, C.B., 1996. Transport of UDP-galactose into the Golgi lumen regulates the biosynthesis of proteoglycans. J Biol Chem 271, 3897-3901.
Tomatsu, S., Montano, A.M., Nishioka, T., Gutierrez, M.A., Pena, O.M., Tranda Firescu, G.G., Lopez, P., Yamaguchi, S., Noguchi, A., Orii, T., 2005. Mutation and polymorphism spectrum of the GALNS gene in mucopolysaccharidosis IVA (Morquio A). Hum Mutat 26, 500-512.
Tompson, S.W., Merriman, B., Funari, V.A., Fresquet, M., Lachman, R.S., Rimoin, D.L., Nelson, S.F., Briggs, M.D., Cohn, D.H., Krakow, D., 2009. A recessive skeletal dysplasia, SEMD aggrecan type, results from a missense mutation affecting the C-type lectin domain of aggrecan. Am J Hum Genet 84, 72-79.
Troeberg, L., Nagase, H., 2012. Proteases involved in cartilage matrix degradation in osteoarthritis. Biochim Biophys Acta 1824, 133-145.
Tumova, S., Woods, A., Couchman, J.R., 2000. Heparan sulfate proteoglycans on the cell surface: versatile coordinators of cellular functions. Int J Biochem Cell Biol 32, 269-288.
Turnbull, J., Powell, A., Guimond, S., 2001. Heparan sulfate: decoding a dynamic multifunctional cell regulator. Trends Cell Biol 11, 75-82.
Twining, B.S., Baines, S.B., Fisher, N.S., Maser, J., Vogt, S., Jacobsen, C., Tovar-Sanchez, A., Sanudo-Wilhelmy, S.A., 2003. Quantifying trace elements in individual aquatic protist cells with a synchrotron X-ray fluorescence microprobe. Anal Chem 75, 3806-3816.
Uchimura, K., Kadomatsu, K., Nishimura, H., Muramatsu, H., Nakamura, E., Kurosawa, N., Habuchi, O., El-Fasakhany, F.M., Yoshikai, Y., Muramatsu, T., 2002. Functional analysis of the chondroitin 6-sulfotransferase gene in relation to lymphocyte subpopulations, brain development, and oversulfated chondroitin sulfates. J Biol Chem 277, 1443-1450.
Uhlin-Hansen, L., Yanagishita, M., 1993. Differential effect of brefeldin A on the biosynthesis of heparan sulfate and chondroitin/dermatan sulfate proteoglycans in rat ovarian granulosa cells in culture. J Biol Chem 268, 17370-17376.
Unlu, G., Levic, D.S., Melville, D.B., Knapik, E.W., 2014. Trafficking mechanisms of extracellular matrix macromolecules: insights from vertebrate development and human diseases. Int J Biochem Cell Biol 47, 57-67.
Upholt, W.B., Chandrasekaran, L., Tanzer, M.L., 1993. Molecular cloning and analysis of the protein modules of aggrecans. Experientia 49, 384-392.
Uyama, T., Ishida, M., Izumikawa, T., Trybala, E., Tufaro, F., Bergstrom, T., Sugahara, K., Kitagawa, H., 2006. Chondroitin 4-O-sulfotransferase-1 regulates E disaccharide expression of chondroitin sulfate required for herpes simplex virus infectivity. J Biol Chem 281, 38668-38674.
Uyama, T., Kitagawa, H., Sugahara, K., 2007. Biosynthesis of glycosaminoglycans and proteoglycans. J.P. Kamerling (Ed.), Comprehensive Glycoscience 3, 79-104.
Uyama, T., Kitagawa, H., Tamura Ji, J., Sugahara, K., 2002. Molecular cloning and expression of human chondroitin N-acetylgalactosaminyltransferase: the key enzyme for chain initiation and elongation of chondroitin/dermatan sulfate on the protein linkage region tetrasaccharide shared by heparin/heparan sulfate. J Biol Chem 277, 8841-8846.
Valayannopoulos, V., Nicely, H., Harmatz, P., Turbeville, S., 2010. Mucopolysaccharidosis VI. Orphanet J Rare Dis 5, 5.

Valdes, A.M., Loughlin, J., Oene, M.V., Chapman, K., Surdulescu, G.L., Doherty, M., Spector, T.D., 2007. Sex and ethnic differences in the association of ASPN, CALM1, COL2A1, COMP, and FRZB with genetic susceptibility to osteoarthritis of the knee. Arthritis Rheum 56, 137-146.
Valdes, A.M., Spector, T.D., 2010. The genetic epidemiology of osteoarthritis. Curr Opin Rheumatol 22, 139-143.
Valhmu, W.B., Palmer, G.D., Rivers, P.A., Ebara, S., Cheng, J.F., Fischer, S., Ratcliffe, A., 1995. Structure of the human aggrecan gene: exon-intron organization and association with the protein domains. Biochem J 309 (Pt 2), 535-542.
Verhoef, R., Schols, H.A., Blanco, A., Siika-aho, M., Ratto, M., Buchert, J., Lenon, G., Voragen, A.G., 2005. Sugar composition and FT-IR analysis of exopolysaccharides produced by microbial isolates from paper mill slime deposits. Biotechnol Bioeng 91, 91-105.
Vertel, B.M., Barkman, L.L., 1984. Immunofluorescence studies of chondroitin sulfate proteoglycan biosynthesis: the use of monoclonal antibodies. Coll Relat Res 4, 1-20.
Vertel, B.M., Hitti, Y., 1987. Biosynthetic precursors of cartilage chondroitin sulfate proteoglycan. Coll Relat Res 7, 57-75.
Vertel, B.M., Walters, L.M., Flay, N., Kearns, A.E., Schwartz, N.B., 1993. Xylosylation is an endoplasmic reticulum to Golgi event. J Biol Chem 268, 11105-11112.
Vortkamp, A., 2000. The Indian hedgehog--PTHrP system in bone development. Ernst Schering Res Found Workshop, 191-209.
Vu, T.H., Werb, Z., 2000. Matrix metalloproteinases: effectors of development and normal physiology. Genes Dev 14, 2123-2133.
Vynios, D.H., 2014. Metabolism of cartilage proteoglycans in health and disease. Biomed Res Int 2014, 452315.
Watanabe, H., Kimata, K., Line, S., Strong, D., Gao, L.Y., Kozak, C.A., Yamada, Y., 1994. Mouse cartilage matrix deficiency (cmd) caused by a 7 bp deletion in the aggrecan gene. Nat Genet 7, 154-157.
Watanabe, Y., Takeuchi, K., Higa Onaga, S., Sato, M., Tsujita, M., Abe, M., Natsume, R., Li, M., Furuichi, T., Saeki, M., Izumikawa, T., Hasegawa, A., Yokoyama, M., Ikegawa, S., Sakimura, K., Amizuka, N., Kitagawa, H., Igarashi, M., 2010. Chondroitin sulfate N-acetylgalactosaminyltransferase-1 is required for normal cartilage development. Biochem J 432, 47-55.
Wen, J., Xiao, J., Rahdar, M., Choudhury, B.P., Cui, J., Taylor, G.S., Esko, J.D., Dixon, J.E., 2014. Xylose phosphorylation functions as a molecular switch to regulate proteoglycan biosynthesis. Proc Natl Acad Sci U S A 111, 15723-15728.
Wiegmann, E.M., Westendorf, E., Kalus, I., Pringle, T.H., Lubke, T., Dierks, T., 2013. bArylsulfatase K, a novel lysosomal sulfatase. J Biol Chem 288, 30019-30028.
Wight, T.N., Heinegard, D., Hascall, V.C., 1991. Cell Biology of Extracellular Matrix 2ed. Plenum Publishing Corp., New York.
Wiweger, M.I., de Andrea, C.E., Scheepstra, K.W., Zhao, Z., Hogendoorn, P.C., 2014. Possible effects of EXT2 on mesenchymal differentiation--lessons from the zebrafish. Orphanet J Rare Dis 9, 35.
Wuyts, W., Van Hul, W., De Boulle, K., Hendrickx, J., Bakker, E., Vanhoenacker, F., Mollica, F., Ludecke, H.J., Sayli, B.S., Pazzaglia, U.E., Mortier, G., Hamel, B., Conrad, E.U., Matsushita, M., Raskind, W.H., Willems, P.J., 1998. Mutations in the EXT1 and EXT2 genes in hereditary multiple exostoses. Am J Hum Genet 62, 346-354.
Yada, T., Gotoh, M., Sato, T., Shionyu, M., Go, M., Kaseyama, H., Iwasaki, H., Kikuchi, N., Kwon, Y.D., Togayachi, A., Kudo, T., Watanabe, H., Narimatsu, H., Kimata, K., 2003. Chondroitin sulfate synthase-2. Molecular cloning and characterization of a novel human

glycosyltransferase homologous to chondroitin sulfate glucuronyltransferase, which has dual enzymatic activities. J Biol Chem 278, 30235-30247.
Yamada, S., 2015. Role of hyaluronidases in the catabolism of chondroitin sulfate. Adv Exp Med Biol 842, 185-197.
Yamauchi, S., Mita, S., Matsubara, T., Fukuta, M., Habuchi, H., Kimata, K., Habuchi, O., 2000. Molecular cloning and expression of chondroitin 4-sulfotransferase. J Biol Chem 275, 8975-8981.
Yan, Y.L., Miller, C.T., Nissen, R.M., Singer, A., Liu, D., Kirn, A., Draper, B., Willoughby, J., Morcos, P.A., Amsterdam, A., Chung, B.C., Westerfield, M., Haffter, P., Hopkins, N., Kimmel, C., Postlethwait, J.H., 2002. A zebrafish sox9 gene required for cartilage morphogenesis. Development 129, 5065-5079.
Yanagishita, M., 1993a. A brief history of proteoglycans. Experientia 49, 366-368.
Yanagishita, M., 1993b. Function of proteoglycans in the extracellular matrix. Acta Pathol Jpn 43, 283-293.
Zimmermann, B., Bagcioglu, M., Sandt, C., Kohler, A., 2015. Vibrational microspectroscopy enables chemical characterization of single pollen grains as well as comparative analysis of plant species based on pollen ultrastructure. Planta 242, 1237-1250.
Zon, L.I., 1999. Zebrafish: a new model for human disease. Genome Res 9, 99-100.